Journal of Molecular Spectroscopy **195,** 194–228 (1999)
Article ID jmsp.1999.7838, available online at http://www.idealibrary.com on IDEAL®

SPECIAL REVIEW LECTURE

# Photoassociation of Ultracold Atoms: A New Spectroscopic Technique

William C. Stwalley and He Wang

*Department of Physics, University of Connecticut, 2152 Hillside Road, Storrs, Connecticut 06269-3046*

E-mail: stwalley@uconnvm.uconn.edu, wang@phys.uconn.edu

Received February 17, 1999

The new spectroscopic technique of photoassociation of ultracold atoms is reviewed, with an emphasis on connecting this area to traditional bound-state molecular spectroscopy. In particular, in contrast to photoassociative spectra at thermal energies, which are broad and of low information content, photoassociative spectra of ultracold atoms are high resolution, permitting observation of small vibrational and rotational spacings of long-range molecular levels near dissociation (typically with outer classical turning points >20 Å). The types of detection and theoretical analysis employed are illustrated, primarily using the example of $^{39}K_2$. Future directions and applications of this field (e.g., to ultracold molecular formation) are also discussed. 

## CONTENTS



## I. INTRODUCTION

The primary purpose of this review is to provide scientists interested in molecular spectroscopy with an overview of the powerful spectroscopic technique of the photoassociation of ultracold atoms. This is a follow-up to the First Annual *Journal of Molecular Spectroscopy* lecture by Stwalley at the 53rd International Symposium on Molecular Spectroscopy at Ohio State University in June 1998 on this topic. Fortunately, there are two existing reviews (primarily for atomic, molecular, and optical physicists) of this field (*1, 2*), and a comprehensive review of cold and ultracold collisions, atom cooling and trapping, and photoassociation has just appeared (*3*). We use as our primary illustrative example the potassium atom and molecule. K, like Li, has relatively small hyperfine splittings, simplifying the spectra considerably when compared to Na, Rb, and Cs. Most techniques for obtaining spectra can be well illustrated using examples from $^{39}K$ photoassociation. All seven attractive excited states (including two "pure long-range" states) at the $n_{min}s + n_{min}p$ asymptote have been observed for $^{39}K$, but not yet for any other species. In addition, the energetics are precisely known for K, as they also are for Li and Na. Finally, we feel there is a considerable pedagogic advantage in considering primarily a single molecular system, although many analogous (referenced) results are available for the other alkali atoms with qualitatively similar interatomic interactions.

In the region below ionization, single-photon two-atom photophysical/photochemical processes can be broken down as summarized in Table 1 into bound–bound, bound–free, free–bound, and free–free processes (*4*). The focus in this review will be on free → bound absorption (photoassociation) of



0022-2852/99 $30.00

**TABLE 1**
**Single-Photon Photoprocesses Involving Two Atoms ($M$) and No Ionization**

| | |
|---|---|
| Absorption | |
| bound → bound | $M_2(v'', J'') + h\nu \rightarrow M_2^*(v', J')$ |
| bound → free (photodissociation) | $M_2(v'', J'') + h\nu \rightarrow M^* + M$ |
| free → bound (photoassociation) | $M + M + h\nu \rightarrow M_2^*(v', J')$ |
| free → free | $M + M + h\nu \rightarrow M^* + M$ |
| Emission (Spontaneous [or Stimulated]) | |
| bound → bound | $M_2^*(v',J') [+ h\nu] \rightarrow M_2(v'',J'') + h\nu [+ h\nu]$ |
| bound → free | $M_2^*(v',J') [+ h\nu] \rightarrow M + M + h\nu [+ h\nu]$ |
| free → bound | $M^* + M [+ h\nu] \rightarrow M_2(v'',J'') + h\nu [+ h\nu]$ |
| free → free | $M^* + M [+ h\nu] \rightarrow M + M + h\nu [+ h\nu]$ |

ultracold ($T \leq 1$ mK) atoms, a new and exciting technique which is providing unprecedented understanding of photoprocesses and long-range interactions.

In Fig. 1, we see a selection of the potential curves and corresponding asymptotes of the $^{39}K_2$ molecule. The ordinary molecular absorption spectrum of $K_2(A^1\Sigma_u^+ \leftarrow X^1\Sigma_g^+$ and $B^1\Pi_u \leftarrow X^1\Sigma_g^+)$ has been known since 1874 (*7*). Laser spectroscopy of the $A^1\Sigma_u^+$ and $B^1\Pi_u$ states correlating to the $4s + 4p$ asymptotes is quite extensive (e.g., (*8*)), and the spectroscopy of higher gerade states through the intermediate $A^1\Sigma_u^+$, $B^1\Pi_u$ and $A^1\Sigma_u^+ \sim b^3\Pi_u$ mixed levels is also quite extensive (e.g., (*9, 10*)). All-optical triple resonance (AOTR) has been used to study the $A^1\Sigma_u^+ \sim b^3\Pi_u$ mixed levels as well as pure $b^3\Pi_u$ levels inaccessible from the ground state (e.g., (*11*)), and also to study state-selected photodissociation of vibrationally excited ground state molecules (e.g., (*12*)).

In addition, laser excitation of singlet ungerade states above the $4s + 4p$ asymptotes has been combined with high-resolution Fourier transform spectroscopy to generate important information on singlet gerade states at the $4s + 4p$ asymptotes. Triplet spectroscopy originating in the $a^3\Sigma_u^+$ state has been carried out using molecules formed on large, cold He clusters (e.g., (*13*)). Finally, high-quality electronic structure calculations are available for most of these states (e.g., (*6*)). Thus a fairly complete picture of molecular states from ~2.5–8 Å is now available for $K_2$. Similar high-quality information is available for other alkalis, e.g., $Li_2$ and $Na_2$.

The connection of these short-range molecular potentials with long-range potentials and various atomic asymptotes is more problematic, with a few exceptions (e.g., in $K_2$ the $1^1\Pi_g$ state (*14, 15*) is now known out to 40 Å). Fortunately, a new and complementary alternative for probing the long-range potentials (typically ≥15 Å) is now available, namely photoassociation of ultracold atoms, the topic of this review. Figure 1 shows the examples of short-range single-photon excitation of the $A^1\Sigma_u^+$ state (laser $L_1$) and short-range optical–optical double resonance (OODR) excitation (lasers $L_1$ and $L_2$) of the $5^1\Pi_g$ state of $K_2$ correlating to the $4s + 4d$ asymptote via the intermediate $A^1\Sigma_u^+$ state. Figure 1 also shows the examples of long-range $A^1\Sigma_u^+ \leftarrow X^1\Sigma_g^+$ photoassociation (laser $L_{PA}$) of two colliding ground state atoms and of long-range OODR excitation (lasers $L_{PA}$ and $L_2'$) of the $5^1\Pi_g$ state near the $4s + 4d$ asymptote (in fact, the long-range states are better described in Hund's case c notation, as discussed here in Section III; thus the photoassociation is labeled $0_u^+ \leftarrow 0_g^+$ and the OODR excitation is $1_g \leftarrow 0_u^+$). It should be clear that the long-range ultracold atom photoassociation is in many ways the perfect complement to ordinary short-range spectroscopy, which we elaborate below.

In this section, we will first examine "ordinary" photoassociation at thermal energies (Section I.A), which can provide important but limited information on atomic interactions. Then we will briefly survey atom cooling and trapping techniques (Section I.B) which allow the possibility of spectroscopically probing relatively dense ($\sim 10^{11}$ atoms/cm$^3$) samples of ultracold atoms. We then discuss the groundbreaking marriage of photoassociation and ultracold atoms (Section I.C) first proposed by Thorsheim, Weiner, and Julienne (*16*) and first reported in back-to-back *Physical Review Letters* on Na (*17*) and Rb (*18*). We note that photoassociation of ultracold atoms is currently the leading approach for producing ultracold molecules (Section I.D; initially translationally ultracold and ultimately both translationally and internally ultracold). Such ul-

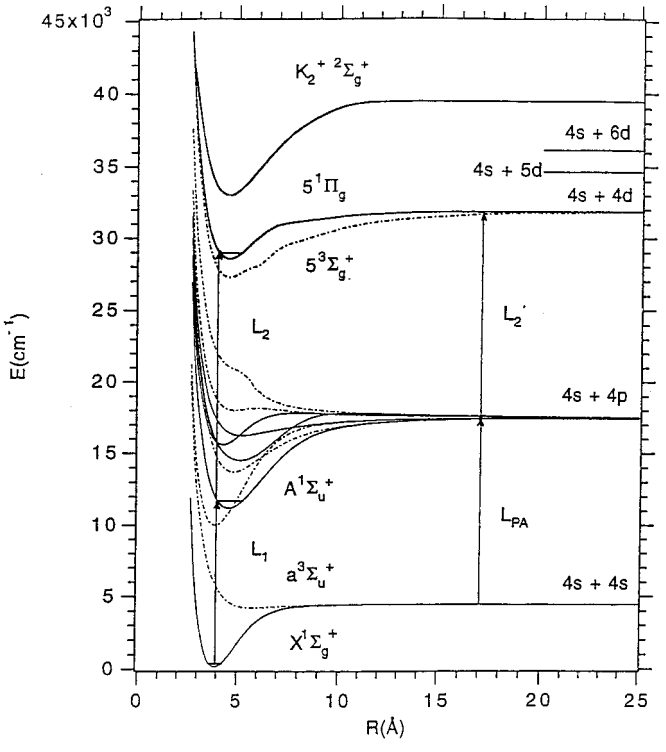


**FIG. 1.** Selected potential energy curves and atomic asymptotes of the $^{39}K_2$ molecule (*5, 6*).

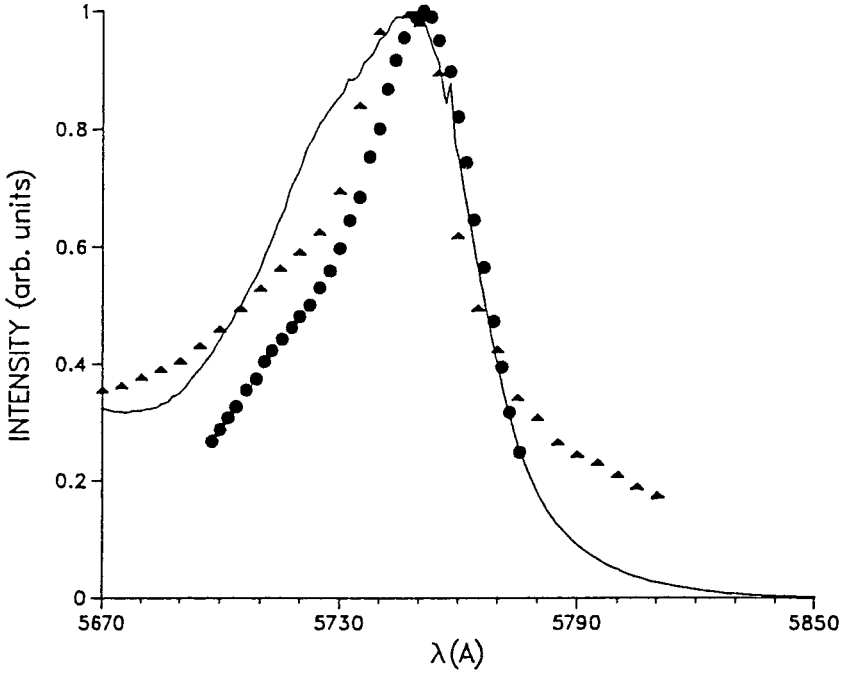


**FIG. 2.** Absorption observations of the $K_2$ diffuse band (corresponding to $2^3\Pi_g \leftarrow a^3\Sigma_u^+$ photoassociation) from (*25*) (▲) at 780–840 K and (*26*) (●) at 845 K compared with a quantum mechanical simulation (*27*) at 800 K (—).

tracold molecules should be of high interest for many reasons (*19*).

Later sections will deal with Observations of Ultracold Photoassociation (Section II), Analysis of Ultracold Photoassociation (Section III), and Future Directions (Section IV) using this fascinating new technique.

In this review, we will focus on the alkali metal atoms and diatomics and especially on potassium, which our group has studied in collaboration with the groups of Professors Phillip Gould and Edward Eyler at the University of Connecticut and which illustrate much of the promise of the ultracold photoassociation technique. Extensive assigned spectroscopic results are also available from groups at Rice University (Li), NIST (Na), Maryland (Na and Rb), Texas (Rb), Lab. Aimé Cotton (Cs), and Utrecht (Na) and are referenced in Table 7 in Section II. Very recently, photoassociation of cold H has also been observed at the University of Amsterdam (*20*).

### *I.A. Photoassociation*

It has long been realized that the absorption of light by colliding atoms results in molecular continua (*21–23*). In particular, such spectra at ordinary temperatures are broad and continuous whether the upper electronic state is bound (photoassociation) or free. This breadth is due not only to the initial thermal energy; the wide range of detunings from atomic resonance over which the absorption can occur provides significant broadening (e.g., when the excited asymptote has states with strong $\pm C_3/R^3$ long-range interactions as in the alkali dimers). Finally, the broad range of rotational quantum numbers/angular momenta of collision provides additional broadening.

In the case of $K_2$ photoassociation, the 575-nm diffuse band, corresponding to free-to-bound $2^3\Pi_g \leftarrow a^3\Sigma_u^+$ absorption, was first observed in 1928 (*24*) and has been extensively studied since (*25–28*). A comparison of two experimental results (*25, 26*) and a simulation (*27*) is shown in Fig. 2. It is clear that the information content in this thermal photoassociation spectrum is low; nevertheless, it does serve to fairly precisely ($\pm 10$ $cm^{-1}$) determine the $T_e$ value of the $2^3\Pi_g$ state of $K_2$, which has not been observed except via this diffuse band. It might be noted that the simulation in Fig. 2 involved calculating the free $\rightarrow$ bound Einstein B coefficients for absorption to thousands of bound $2^3\Pi_g$ levels ($v' \leq 50$, $J' \leq 300$) from the thermal distribution of atoms colliding on the lower $a^3\Sigma_u^+$ potential, since $kT \gg \Delta G_{v'+1/2}$, the upper state vibrational spacing. This is in contrast to the ultracold photoassociation described below, where not only is $kT \ll \Delta G_{v'+1/2}$, but also $kT \ll B_{v'}$ and only $J'' \leq 2$ collisions penetrate inside 100 Å.

### *I.B. Atom Cooling and Trapping*

One of the most remarkable developments in recent years has been the arsenal of techniques to cool atoms to ultracold temperatures ($<1$ mK) using lasers but no cryogenics, and then to trap them in high vacuum. These techniques include Zeeman, chirp, and other techniques to slow, stop, or even accelerate an atomic beam; optical molasses to damp the motion of atoms away from an intersection of laser beams; the magneto–optical trap (MOT) to confine atoms in a three-dimensional

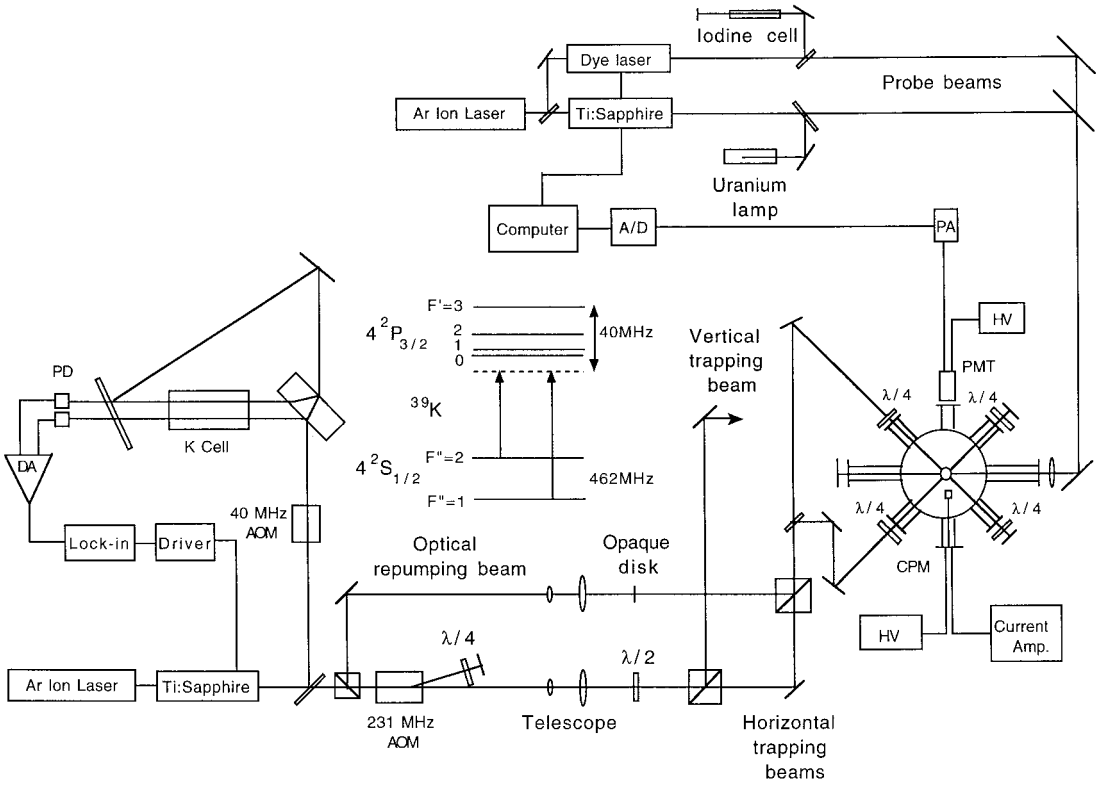


**FIG. 3.** Schematic diagram of our cell dark spot magneto–optical trap (CDSMOT), described in detail in (*36, 37*). Trap-loss detection (with a photomultiplier tube (PMT)) and ion detection (with a channeltron particle multiplier (CPM)) are shown here; for other detection methods, see Section II. Note also the inset showing hyperfine structure in the ground and excited states for $^{39}$K.

trap of depth ~1 K at temperatures of hundreds of microkelvins and densities of $\sim 10^{11}$ atoms/cm$^3$; and Bose–Einstein condensation (BEC) of atoms in magnetic traps at nanokelvin temperatures and densities of $\sim 10^{14}$ atoms/cm$^3$. A full survey of these techniques is far beyond the scope of this review. We refer the interested reader to (*3, 29–35*).

For the purposes of this review, it is sufficient to understand the operation of a so-called cell dark spot magneto–optical trap (CDSMOT), although photoassociation can certainly be carried out in either a beam-loaded (rather than cell) or regular (rather than dark spot) MOT or in another type of trap (e.g., far-off resonance traps (FORTs)). A schematic diagram of our CDSMOT (*36, 37*) is shown in Fig. 3. Operationally, our CDSMOT is a robust sample of isotopically selected ultracold atoms with properties listed in Table 2, analogous in many ways to a transparent $I_2$ cell or a metal vapor heat pipe oven. It is composed of three major parts: 1) an ultrahigh vacuum chamber; 2) three pairs of circularly polarized, red-detuned, counterpropagating laser beams; and 3) a pair of anti-Helmholtz coils. Our potassium cell MOT was built in a ten-arm stainless steel UHV chamber with a background pressure of $5 \times 10^{-10}$ Torr and a room temperature potassium vapor pressure of $\sim 10^{-8}$ Torr. The three pairs of orthogonal laser beams are provided by a single mode tunable ring Ti:Sapphire laser (Coherent 899-29) with output power ~300 mW at 766.5 nm. The ring-laser frequency is locked to the $^{39}$K $4^2S_{1/2}$ ($F'' = 2$) $\rightarrow 4^2P_{3/2}$ ($F' = 3$) transition using saturated absorption for long-term frequency stability ($\Delta\nu < 1$ MHz). The case of potassium is unique among the alkalis because the hyperfine levels of the excited state are closely spaced (all within 34 MHz of each other as shown in the insert of Fig. 3), resulting in strong optical pumping (i.e., no effective cycling transition)

**TABLE 2**
**Selected Properties of Our Cell Magneto–Optical Trap of $^{39}$K (*36, 37*)**

| | |
|---|---|
| Background vacuum: | $5 \times 10^{-10}$ Torr |
| K vapor pressure: | ~$1 \times 10^{-8}$ Torr (room temp.) |
| $B_z$ gradient: | 20 Gauss / cm |
| Trapping beam intensity: | 90 mW / cm$^2$ |
| Repumping beam intensity: | 40 mW / cm$^2$ |
| Red-detuning $\Delta\nu$: | -40 MHz (from the F′ = 3 level) |
| Total trapped atoms: | $2 \times 10^7$ |
| Regular MOT (mainly F = 2): | |
| Density | $3 \times 10^{10}$ atoms / cm$^3$ |
| Trap temperature | 500 μK |
| Dark Spot MOT (mainly F = 1): | |
| Density | ~$10^{11}$ atoms / cm$^3$ |
| Trap temperature: | 350 μK |

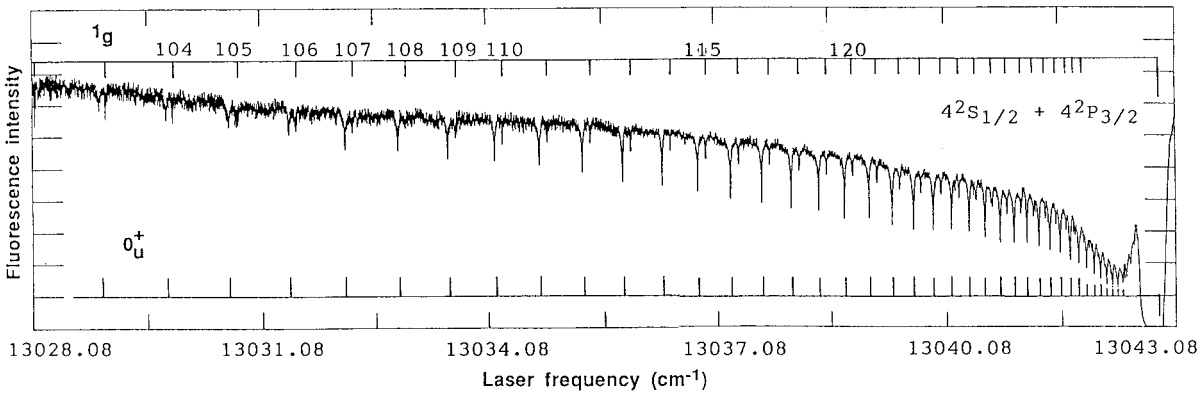


**FIG. 4.** A high-resolution trap-loss spectrum corresponding to single-photon excitation of the $1_g$ and $0_u^+$ electronic states of $^{39}K_2$ immediately below the $4p_{3/2} + 4s_{1/2}$ asymptote (marked at the right top). This 15 $cm^{-1}$ scan clearly shows $1_g$ vibrational levels from $v = 102$–135 and an even larger number of $0_u^+$ vibrational levels (quantum numbers not yet assigned). Each level has rotational structure such as is shown in Fig. 5 and discussed in Section II.

when typical laser detunings (~10 MHz) are used. As a direct consequence of the small hyperfine splittings, detuning below all excited state hyperfine components is found to optimize the capture and confinement of potassium atoms. A 40-MHz red-detuning below the upper $F' = 3$ level is generated by an acousto–optical modulator (AOM). The optical repumping beam with a 462-MHz frequency shift is obtained by double passing through a 231-MHz AOM. The anti-Helmholtz coils generate a quadrupole field with an axial magnetic field gradient of 20 G/cm. To achieve a higher density of trapped atoms, we used a "dark spot" MOT (*38*), which was formed by blocking the center region of the two horizontal optical repumping beams with an opaque disk of 2–3 mm in diameter. Both the trapping and repumping beams are expanded by a telescope to a beam size of 20 mm in diameter. With such a CDSMOT, a sample of $10^7$ $^{39}K$ atoms with a density $> 10^{11}$ atoms/$cm^3$ and a temperature ~350 $\mu$K was obtained.

The photoassociation is induced by a second Ti:sapphire laser (Coherent 899-29) with a typical output power of ~500 mW. This intense laser beam is focused to a diameter of ~0.5 mm at the trap region. The absolute laser frequency is calibrated by uranium atomic lines as well as the potassium resonance lines. The detection schemes shown in Fig. 3 are atomic fluorescence ($4p_{3/2} \rightarrow 4s_{1/2}$) and ion detection. This fluorescence detection versus probe laser frequency, such as shown in Figs. 4 and 5, provides a so-called "trap-loss spectrum," discussed further in Section II with other detection schemes. Note that these Figs. 4 and 5 spectra are quite different from the classic photoassociation spectrum (Fig. 2).

### *I.C. Photoassociation of Ultracold Atoms*

Recent advances in atom cooling and trapping have provided samples of isotopically selected atomic gases at densities of $>10^{11}$/$cm^3$ and ultracold temperatures (without using cryogenics) below 1 mK. Here the thermal kinetic energy ($kT$/h = 21 MHz at 1 mK) is comparable to or smaller than many terms in the Hamiltonian (Table 3), including, for example, the natural energy linewidth of excited states! For example, Fig. 6 shows the long-range potential ($J = 0$), well approximated by an inverse power sum ($-C_6R^{-6} - C_8R^{-8} - C_{10}R^{-10}$) (*39*), and the corresponding effective potentials ($J = 1, 2, 3$) for the $X^1\Sigma_g^+$ ($0_g^+$) state of $K_2$. The curves for the $a^3\Sigma_u^+(0_u^-)$ state are identical; those for the $a^3\Sigma_u^+(1_u)$ state are quite similar but lower, since the effective potential $U_J(R) = V(R) + \{\hbar^2[J(J+1) - \Omega^2]\}/2\mu R^2$. At a collision energy of 1 mK in our trap (approximately three times $kT$), only $J = 0$ ($s$ wave) and $J = 1$ ($p$ wave) collisions reach short distances. $J = 2$ ($d$ wave) collisions are reflected at ~80 Å unless

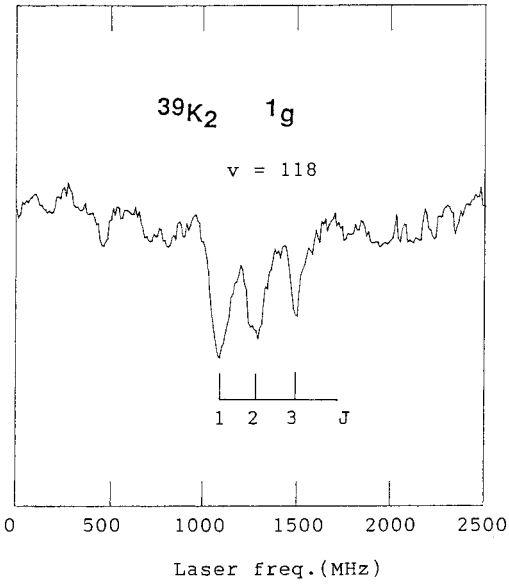


**FIG. 5.** A very high-resolution trap-loss spectrum corresponding to single-photon excitation of the $v = 118$ vibrational level of the $1_g(4p_{3/2})$ electronic state of $^{39}K_2$ immediately below the $4p_{3/2} + 4s_{1/2}$ asymptote, previously shown in lower resolution in Fig. 4. The 2.5 GHz scan clearly shows the three rotational levels ($J' = 1, 2, 3$) expected for excitation from $J'' = 0$, 1, and 2 continuum states. Line broadening is primarily attributable to the AC Stark effect.

**TABLE 3**

**Ultracold Collisions ($T \lesssim 1$ mK) Take Place in a Regime Where the Kinetic Energy of the Colliding Atoms Is Comparable to or Smaller than the Following Quantities**

| | |
|---|---|
| Electronic Splittings | AC/DC Stark Splittings |
| Vibrational Splittings | Electronic and Nuclear Zeeman Splittings |
| Rotational Splittings | Isotope Shifts |
| Fine Structure Splittings | Centrifugal Barriers |
| Hyperfine Structure Splittings | Natural Linewidths |

tunneling occurs (which has significant probability because of the long deBroglie wavelength) and $J = 3$ ($f$ wave) collisions are reflected at ~120 Å. Thus our photoassociation spectra are dominated by lower $s$-, $p$-, and $d$-wave free states, giving very simple rotational spectra as shown in Fig. 5 and discussed in Section II.

This provides new (and relatively simple and inexpensive) opportunities to study high-resolution long-range molecular spectroscopy by free → bound photoassociation of ultracold atoms as first pointed out in (*16*) and recently reviewed (*1–3*). This is because, compared to $kT$, the vibrational splittings ($kT \ll \Delta G_{v'+1/2}$) and even the rotational splittings ($kT \ll B_{v'}$) are large. Moreover, the $4p$ fine-structure splitting (57.7 $cm^{-1}$) and even the $^{39}$K ground state hyperfine splitting (462 MHz) are large. Only the excited state hyperfine splittings (Fig. 3), natural linewidths, Zeeman splittings, pressure broadening shifts and widths, and AC Stark shifts and widths are less than $10kT$ in our experiments.

Important concerns in spectroscopy are the shape and shifts of spectral lines. These issues have been reviewed in detail in (*3*) and will only be briefly discussed here. The thermal distribution of ultracold collisions yields sharp asymmetric photoassociative lines of width on the order of $kT$ (~7 MHz for $^{39}$K discussed here). There is a sharp onset at high frequency (zero collision energy) which exponentially decays to the red. These asymmetric lines must then be summed over the various optically connected upper state hyperfine components. The individual asymmetric lines are also broadened by natural linewidth, Zeeman splittings (which vary with position in the MOT), pressure broadening, and AC Stark widths (and shifts). Examples of such considerations include hyperfine structure (*40–42*), general theory for single (*43, 44*) and two-color spectra (*45*), and the effects of Bose–Einstein condensation (*46*).

### *I.D. Applications of Photoassociation*

As noted above, ultracold photoassociation provides a simple way to determine long-range interactions between atoms

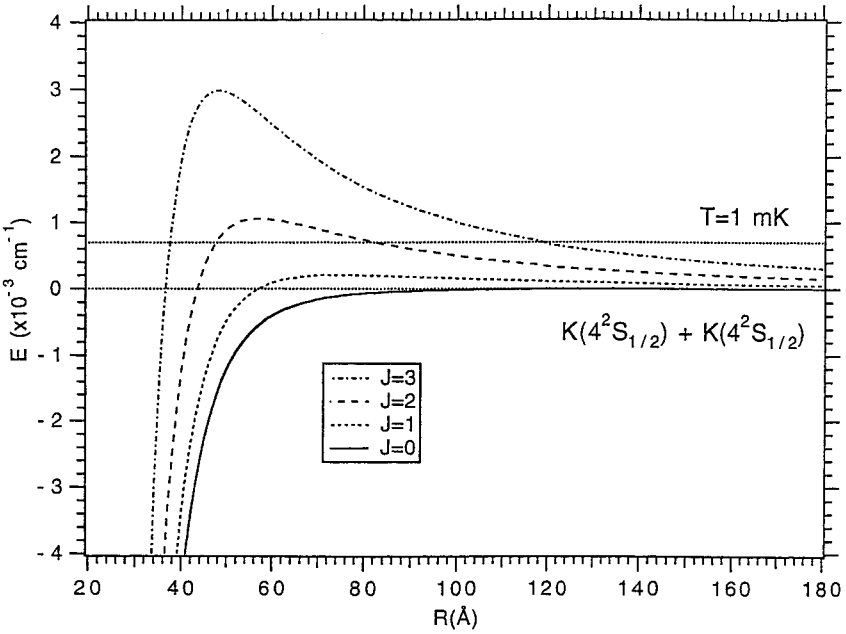


**FIG. 6.** Long-range potential ($J = 0$) and $J = 1$, 2, and 3 effective potentials ($U_J = V + \{\hbar^2[J(J+1) - \Omega^2]/2\mu R^2)\}$ for the $\Omega = 0$ states ($0_g^+$ and $0_u^-$) of two colliding $^{39}$K ground state atoms.

and precise binding energies (and dissociation energies; e.g., (*47*)), complementary to ordinary short-range molecular spectroscopy. A side benefit is improved determination of atomic properties (e.g., radiative lifetimes; see (*48–51*) and references therein).

Ultracold dynamics (photodissociation, predissociation, autoionization, energy transfer) can also be studied using related techniques. A particularly interesting topic is the low temperature limit of atomic resonant line broadening, since ultracold photoassociation provides complete information on all the potential curves near dissociation.

The use of ultracold photoassociation to form ultracold molecules is a major long-term goal, discussed further in Section IV.D. Such ultracold molecules could be used for trapping; for the molecular analog of atom optics; for study of highly quantum-mechanical, resonance-dominated ultracold collisions; for fundamental nucleation studies; and for formation of molecular BECs and molecule lasers. A separate review of ultracold molecule formation has been submitted for publication (*19*).

## II. OBSERVATIONS OF ULTRACOLD PHOTOASSOCIATION

The ultracold photoassociative process is exemplified by the reaction

$$K + K + h\nu_1 \rightarrow K_2^*(v', J'), \qquad [1]$$

where the small magnitude of $kT$ allows for excitation of a single low-$J'$ rovibrational level in a specific electronically excited state, just as in bound–bound laser-induced fluorescence transitions of $K_2$. The singly excited $K_2^*(v', J')$ molecules (here assumed to be near the $4s + 4p$ asymptotes) then decay radiatively in bound $\rightarrow$ bound

$$K_2^*(v', J') \rightarrow K_2(v'', J') + h\nu_2 \qquad [2]$$

or bound $\rightarrow$ free emission

$$K_2^*(v', J') \rightarrow K + K + h\nu_3, \qquad [3]$$

where $K_2(v'', J'')$ is either the ground $X^1\Sigma_g^+$ state or the lowest triplet state ($a^3\Sigma_u^+$).

Since significant atomic fluorescence ($4p_{3/2} \rightarrow 4s_{1/2}$) is excited by the very near resonance trap laser (see Fig. 3), the atom density is readily monitored. Process 1 yields a decrease in atomic density, dependent on the fate of the excited molecules. If Process 2 occurred exclusively, trap loss would occur with maximum efficiency (two atoms lost per photoassociative photon absorbed), assuming the excited molecule cannot emit bound–bound photons with a wavelength in the narrow band pass of the $4p_{3/2} \rightarrow 4s_{1/2}$ filter (which is very likely). However, Process 2 is a relatively minor process for levels near dissociation and Process 3 dominates as is well known from earlier laser-induced fluorescence studies starting from ground state molecules. If Process 3 occurs nearly exclusively, the question becomes the distribution of final kinetic energies in the bound $\rightarrow$ free emission. In particular, if the identical kinetic energies of the two separating atoms are greater than the trap depth (typically $\sim$1 K for a MOT such as ours), the atoms will escape and trap loss will be detected by diminished atomic fluorescence. If no such "hot" atoms (KE $\geq$ 1 K) are formed by bound–free emission, there will be no trap loss and no photoassociation detection by trap loss. Examples of levels showing negligible trap loss in a MOT are the zero-point levels of the pure long-range states ($0_g^-$ and $1_u$) at 28 and 39 Å, respectively, and are discussed in detail in Section III. Alternatively, a much weaker trap could be employed, e.g., a far-off resonant trap with a milliKelvin trap depth (*52*), to observe trap loss of such levels.

Alternatively, the singly excited $K_2^*(v', J')$ molecules can be further excited as

$$K_2^*(v', J') + h\nu_4 \rightarrow K_2^{**}(v, J), \qquad [4]$$

or single- or multiphoton ionized to form molecular

$$K_2^*(v', J') + nh\nu_5 \rightarrow K_2^+(v^+, N^+) + e^- \qquad [5]$$

or atomic ions

$$K_2^*(v', J') + n'h\nu_6 \rightarrow K + K^+ + e^-. \qquad [6]$$

The singly excited $K_2^*(v', J')$ molecules in some cases nonradiatively decay (predissociate) to fragments as

$$K_2^*(v', J') \rightarrow K^*(4p_{1/2}) + K(4s_{1/2}). \qquad [7]$$

Finally, the doubly excited molecules $K_2^{**}(v, J)$ can decay radiatively (as in [2] and [3]), nonradiatively by predissociation (as in [7]), by autoionization as in

$$K_2^{**}(v, J) \rightarrow K_2^+(v^+, N^+) + e^-, \qquad [8]$$

or by ion pair formation as in

$$K_2^{**}(v, J) \rightarrow K^+ + K^-. \qquad [9]$$

The $K_2(v'', J'')$ and $K_2^{**}(v, J)$ can also be single- or multiphoton ionized as in [5]. In addition, singly and doubly excited atomic fragments from predissociation of $K_2^*$ and $K_2^{**}$ undergo radiative decay such as

$$K^*(4p_{1/2}) \rightarrow K(4s_{1/2}) + h\nu_7. \qquad [10]$$

The doubly excited fragments (e.g., K**(5*d*)) undergo associative ionization as well as shown in

$$K^{**}(5d) + K(4s_{1/2}) \rightarrow K_2^+(v^+, N^+) + e^- \quad [11]$$

and ion pair formation (e.g., K**(6*d*)) as shown in

$$K^{**}(6d) + K(4s_{1/2}) \rightarrow K^+ + K^-. \quad [12]$$

Collisional energy transfer is a final possibility, e.g.,

$$K^{**}(6s) + K(4s_{1/2}) \rightarrow K^{**}(4d) + K(4s_{1/2}). \quad [13]$$

All these processes are significantly constrained by the well-known energetics of the K atom [e.g., IP = 35 009.815 ± 0.003 $cm^{-1}$ (*53*)] and of the $K_2$ molecule [e.g., $D_0^0(K_2)$ = 4404.583 ± 0.072 $cm^{-1}$ (*39*), IP ($K_2$) = $E_x(v^+ = 0, N^+ = 0) - E_x(v'' = 0, J'' = 0)$ = 32 775.5 ± 0.15 $cm^{-1}$ (*54*) and $D_0^0(K_2^+)$ = 6633.26 ± 0.16 $cm^{-1}$], summarized in Table 4.

The above processes suggest a wide variety of detection schemes for single-color (Section II.A) and two-color (Section II.B) ultracold photoassociation, four of which have been implemented as summarized in Table 5 and discussed below. Molecular absorption and fluorescence are difficult to detect because of the small number of molecules produced (see Section IV.D also). Other schemes, such as $4p_{1/2} \rightarrow 4s_{1/2}$ fluorescence detection of predissociation [7] and $K^-$ detection of ion pair formation ([9] and [12]), should be feasible, but have not been implemented.

**TABLE 4**
**Energetics of Atomic and Diatomic $^{39}K$ (All Values in $cm^{-1}$) Relevant to Published Ultracold Photoassociative Spectra**

| Quantity | Value | Uncertainty | Reference |
|---|---|---|---|
| $^{39}K$ ($4s\ ^2S_{1/2}$) | 0 | — | definition |
| $^{39}K$ ($4p\ ^2P_{1/2}$) | 12985.170 | <0.01 | 55 |
| $^{39}K$ ($4p\ ^2P_{3/2}$) | 13042.876 | <0.01 | 55 |
| $^{39}K$ ($4d\ ^2D_{3/2}$) | 27398.11 | 0.01 | 56, 57 |
| $^{39}K$ ($4d\ ^2D_{5/2}$) | 27397.01 | 0.01 | 56, 57 |
| $^{39}K$ ($6s\ ^2S_{1/2}$) | 27450.65 | 0.01 | 56, 57 |
| $^{39}K$ ($5d\ ^2D_{3/2}$) | 30185.69 | 0.01 | 56, 57 |
| $^{39}K$ ($5d\ ^2D_{5/2}$) | 30185.18 | 0.01 | 56, 57 |
| $^{39}K$ ($7s\ ^2S_{1/2}$) | 30274.26 | 0.01 | 56, 57 |
| $^{39}K$ ($6d\ ^2D_{3/2}$) | 31695.75 | 0.01 | 56, 57 |
| $^{39}K$ ($6d\ ^2D_{5/2}$) | 31695.51 | 0.01 | 56, 57 |
| $^{39}K^+ = {}^{39}K$ (IP) | 35009.815 | <0.01 | 53 |
| $^{39}K_2$ (v=0, J=0) ($-D_0^0$) | 4404.583 | 0.072 | 39 |
| $^{39}K_2$ (zero point energy) | 46.0910 | <0.001 | 58 |
| $^{39}K_2$ ($-D_e$) | 4450.674 | 0.072 | 39 |
| $^{39}K_2^*$ ($a^3\Sigma_u^+$, $-D_0$) | 242.00 | 0.12 | 39 |
| $^{39}K_2^*$ ($a^3\Sigma_u^+$, zero point energy) | 10.737 | <0.01 | 59 |
| $^{39}K_2^*$ ($a^3\Sigma_u^+$, $-D_e$) | 252.74 | 0.12 | 39 |
| $^{39}K_2$ (IP) | 32775.50 | 0.15 | 54 |
| $^{39}K_2^+$ (v=0, N=0) ($-D_0^0$) | 6633.26 | 0.16 | this work |
| $^{39}K_2^+$ (zero point energy) | 36.65 | 0.3 | 60, 61 |
| $^{39}K_2^+$ ($-D_e$) | 6669.9 | 0.5 | this work |
| $^{39}K^+ + {}^{39}K^-$ | 30965.2 | 0.8 | 53, 62 |

**TABLE 5**
**Ultracold Photoassociative Spectroscopy Detection Techniques Used in Studies of $^{39}K_2$**

I. Trap Loss (Decrease of Atomic Fluorescence) (36, 37)

$K + K + h\nu \rightarrow K_2^* \rightarrow K + K + h\nu'$ "hot" loss
"cold" no loss
$\rightarrow K_2 + h\nu''$ loss

II. Direct Molecular Ionization (37, 63)

$K + K + h\nu \rightarrow K_2^* \xrightarrow{(1 \text{ or } 2)\ h\nu'} K_2^+ + e^-$ or $K^+ + K + e^-$

III. Fragmentation Spectroscopy (64)

$K + K + h\nu \rightarrow K_2^* \rightarrow K^*(^2P_{1/2}) + K$
$K^*(^2P_{1/2}) + 2h\nu' \rightarrow K^+ + e^-$ REMPI (via 5d)

IV. Ground State Molecule Detection (65)

$K + K + h\nu \rightarrow K_2^* \rightarrow K_2(v') + h\nu'$
$K_2(v') + h\nu'' + h\nu''' \rightarrow K_2^+ + e^-$ REMPI (via $B\ ^1\Pi_u$)

We measure the trap-loss rate (Table 5, I) by monitoring the $4p_{3/2} \rightarrow 4s_{1/2}$ atomic fluorescence of trapped K atoms using a photomultiplier-filter system. A third CW ring laser (Coherent 899-29, operating in dye laser mode with R-6G, DCM, or R-110 laser dye), provides the second photon for the two-color optical–optical double-resonance photoassociative spectroscopy (Table 5, II) and the fragmentation atomic resonance-enhanced multiphoton ionization spectroscopy (Table 5, III). The dye laser frequency is calibrated by the standard iodine spectrum. Molecular and atomic ions generated in Techniques 2. and 3. are collected by a channeltron particle multiplier (Galileo model 4869). Alternatively, the translationally ultracold ground state molecules formed by photoassociation followed by bound–bound emission (Table 5, IV) are detected with pulsed laser resonance-enhanced multiphoton ionization.

### *II.A. Detection of Single-Color Spectra*

*II.A.1. Trap loss.* The decrease in atomic fluorescence versus photoassociative laser frequency because of ultracold photoassociation has been designated a trap-loss spectrum. Any $K_2^*(v', J')$ formation [1] which does not subsequently yield exclusively "cold" atoms (KE ≤ 1 K) by bound → free emission [3] will yield some loss of atomic ($4p_{3/2} \rightarrow 4s_{1/2}$) fluorescence and is potentially detectable in trap loss. These alternate decay paths include hot atom formation by bound–free emission [3], bound → bound emission [2], and predisso-

**TABLE 6**
**Single-Photon Long-Range Ultracold Photoassociation Forming $^{39}K_2^*$ (*37, 63*)**

| Hund's Case (c) State | Range of Binding Energies Observed ($cm^{-1}$) (v assignments) | Range of $R_+(v)$ Observed (Å) | Short Range Correlate [Hund's Case (a)] | Detection Techniques (Table V) |
|---|---|---|---|---|
| $4^2S_{1/2} + 4^2P_{3/2}$ Asymptote: | | | | |
| $1_u$ ($4p_{3/2}$) | 0.489 - 0.087 (v = 0-7) | 31.7 - 86.5 $R_-/R_+$ (v = 7) pure long range | $B^1\Pi_u$, 315 $cm^{-1}$ barrier at 8.1Å, last quasibound v=43, J=43 | 2. |
| $0_g^-$ ($4p_{3/2}$) | 6.26 - 0.26 (v = 0-30) | 21.0 - 102 $R_-/R_+$ (v = 30) pure long range | $1^3\Pi_g$ ($\Omega$=0$^-$), purely repulsive at short range | 1.,2. |
| $1_g$ ($4p_{3/2}$) | 35.8 - 0.33 (v = 87-145) | 22.1 - 109 | $1^1\Pi_g$, last observed v=107, bound by 10.62 $cm^{-1}$ with $R_+$ (107) = 34.0Å | 1.,3. |
| $0_u^+$ ($4p_{3/2}$) | 17.0 - 0.03 | 29.4 - 250 | $b^3\Pi_u$ ($\Omega = 0^+$), last observed v = 24, bound by 5455.6 $cm^{-1}$ with $R_+$ (24) = 5.1Å | 1.,3. |
| $4^2S_{1/2} + 4^2P_{1/2}$ Asymptote: | | | | |
| $0_u^+$ ($4p_{1/2}$) | 14.1 - 0.76 | 29.9 - 78.3 | $A^1\Sigma_u^+$, last observed v = 84, bound by 1555.54 $cm^{-1}$ with $R_+$ (84) = 8.2Å | 1.,4. |
| $0_g^-$ ($4p_{1/2}$) | 22.4 - 0.73 | 22.4 - 39.3 | $1^3\Sigma_g^+$ ($\Omega = 0^-$) | 1. |
| $1_g$ ($4p_{1/2}$) | 34.5 - 0.70 | 21.4 - 65.0 | $1^3\Sigma_g^+$ ($\Omega = 1$) | 1. |

ciation [7]. Sample single-color trap-loss spectra showing the $1_g(4p_{3/2})$ and $0_u^+(4p_{3/2})$ states were given in Figs. 4 and 5. Note that in Fig. 4 the magnitude of trap loss (with respect to 0 near the atomic line) can be quite significant with decreases up to 30% in atomic fluorescence. An attempt to quantitatively understand such trap loss in the case of $Li_2$ should be noted (*66*).

Note that the background fluorescence among photoassociation resonances varies slowly with wavelength for reasons not fully understood (and related to the $4p + 4p$ asymptotes (Section IV.A)). Most of the single-color ultracold photoassociative spectra we have observed (summarized in Table 6) have been observed via trap-loss spectra. Only the low levels of the weakly bound pure long-range $0_g^-(4p_{3/2})$ and $1_u(4p_{3/2})$ states (bound by 6 and 0.5 $cm^{-1}$ at 28 and 39 Å, respectively) require an alternate detection technique. This is because the local kinetic energy as the molecule vibrates remains very small (0.24 and 0.055 $cm^{-1}$ maximum at $R_e'$ in $v' = 0$ of the $0_g^-$ and $1_u$ states, respectively (*37*)) compared to the trap depth ($\sim$1 K = 0.7 $cm^{-1}$); by the Franck–Condon Principle, "no change in the velocity or kinetic energy of nuclear motion during a virtually instantaneous electronic transition," bound–free emission from these two $v' = 0$ levels will yield two atoms each with at most 0.12 and 0.028 $cm^{-1}$ kinetic energy, respectively, which cannot escape the CDSMOT.

The seven electronic states listed in Table 6 represent all the states from two colliding ground state atoms (electronic states $0_g^+$, $0_u^-$, and $1_u$) that are theoretically expected to have bound levels and to be optically allowed, as discussed in Section III. $^{39}K_2$ is the only species for which this has been achieved. In this and the following sections (II.A.2–II.A.4) we will discuss observations of the other states in Table 6 not already shown in Figs. 4 and 5. Work and references for the other alkali dimers are given in Table 7; for the most part, these other species have been detected by trap loss, although most results for $Na_2$ employ direct ionization detection ($3p + 3p$ collisions yield ionization, which does not occur for $n_{\min}p + n_{\min}p$ collisions of the other alkalis). The detection of the molecule in the lowest triplet state has been used in $Cs_2$ (*67, 68*).

In Fig. 7, we show a blow-up of a portion of Fig. 4, which clearly shows the $0_g^-(4p_{3/2})$ state as well as the much stronger $0_u^+(4p_{3/2})$ series and the somewhat stronger $1_g(4p_{3/2})$ series previously shown. Note that the convergence pattern of vibrational levels of the $0_u^+$ and $1_g$ states is very similar, with a significantly different convergence pattern for the $0_g^-$ state. This is because, as detailed in Section III, the long-range $C_3$ coefficient for the $0_g^-$ state is about two-thirds that of the $0_u^+$ and $1_g$ states. However, it is difficult to observe $0_g^-$ levels below $v' = 9$ and virtually impossible to detect the lowest few levels ($v' = 0$–3), where the kinetic energy of atoms produced by bound–free emission (*3*) does not exceed 0.7 $cm^{-1}$. Observation of these levels is discussed in the next subsection.

In Figs. 7b and 8 in this review, we show two examples of our trap-loss spectra near the $4p_{1/2} + 4s_{1/2}$ asymptote (we emphasize the $4p_{3/2} + 4s_{1/2}$ asymptote results in this Section and in Section III), along with a "molecular ion" spectrum

**TABLE 7**
**Single-Photon Long-Range Ultracold Photoassociation Forming Alkali Dimers near the $n^2_{min}P + n^2_{min}S$ Asymptotes**

| Hund's Case c and Short Range Correlate States | $Li_2$ | $Na_2$ | $K_2$ | $Rb_2$ | $Cs_2$ |
|---|---|---|---|---|---|
| $n_{min}\ ^2P_{3/2} + n_{min}\ ^2S_{1/2}$: | | | | | |
| $1_u\ (n_{min}\ p_{3/2})\ B\ ^1\Pi_u$ | | | X | | X |
| $0_g^-\ (n_{min}\ p_{3/2})\ 1\ ^3\Pi_g\ (\Omega = 0^-)$ | | X | X | X | X |
| $1_g\ (n_{min}\ p_{3/2})\ 1\ ^1\Pi_g$ | | X | X | X | X |
| $0_u^+\ (n_{min}\ p_{3/2})\ b\ ^3\Pi_u\ (\Omega = 0^+)$ | | X | X | X | X |
| $n_{min}\ ^2P_{1/2} + n_{min}\ ^2S_{1/2}$: | | | | | |
| $0_u^+\ (n_{min}\ p_{1/2})\ A\ ^1\Sigma_u^+$ | X | X | X | X | |
| $0_g^-\ (n_{min}\ p_{1/2})\ 1\ ^3\Sigma_g^+\ (\Omega = 0^-)$ | X | | X | X | |
| $1_g\ (n_{min}\ p_{1/2})\ 1\ ^3\Sigma_g^+\ (\Omega = 1)$ | X | | X | X | |

References:

$Li_2$: (48, 66, 69-76)

$Na_2$: (1, 47, 49, 77-86)

$K_2$: (36, 37, 50, 63-65, 87, 88)

$Rb_2$: (2, 18, 51, 52, 89-98)

$Cs_2$: (67, 68, 99, 100)

(obtained by resonance-enhanced multiphoton ionization (REMPI) of ground state $K_2$ as discussed in Section II.A.4). The trap-loss spectrum in Fig. 8 clearly shows a single vibrational level of the $0_g^-(4p_{1/2})$ and $1_g(4p_{1/2})$ states, which correlate to $1\,^3\Sigma_g^+$ at short range. Barely visible but reproducible, is a vibrational level (approximately $v = 191$) of the $0_u^+(4p_{1/2})$ state, which correlates to the $A\,^1\Sigma_u^+$ state at short range. Levels closer to the $4p_{1/2} + 4s_{1/2}$ asymptote show significantly better trap-loss signal-to-noise, but since their analysis is not complete, will not be presented here. It is worth noting that the nearby $0_g^-$, $1_g$, and $0_u^+$ states at the $4p_{1/2} + 4s_{1/2}$ asymptote show very different vibrational level convergence patterns as seen in Fig. 7b, since they have very different long-range $C_3$ coefficients, as discussed in Section III.

*II.A.2. Direct ionization.* To observe photoassociation of levels unobservable by trap loss, i.e. the low levels of the $0_g^-(4p_{3/2})$ pure long-range state and all levels of the $1_u(4p_{3/2})$ pure long-range state, we provided a second ionizing laser tuned to broad resonances slightly below the $4s + 5d$ or $4s + 6d$ asymptotes. These broad resonances and related sharp levels have themselves been assigned in other experiments (Sections II.B and III.E). The "direct ionization" excitation scheme is shown in Fig. 9, along with sample spectra in Figs. 10 and 11 of the rotational structure of the $0_g^-(4p_{3/2})$ and $1_u(4p_{3/2})v' = 0$ levels.

The primary process here is thought to be excitation [4] of a photoassociated $K_2^*(v', J')$ level, followed by autoionization [8], although other photoionization ([5] and [6]) and ion pair formation [12] (for $4s + 6d$) have not been ruled out. However, the laser frequencies used establish that it is excitation/ionization of a $K_2^*(v', J')$ level and not that of a ground state molecule (or lowest triplet state molecule) formed by radiative decay [2] (used in Section II.A.4).

The $0_g^-v' = 0$ spectrum in Fig. 10 is readily assignable (*37*), since there are no significant splittings due to hyperfine structure (which is smaller in $^{39}K$ than in $^{23}Na$, $^{85}Rb$, $^{87}Rb$, and $^{133}Cs$). Note the extremely small rotational splittings, corresponding to the very long-range nature of this state ($R_e = 28$ Å).

The $1_uv' = 0$ spectrum in Fig. 11, on the other hand, is more challenging to assign (*88*). In particular, the hyperfine splittings are comparable to the very small rotational splittings ($R_e(1_u) = 39$ Å) for low rotation ($J' \leq 3$), which are the only rotational levels excited here. The bottom diagram in Fig. 11 shows the simplification that results for higher $J'$.

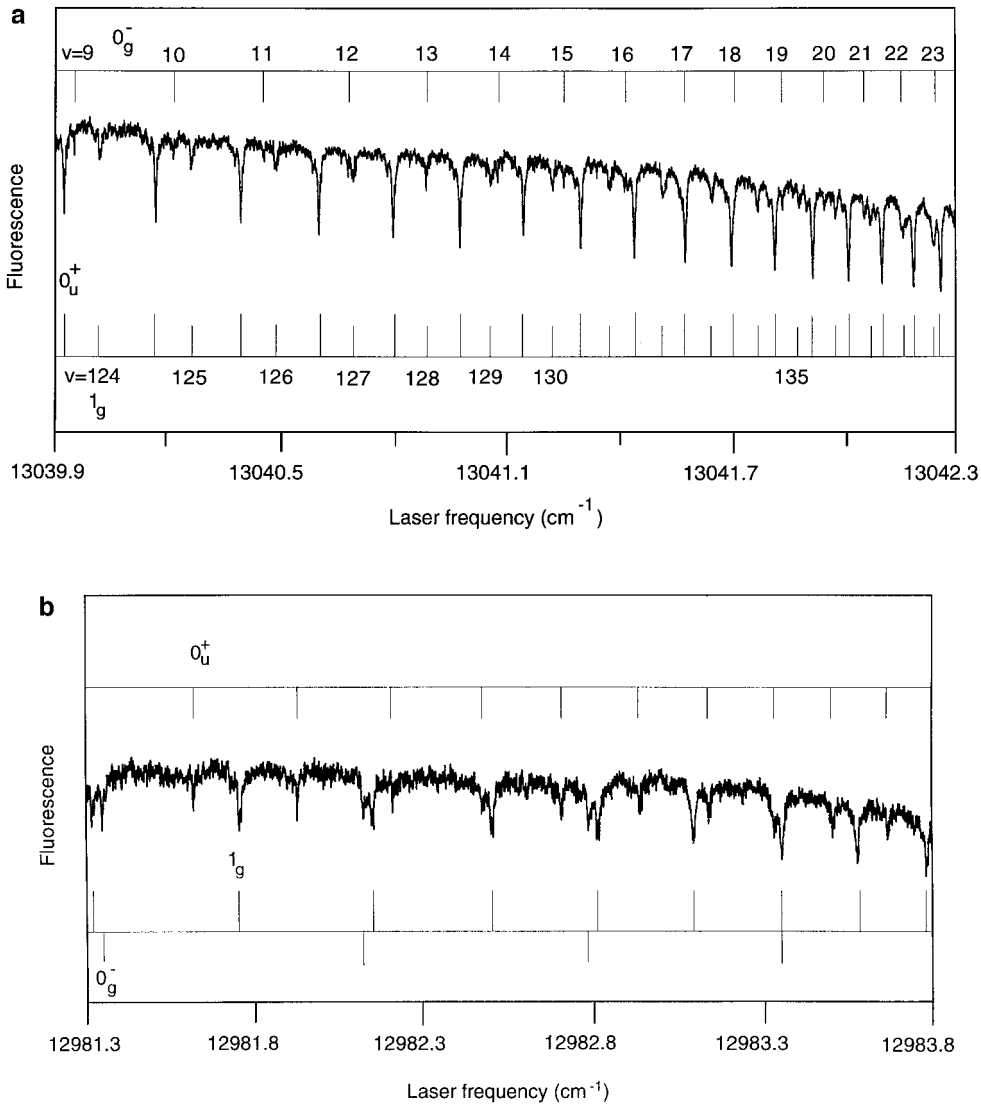


**FIG. 7.** Trap-loss spectra (a) near the $4p_{3/2} + 4s_{1/2}$ asymptote which clearly shows the $0_g^-$ vibrational levels as well as the $0_u^+$ and $1_g$ vibrational levels previously shown in Figure 4; (b) near the $4p_{1/2} + 4s_{1/2}$ asymptote which shows the $0_u^+$, $0_g^-$, and $1_g$ vibrational levels.

*II.A.3. Fragmentation spectroscopy.* Fragmentation spectroscopy is a well-known technique for studying photodissociation (including predissociation resonances). There are many studies of such fragmentation spectra in the alkali dimers; e.g., the fragmentation of $^{133}Cs_2$ to produce the $6p_{3/2}$, $6p_{1/2}$, $5d_{5/2}$, and $5d_{3/2}$ levels of Cs, which were detected by what is now called REMPI (see, e.g., (*101*) and references therein), and the state-selected fragmentation of $^{39}K_2$ to produce the $4p_{3/2}$ level (aligned) of K, which was detected by fluorescence (see, e.g., (*12, 102*) and references therein).

These same techniques can be used to detect even weak predissociation of levels formed by photoassociation (*64*). Here we use REMPI detection, because detection of $4p_{1/2} \rightarrow 4s_{1/2}$ fluorescence cannot be easily done due to the strong atomic fluorescence ($4p_{3/2} \rightarrow 4s_{1/2}$) from the MOT and the scattered light of the photoassociation laser. A schematic diagram of excitation of a $1_g(4p_{3/2})$ predissociative level between the $(4p_{3/2} + 4s_{1/2})$ and the $(4p_{1/2} + 4s_{1/2})$ asymptotes of $K_2$ is shown in Fig. 12. The excitation event is followed by crossing with the $0_g^+(4p_{1/2})$ state and fragmentation to a $4p_{1/2}$ atom and a $4s_{1/2}$ atom, the former being then detected by one-photon resonant two-photon ionization via the $5d_{3/2}$ level of K. The fragmentation spectrum is shown in Figs. 13–15, in comparison in some regions with the previously shown trap-loss spectra (Figs. 4 and 7).

Starting from the $(4p_{1/2} + 4s_{1/2})$ asymptote and scanning the photoassociative laser toward the $(4p_{3/2} + 4s_{1/2})$ asymptote, the first predissociation (fragmentation) observed corresponds to $v' = 91$ of the $1_g(4p_{3/2})$ state, even though trap-loss spectra down to $v' = 87$ have been observed. Since the lower states ($0_u^-$, $1_u$) become the $a^3\Sigma_u^+$ state at short range, while the upper state ($1_g$) becomes the $1^1\Pi_g$ state, the radiative transition probability for photoassociation vanishes at intermediate range

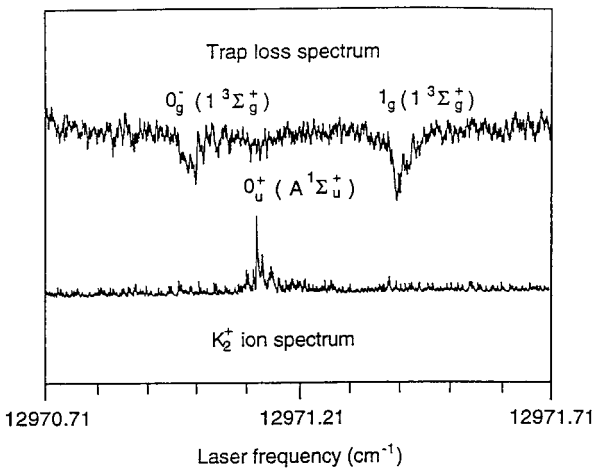


**FIG. 8.** Trap loss and molecular ion (molecule formation) signals versus photoassociation laser frequency for $^{39}K_2$ slightly below the $4p_{1/2} + 4s_{1/2}$ asymptote (*65*). The trap-loss spectrum is discussed in Section II.A.1 and the molecule formation spectrum in Section II.A.4.

and lower $v'$, where the total electronic spin $S$ becomes a good quantum number.

The analysis of these predissociations is discussed in Section III.C.

*II.A.4. Molecule formation.* One of the important goals of photoassociation is the formation of ultracold molecules for a variety of applications as mentioned in Section I.D and discussed in Section IV.D. Here we simply note that the detection of such ground state molecules is an alternate (but difficult) way of observing photoassociative spectra (Fig. 8), sometimes with better signal-to-noise than with trap loss. To form the molecule in the $X^1\Sigma_g^+$ ground state at short range, it is necessary to photoassociate into a bound $1_u$ or $0_u^+$ Hund's Case c state, which correlates with a $^1\Lambda_u$ state at short range. For the $K_2$ $4s + 4p$ asymptotes, these are the $1_u(4p_{3/2})$ and $0_u^+(4p_{1/2})$ states, as noted in Table 6. However, the $1_u(4p_{3/2})$ state, which correlates to the $B^1\Pi_u$ state at short-range, is not suitable as there is a potential barrier of 315 $cm^{-1}$, which our ultracold atoms can neither surmount nor tunnel through. Thus we must use the $0_u^+(4p_{1/2})$ state which correlates to the $A^1\Sigma_u^+$ state to form ground state molecules (*65*) as shown in Fig. 16. In model potential calculations, our photoassociative laser frequency produces $v' = 191$, which then spontaneously emits to $v'' = 36$ of the ground state. Such a ground state molecule will be translationally ultracold since the original ultracold atoms ($\sim$350 $\mu$K) experience only two random photon recoils (on the order of a few microKelvins) in forming the molecule. The ground state molecules ($v'' = 36$) are then state-selectively detected by one-photon resonant two-photon ionization via the $B^1\Pi_u$ state (e.g., $v' = 26$). Such a "molecule formation" spectrum is shown in Fig. 8.

It is also possible to produce long-lived metastable states (e.g., the $a^3\Sigma_u^+$ and $b^3\Pi_u$ states of the alkali dimers). The Orsay group has clearly produced translationally ultracold $a^3\Sigma_u^+$ molecules (*67, 68*) as well as $X^1\Sigma_g^+$ molecules (*68*), although their REMPI spectra are not yet well understood. In addition, the Colorado Springs group has produced translationally ultracold molecules detected by time-of-flight mass spectrometry, but it is unclear in what electronic states the molecules are (*103*). They have also recently trapped these molecules in an optical trap (*104*).

### *II.B. Detection of Two-Color Spectra*

The use of lasers of two distinct colors allows the possibility of photoassociative OODR experiments (*45*), as illustrated in Fig. 1. For OODR there are basically two schemes, the "ladder" and the "lambda" schemes, as shown in Fig. 17.

Lambda OODR, starting with colliding ultracold atoms, has recently been carried out for $Li_2$ (*70*), $Rb_2$ (*94*), and $K_2$ (work in progress). Such experiments very precisely determine the long-range interactions of ground state atoms and also the scattering lengths of the ground $X^1\Sigma_g^+$ state and the lowest triplet $a^3\Sigma_u^+$ state. The triplet scattering length is particularly significant (see also Section III.D) in determining the low temperature elastic scattering cross section (critical for evapo-

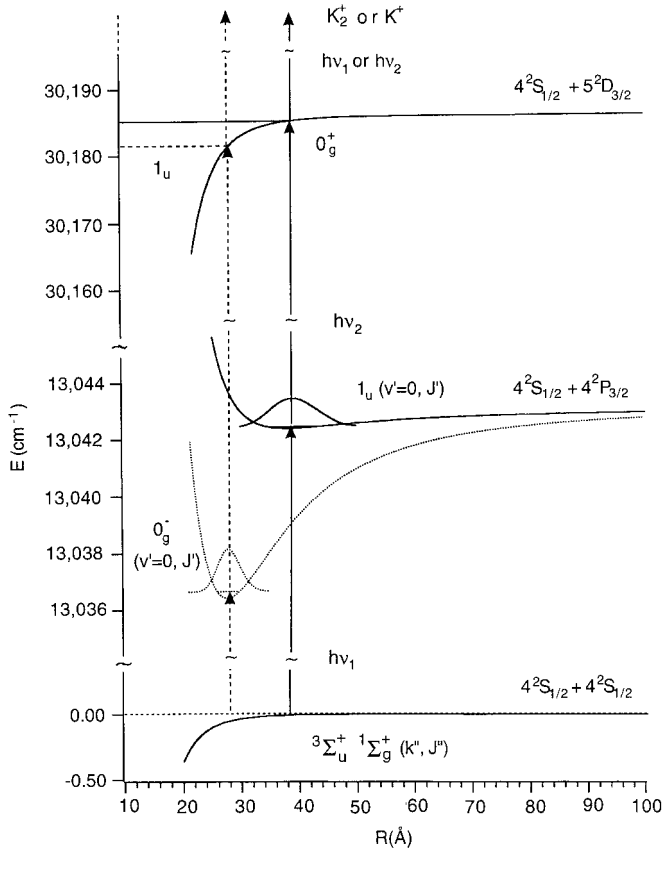


**FIG. 9.** Schemes for direct ionization detection of photoassociation spectra for the lowest levels of the $0_g^-(4p_{3/2})$ and $1_u(4p_{3/2})$ pure long-range states, where detection via trap loss is not possible. The upper $1_u(5d_{3/2})$ and $0_g^+(5d_{3/2})$ states have very similar long-range interactions and are thought to be broadened by autoionization (see Sections II.B.1 and III.D.).

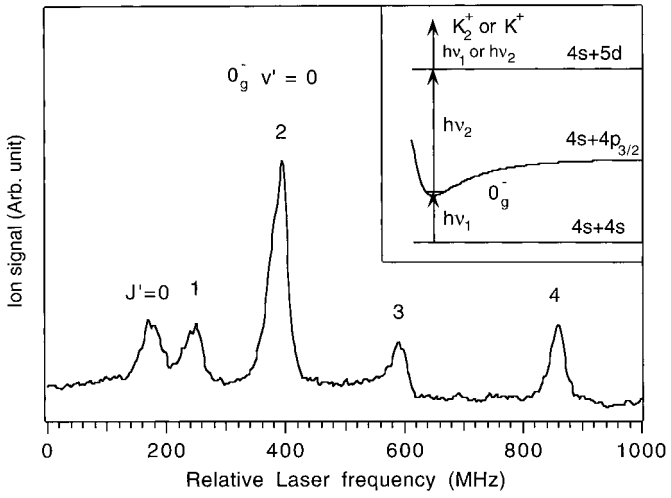


**FIG. 10.** A direct ionization spectrum of the rotational structure of the $0_g^-(4p_{3/2})v' = 0$ level, showing total ionization (atomic and molecular) versus relative photoassociation laser frequency $\nu_1$.

rative cooling to BEC) and the mean field interaction in the BEC (a positive scattering length indicating a repulsive mean field interaction and a stable condensate; a negative scattering length indicating an attractive mean field interaction and an unstable condensate, except for small numbers of atoms in a trap).

Ladder-type two-color photoassociative OODR experiments have been carried out for $K_2$ (*37, 63, 88*) and for $Na_2$ (*49, 83, 84, 86, 105*). Figure 18 shows representative direct ionization signals for three ($4s + 6s$, $4s + 5d$, $4s + 6d$) of the five asymptotes studied ($4s + 4d$ and $4s + 7s$ are not shown). The detection scheme is that of Fig. 9, where laser frequency $\nu_1$ is fixed at the maximum of the $J' = 2$ line in Fig. 10 and laser frequency $\nu_2$ is now scanned. Note that as shown in Fig. 1, the vibrational levels slightly below the $4s + 4d$ and $4s + 6s$ asymptotes do not have enough energy to autoionize to $K_2^+ + e^-$, whereas those slightly below the $4s + 5d$, $4s + 6d$, and $4s + 7s$ asymptotes do have enough energy to autoionize to $K_2^+ + e^-$. Those near the $4s + 6d$ asymptote can also autoionize to $K^+ + K^-$.

The readily assignable top spectrum shows the advantages of going through the "Franck–Condon window" of $v' = 0$ of the pure long-range $0_g^-$ state near 28 Å. The $v' = 0$ level of the pure long-range $1_u$ state offers a similar Franck–Condon window at 39 Å, but will not be detailed here. The "shelf" states of $Na_2$ (*106–110*) offer similar Franck–Condon windows in the intermediate internuclear distance range of 6–20 Å, which have recently been used to study highly excited states at intermediate $R$ through the $3^1\Sigma_g^+$ $v = 23$ level, which "sits" at approximately 6.4 Å on the intermediate shelf (*111*). The lowest frequency group of lines represents the rotational levels $J = 1$, 2, 3, and 4 of a vibrational level $v^*$ of the $1_u$ state dissociating to the $4s + 6s$ asymptote. This correlates with the $1_u$ component of the $^3\Sigma_u^+$ state at short range. Only $J = 1$, 2 and 3 levels would be expected via the $0_g^- v' = 0$, $J' = 2$ level. We believe the explanation for the $J = 4$ peak lies in a very near resonance two-photon transition to the $1_u v^*$, $J = 4$ level via the $0_g^- v' = 0$, $J' = 3$ level, which is detuned by only 200 MHz from the $J' = 2$ level. The absence of a $J = 0$ peak (accessible via a very near resonant two-photon transition via the $J' = 1$ intermediate level) suggests this is the $1_u$ and not the $0_u^-$ component of the $^3\Sigma_u^+$ state correlating to $4s + 6s$.

A similar explanation can be found for strong features at higher frequency, namely $J = 1$–4 of $v = v^* + 1$ to $v^* + 4$ of the same $1_u$ state. As noted in Section III.E, these five vibrational levels show the convergence to the $4s + 6s$ asymptote expected from long-range theory (*112, 113*) and agree fairly well with the eigenvalues of a long-range potential well calculated (minimum at 24 Å) by Marinescu from long-range exchange plus long-range dispersion (*114*). The features between $v = v^* + 1$ and $v^* + 2$ and between $v = v^* + 2$ and $v^* + 3$ are too weak to assign at this time.

The spectrum in the central panel in Fig. 18 is also readily assignable to vibrational levels $v = v^*$ to $v^* + 3$, respectively,

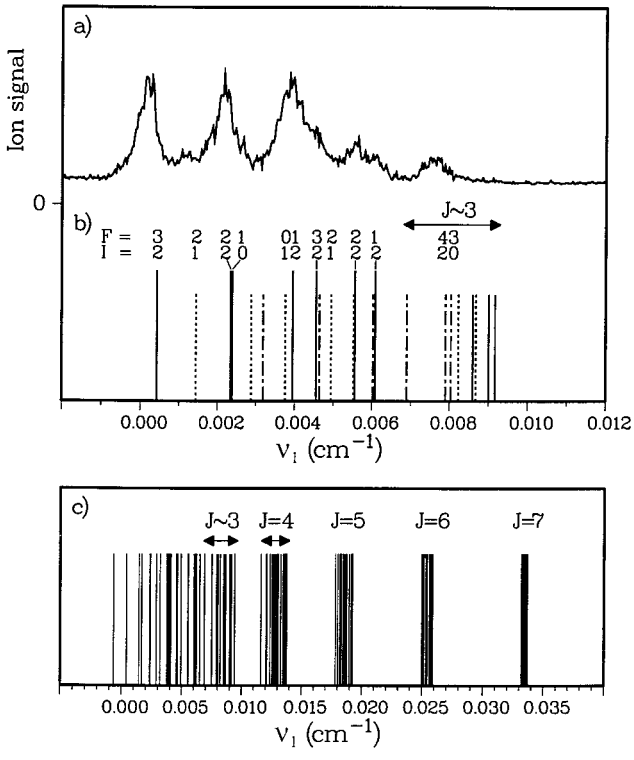


**FIG. 11.** (a) A direct ionization spectrum of the rotational–hyperfine structure of the $1_u(4p_{3/2})v' = 0$ level, showing total ionization (atomic and molecular) versus relative photoassociation laser frequency $\nu_1$ (*88*). (b) Theoretical rotation–hyperfine level structure arising from *s*-, *p*-, and *d*-wave collisions. Selected lines are labeled with total angular momentum $F$ and total nuclear spin $I$. The full lines correspond to lines with both *s*- and *d*-wave contributions. The dotted lines and the dash–dotted lines correspond to *p*-wave scattering only and *d*-wave scattering only, respectively. (c) An expanded view of the level structure showing the complicated region of (b) where hyperfine and rotation are thoroughly mixed as well as the higher $J$ region where rotation dominates. All levels with $F \leq 6$ are included.

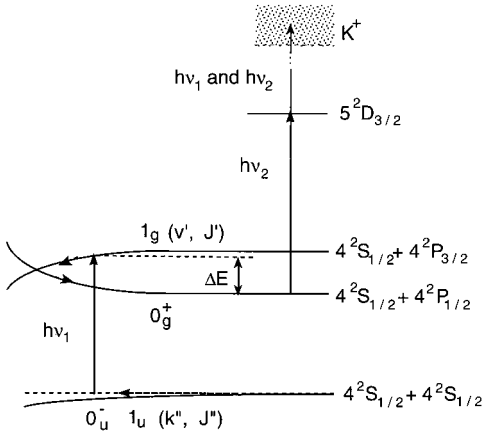


**FIG. 12.** Schematic diagram of the fragmentation spectroscopy of the $1_g(4p_{3/2})$ state of $^{39}K_2$.

of a $1_u$ state. Note, however, that while the $v = v^*$ band shows clear rotational structure (expanded in Fig. 19), the $v = v^* + 1$ band shows reduced rotational structure and the structure is absent in the $v = v^* + 2$ and $v^* + 3$ bands. We interpret this change in rotational structure as being due to an increased rate of autoionization (and thus lifetime broadening) with increased $v$, although another decay channel (e.g., predissociation) cannot be absolutely excluded.

In the bottom panel of Fig. 18, we see the readily assignable $v = v^*$ to $v^* + 3$ levels of an unknown combination of $1_u$ and $0_u^-$ bands from the $0_g^-(4p_{3/2})v' = 0$, $J' = 2$ level. Note that no rotational structure is observed, so the absence of a $J = 0$ line cannot be used to rule out $0_u^-$ symmetry. The lines here are all broader than $v = v^* + 2$ and $v^* + 3$ in the center panel, suggesting somewhat faster autoionization.

In Fig. 19, the bottom panel shows a $v = v^*$ rotationally resolved band similar to that in Fig. 18, again with "forbidden" $J$ lines (here 4 and 5), attributable to very near resonance two-photon excitation as for the $1_u(6s_{1/2})$ state discussed above. However, when the pump laser power at frequency $\nu_1$ is drastically reduced (by a factor of 1000), only the allowed $J = 1$, 2, and 3 lines remain. Note that such additional rotational lines could be labeled "strong field effects," but because of the very small splittings between rotational levels, they occur at relatively weak fields.

Finally, we have opened the Franck–Condon window by using the $0_g^-(4p_{3/2})v' = 2$, $J' = 2$ level as an intermediate in Fig. 20. This allows us to see many more vibrational levels ($v = v^* + 4$, $v^* + 6$, $v^* + 7$, and $v^* + 8$), where $v^* + 8$ is extremely weakly bound ($<0.1$ cm$^{-1}$). Moreover, it is clear that these new levels are becoming less broad with increasing $v$, suggesting a slowdown in autoionization because of a lengthening of vibrational period (see Section III.E). A new electronic state is also visible below $v = v^*$, between $v = v^*$ and $v^* + 1$, and between $v = v^* + 1$ and $v^* + 2$, but that structure has not been assigned.

## III. ANALYSIS OF ULTRACOLD PHOTOASSOCIATION

The analysis of ultracold photoassociation begins with an understanding of the adiabatic potential energy curves of the upper and lower states of photoassociation. For example, considering the first three asymptotes of $K_2$, shown in Fig. 21, we see a wide variety of long-range states (Hund's case c) characterized by an $\Omega$ quantum number, by $g$ (gerade) or $u$ (ungerade) parity, and by reflection symmetry $\pm$ for $\Omega = 0$. These long-range states in turn correlate with a variety of short-range

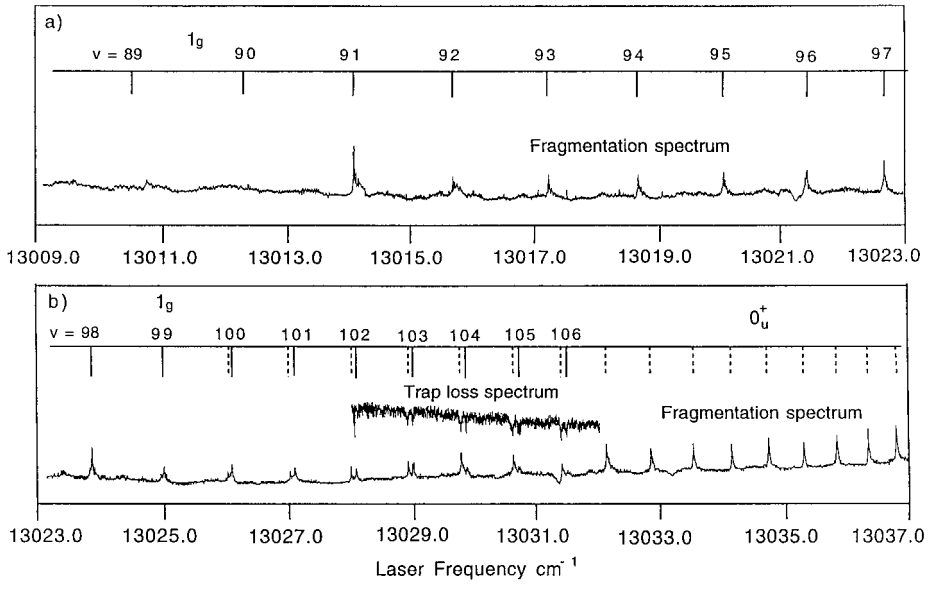


**FIG. 13.** The high-resolution fragmentation spectrum of the $K_2$ molecule (a) from 13 009 to 13 023 cm$^{-1}$ and (b) from 13 023 to 13 037 cm$^{-1}$. A portion of the trap-loss spectrum is also shown in (b) for comparison. Part (a) shows the abrupt onset of $1_g$ predissociation at $v' = 91$ with increasing energy (frequency), while part (b) shows the slow falloff at high $v'$; part (b) also shows the onset of $0_u^+$ predissociation at $\sim$13 026 cm$^{-1}$, which continues in Figure 14.

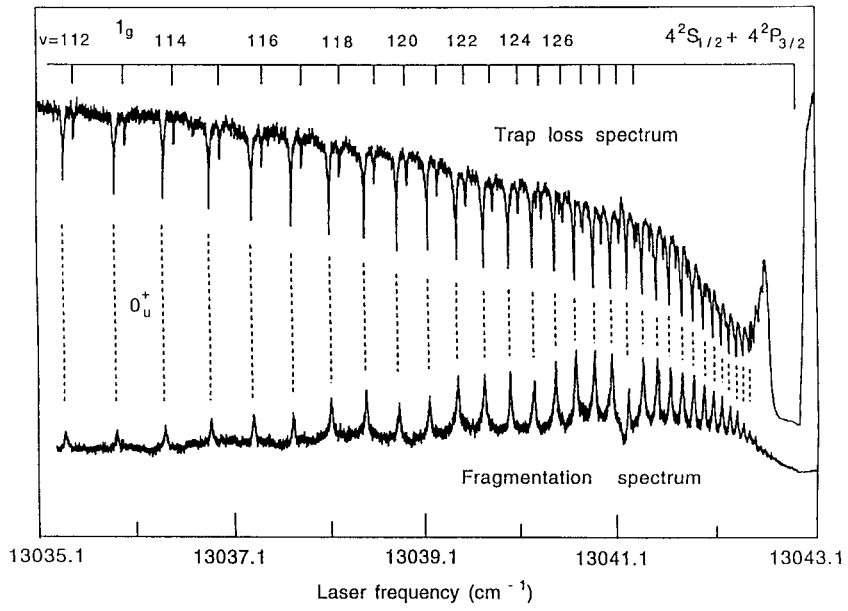


**FIG. 14.** The high-resolution fragmentation spectrum of the $K_2$ molecule from 13 035.1 to 13 043.1 cm$^{-1}$ showing the $0_u^+$ predissociation to a $4p_{1/2}$ fragment. Also shown at the top is a trap-loss spectrum similar to that in Figure 4, which clearly shows that it is the $0_u^+$ state (only) which predissociates in this region.

(Hund's case a or b) states characterized by an electronic angular momentum projection on the internuclear axis $\Lambda$, an electronic spin angular momentum $S$, by $g$ (gerade) or $u$ (ungerade) parity, and by $\pm$ reflection symmetry for $\Lambda = 0$. Ordinary molecular spectroscopy (inside 10 Å for alkali dimers) is concerned with Hund's case a and b states, while ultracold photoassociative spectroscopy (outside 20 Å) is concerned with Hund's case c states. For this long-range region, it is often possible to make a simple long-range inverse power expansion (e.g., for two K(4$s$) atoms or the $2_g$ and $2_u$ states corresponding to K(4$s$) + K(4$p$)). The short distance portions of the corresponding potentials provide only a phase (or effective number of vibrational levels) as far as long-range properties go. Such long-range potentials are discussed in Section III.A. However, more generally fine-structure splittings must also be considered, as pointed out by Dashevskaya, Voronin, and Nikitin (*115*) and Movre and Pichler (*116*). Thus, for example, the potential energy curves of the $\Omega = 0$ states at the $4s + 4p$ asymptotes are eigenvalues of $2 \times 2$ matrices (quadratic equations) while those of the $\Omega = 1$ states are eigenvalues of $3 \times 3$ matrices (cubic equations). Such long-range potentials for $K_2$ are discussed in (*37*) and shown in Fig. 22. There are two potentials showing minima in Fig. 22, the $0_g^-(4p_{3/2})$ and $1_u(4p_{3/2})$ states; these are the observed pure long-range molecule states (Table 6 and Section II.A.2) (*117–119*) discussed in Section III.B. The remaining observed attractive curves (Table 6 and Section II.A.1.) [$0_u^+(4p_{3/2})$, $1_g(4p_{3/2})$, $0_u^+(4p_{1/2})$, $0_g^-(4p_{1/2})$, and $1_g(4p_{1/2})$] are discussed in Section III.C. The states at the two ground state atom ($4s + 4s$) asymptote and at the excited ($4s + ns$, $nd$) asymptotes are discussed in Sections III.D and III.E, respectively. The con-

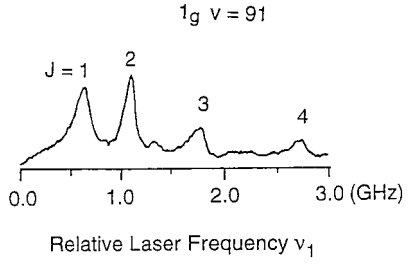


**FIG. 15.** The very high-resolution fragmentation spectrum of the rotational structure of the $v' = 91$ vibrational level of the $1_g(4p_{3/2})$ state of $^{39}K_2$.

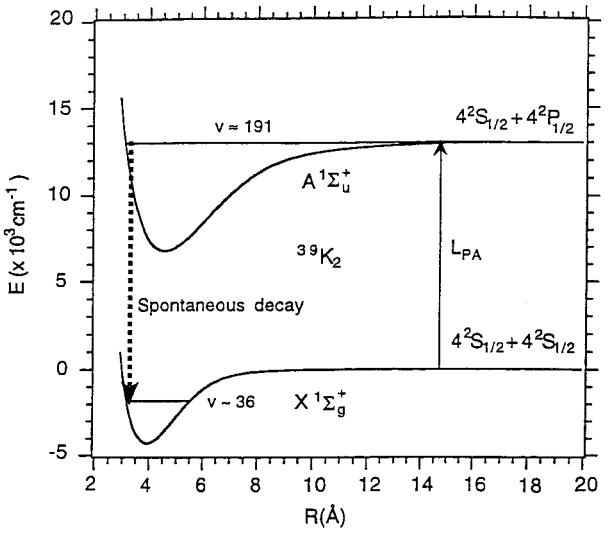


**FIG. 16.** Schematic diagram of the "molecule formation" process used, with time-of-flight mass spectrometry, to generate the photoassociation spectrum in Figure 8.

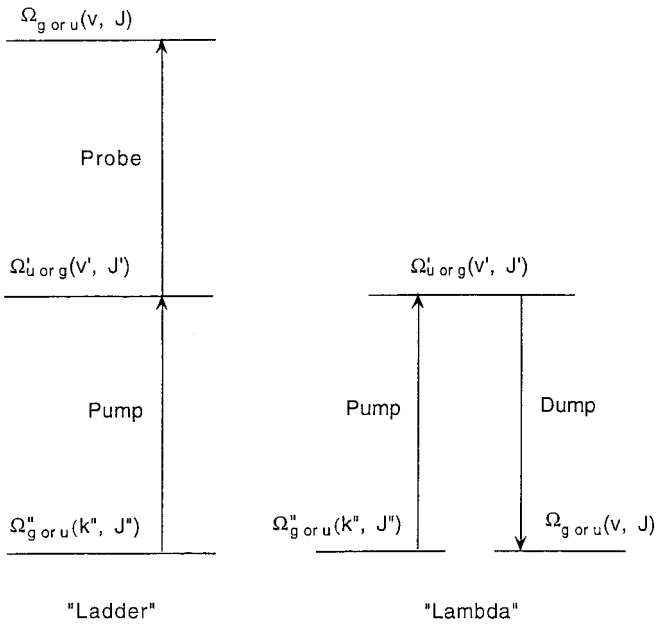


**FIG. 17.** The two schemes for free–bound–bound optical–optical double resonance, the "ladder" and the "lambda," both starting in a continuum state $\Omega''_{g/u}(k'', J'')$.

nections of the long-range states at the $4s + 4s$, $4s + 4p$, and $4s + ns$, $nd$ asymptotes to short-range states observed by traditional molecular spectroscopy are discussed in Section III.F. The other scientific significance of this work is summarized in Section III.G.

### *III.A. Long-Range Potential Energy Curves*

At large internuclear distances, the potential energy of a diatomic molecule can be calculated accurately by perturbation theory from the properties of its separated atoms alone (*120, 121*). If the overlap of the charge distributions of the two atoms is negligible, one may express the asymptotic potential energy as a sum of terms involving inverse powers of the internuclear distance $R$: $V(R) = -\sum C_k R^{-k}$, where $V(\infty) = 0$ and the leading exponent depends on the states of the two atoms. For example, $k = 6$ for the van der Waals interactions of an $ns + ns$ atomic asymptote, $k = 3$ for the resonant dipole–dipole interaction of an $ns + np$ atomic asymptote, and $k = 5$ for the quadrupole–quadrupole interaction of an $np + np$ asymptote and the resonant quadrupole–quadrupole interaction of an $ns + nd$ atomic asymptote, respectively (Table 8).

A reasonable estimate for the smallest distance at which the above equations can be used with better than 10% accuracy (because electron exchange is improbable) is the Le Roy radius (*112*).

$$R_{\mathrm{LR}} = 2\,[\langle r^2\rangle_A^{1/2} + \langle r^2\rangle_B^{1/2}]$$

where $\langle r^2\rangle^{1/2}$ is the rms distance of the electron from the nucleus in the outermost orbital of a given $s$-state atom. More generally the modified Le Roy radius (*122*) as follows should be used

$$2\sqrt{3}[\langle z^2\rangle_A^{1/2} + \langle z^2\rangle_B^{1/2}]$$

for atoms which may not be in $s$ states ($z$ is along the internuclear axis). The $R_{\mathrm{LR}m}$ values relevant to this review are listed in Table 9.

Another useful distance at spin–orbit split asymptotes is the distance at which the spin–orbit splitting $\Delta$ is comparable to the interatomic interaction

$$|C_n| R_{\mathrm{FS}}^{-n} = \Delta.$$

For the states corresponding to the $4s + 4p$ asymptotes where the spin–orbit splitting is 57.71 $\mathrm{cm}^{-1}$, this distance $R_{\mathrm{FS}}$

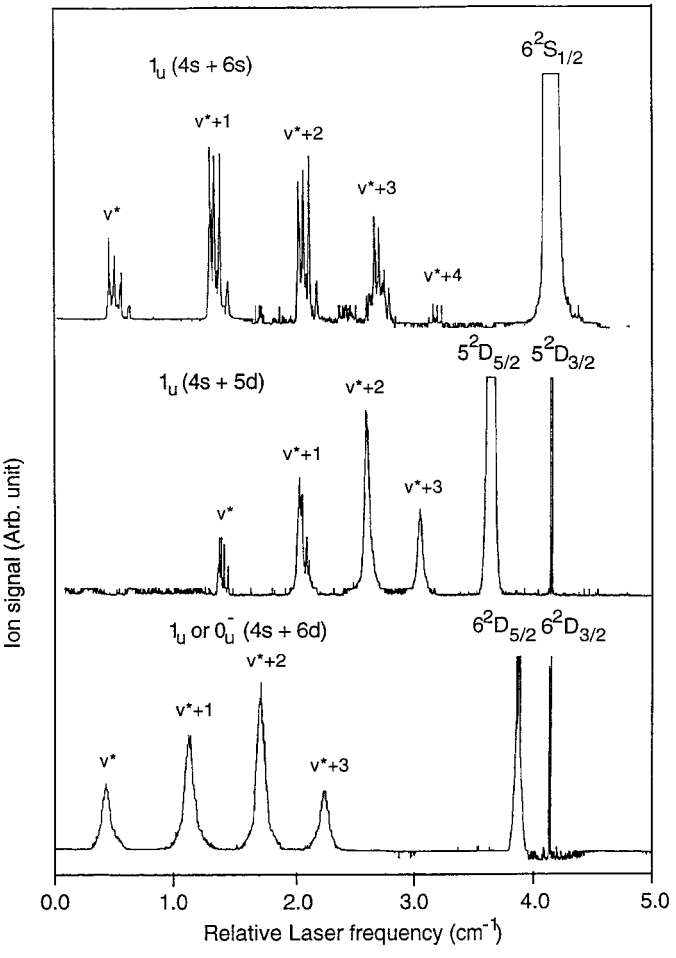


**FIG. 18.** Two-color photoassociative optical–optical double resonance spectra via the $0_g^-(4p_{3/2})v' = 0$, $J' = 2$ level (see Fig. 10). The top panel shows the spectrum of the $1_u$ state below the $4s + 6s$ asymptote; the center panel shows the spectrum of the $1_u$ state below the $4s + 5d$ asymptote; and the bottom panel shows an unspecified combination of the spectra of the $1_u$ and $0_u^-$ states below the $4s + 6d$ asymptote. The absolute vibrational quantum numbers are unknown ($v^*$ is an unknown positive integer or 0 for each state).

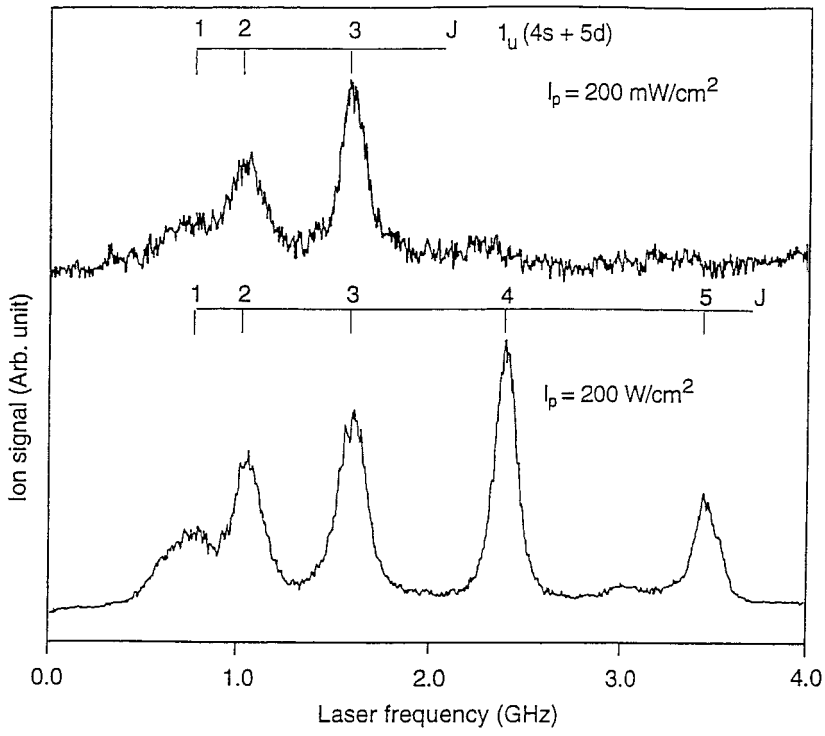


**FIG. 19.** The rotational structure of the central panel spectrum of Figure 18 for the lowest frequency $v = v^*$ band at two different laser intensities. The higher laser intensity shows "strong field effects," i.e. nominally forbidden lines corresponding to $J = 4$ and 5 appear because of two-photon very near resonance transitions via the $v' = 0$, $J' = 3$ and 4 levels of the $0_g^-(4p_{3/2})$ state.

is 16.82 Å for the Π states and $(2)^{1/3}$ times larger (21.19 Å) for the $\Sigma^+$ states. For higher states, the simple equation is less useful, since for the $4s + np$ asymptotes ($n > 4$) the $R^{-3}$ first-order term is comparable to or smaller than the $R^{-6}$ second-order term, and for the $4s + nd$ asymptotes ($n \geq 3$) the $R^{-5}$ first-order term is comparable to or smaller than the $R^{-6}$ second-order term. Nevertheless, it is easy to estimate $R_{FS}$ for a sum of inverse powers.

It should also be noted that the properties of diatomic vibrational levels with outer classical turning points in the attractive $C_nR^{-n}$ long-range region are approximately determined by $C_n$, the coefficient of the long-range potential, and by $n$, the inverse power of $R$ (*112, 113*). These properties include binding energy ($D_e - G(v)$), vibrational spacing ($\Delta G_{v+1/2}$), kinetic energy ($\langle T_v \rangle$), potential energy ($\langle V_v \rangle$), oscillator strength ($f_{ov}$), density of states ($dv/dG$), classical vibrational period ($\tau_v$), outer classical turning point ($R_{v+}$), powers of $R(\langle R^m \rangle_v)$, rotational constant ($B_v \sim \langle R^{-2} \rangle_v$), and centrifugal distortion constant ($D_v$) (*113*). For example, the binding energy of these vibrational levels is related to the vibrational quantum number $v$ (with respect to its (noninteger) value at dissociation $v_D$) by the relation

$$D_e - G(v) = a_n^\infty (v_D - v)^{2n/(n-2)},$$

where $a_n^\infty$ depends only on $n$, $C_n$, and the reduced mass $\mu$ (*123, 124*). For the $n = 3$ and $n = 6$ cases considered here in Sections III.B and III.C and in Sections III.D and III.E, respectively, the powers of $(v_D - v)$ are 6 and 3, respectively. Alternatively, a plot of vibrational quantum numbers for long-range levels versus the $\frac{1}{6}$ and $\frac{1}{3}$ powers of the levels' binding energies is a linear plot yielding $C_n$, $v_D$, and $D_e$ (see, e.g., (*124*)). However, it is worth noting that in ultracold photoassociative spectroscopy (in contrast to traditional short-range molecular spectroscopy), the binding energy is measured directly with respect to a known atomic limit (rather than the minimum of the ground state) and one does not obtain $D_e$ unless lower short-range levels optically connected to high long-range levels are known (see, e.g., (*4*)). Dissociation energies for the alkali dimers based on these and related long-range considerations are given in Table 10.

### *III.B. Pure Long-Range Molecules*

However, this simple expansion in inverse powers of $R$ breaks down as one goes to increasingly large internuclear distance if there is a significant spin–orbit splitting. In particular, there is a change in angular momentum coupling (Hund's case) when the atomic interaction is comparable to the atomic fine-structure splitting (and again when the atomic interaction is comparable to the hyperfine splittings). Finally, at very long range, retardation becomes important (*128*). For example, consider the case of two potassium atoms shown in Fig. 21. Two ground state K atoms interact in the $X^1\Sigma_g^+$ and the $a^3\Sigma_u^+$

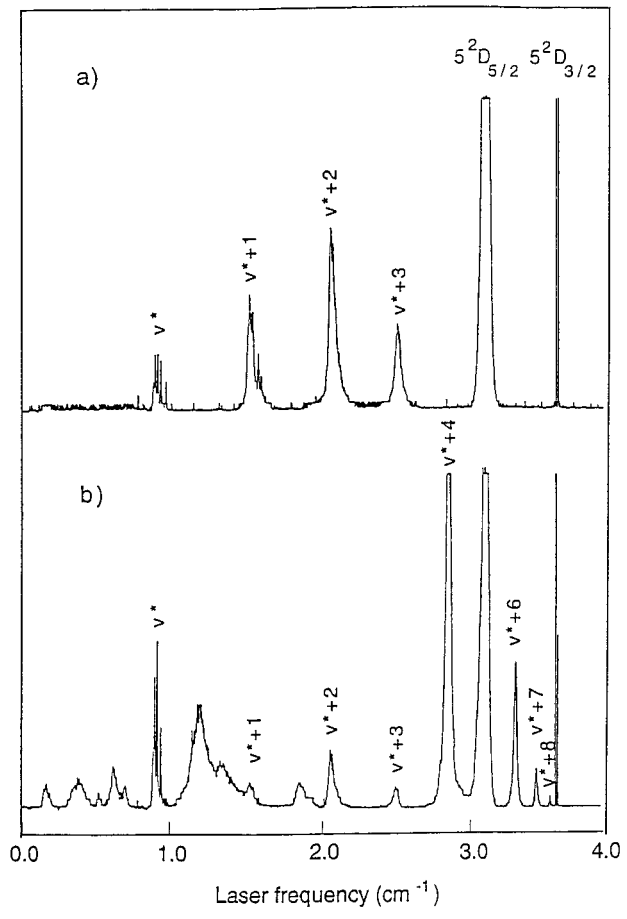


**FIG. 20.** Comparison of the two-color photoassociative optical–optical double resonance spectrum of the $1_u$ state slightly below the $4s + 5d_{3/2}$ asymptote via the following levels of the $0_g^-(4p_{3/2})$ intermediate state: (a) $v' = 0$, $J' = 2$; (b) $v' = 2$, $J' = 2$, the latter corresponding to the wider Franck–Condon window.

molecular electronic states in the Hund's case (a) representation. These two states at large internuclear distance reduce to a pair of degenerate states $^1\Sigma_g^+ - ^3\Sigma_u^+$ corresponding to three degenerate Hund's case (c) components, $0_g^+$, $0_u^-$, and $1_u$, each well described by a sum of inverse power terms.

However, for the excited asymptotes $4s^2S + 4p^2P$ at large internuclear distance (Fig. 21), eight case (a) electronic states, including the well-known $A^1\Sigma_u^+$, $b^3\Pi_u$, and $B^1\Pi_u$ states, reduce to four pairs of degenerate states $^1\Sigma_g^+ - ^3\Sigma_u^+$, $^1\Sigma_u^+ - ^3\Sigma_g^+$, $^1\Pi_u^+ - ^3\Pi_g$, and $^1\Pi_g - ^3\Pi_u$, which further correlate at very large $R$ with 16 Hund's case (c) molecular states due to angular momentum recoupling. The correlation diagram and the Hund's case (c) long-range potentials corresponding to the $4s^2S_{1/2} + 4p^2P_{1/2}$ and $4s^2S_{1/2} + 4p^2P_{3/2}$ asymptotes are given in Figs. 21 and 22, respectively (*37*).

Among the 16 case (c) components, we have observed (Table 6) those that are attractive and dipole allowed from the three ground state components, $0_g^+$, $0_u^-$, and $1_u$ based on the Hund's case (c) selection rules [$\Delta\Omega = 0, \pm 1$; $+ \leftrightarrow +$, $- \leftrightarrow -$, $+ \leftarrow/\rightarrow -$; and $g \leftrightarrow u$, $g \leftarrow/\rightarrow g$, $u \leftarrow/\rightarrow u$]. The three long-range potentials $1_u(4p_{1/2})$, $0_g^-(4p_{3/2})$, and $1_u(4p_{3/2})$, which show local extrema at large $R$, are of special interest (*87, 117*) and are discussed here.

Let us first consider the $0_g^-(4p_{3/2})$ state shown in Fig. 23. As shown there, long-range calculations of $C_3$, $C_6$, and $C_8$ for $\Sigma^+$ and $\Pi$ configurations, followed by diagonalization of a $2 \times 2$ matrix (solution of a quadratic equation) yield theoretical predictions (*118, 119, 129–131*) of the potential energy curve in apparently very good agreement with experiment (*37, 50*) (also shown). It should be noted that these results involve corrections for retardation and nonadiabatic effects and very slightly different models (*37, 50*), and that the long-range coefficients are in excellent agreement with theory (*118, 119, 129–131*) and with a very recent result from molecular spectroscopy (*15*), summarized in Table 11. In particular, the three experimentally based long-range potentials (*15, 37, 50*) are virtually indistinguishable from the RKR potential curve (*15*) outside 15 Å (differences $<0.2$ cm$^{-1}$). A careful global fit, incorporating both traditional molecular spectroscopy and ultracold photoassociative spectroscopy, is in progress for the $1^1\Pi_g \sim 1_g(4p_{3/2})$ state. Such a fit should yield an improved set of $C_n$ coefficients and a significantly more accurate $D_e$, as discussed in Section III.F.

The $0_g^-(4p_{3/2})$ state can be simply thought of as a state whose $C_3$ coefficient changes as a function of $R$. At very large $R$, where the interatomic interaction is small compared to the spin–orbit splitting, there is an interatomic attraction

$$V_{0_g^-}^{\infty} = -(C_3/3)\,R^{-3},$$

where $C_3 = |\langle 4s|\mathbf{r}|4p\rangle|^2$. However, at shorter distance, the two $0_g^-$ states mix (the electronic angular momenta recouple), and the $0_g^-(4p_{3/2})$ potential is approximately described by

$$V_{0_g^-} = +(C_3)\,R^{-3},$$

as previously shown in Fig. 21. Since the change from a $(-1/3)$ to a $(+1)$ occurs entirely in the long-range overlap-free region ($R \gg R_{\mathrm{LR}m}$ in Table 9), it is appropriate to call this a pure long-range molecular state (*87, 117, 132*).

It should also be noted that the $C_n$ coefficients from this state (or from molecular spectra or theory) in Table 11 allow one to calculate the full set of potential energy curves shown in Fig. 22. In particular, the $C_n$ coefficients from the $0_g^-(4p_{3/2})$ state (*37*) allowed us to accurately calculate and subsequently observe the $1_u(4p_{3/2})$ state discussed next, to accurately calculate the $1_g(4p_{3/2})$ state which correlates with the $1^1\Pi_g$ state (*14, 15*) as discussed in Section III.F, and to accurately calculate the $0_g^+(4p_{3/2})$ state which predissociates the $1_g$ state as discussed in Section III.C.

It is worth noting that this $0_g^-$ state has now been observed (Table 5) for $Na_2$, $Rb_2$, and $Cs_2$ as well as for $K_2$. The best theoretical calculations (based on (*130, 131*)) agree remarkably well with the ultracold photoassociation results ($Na_2$: (*49, 84*);

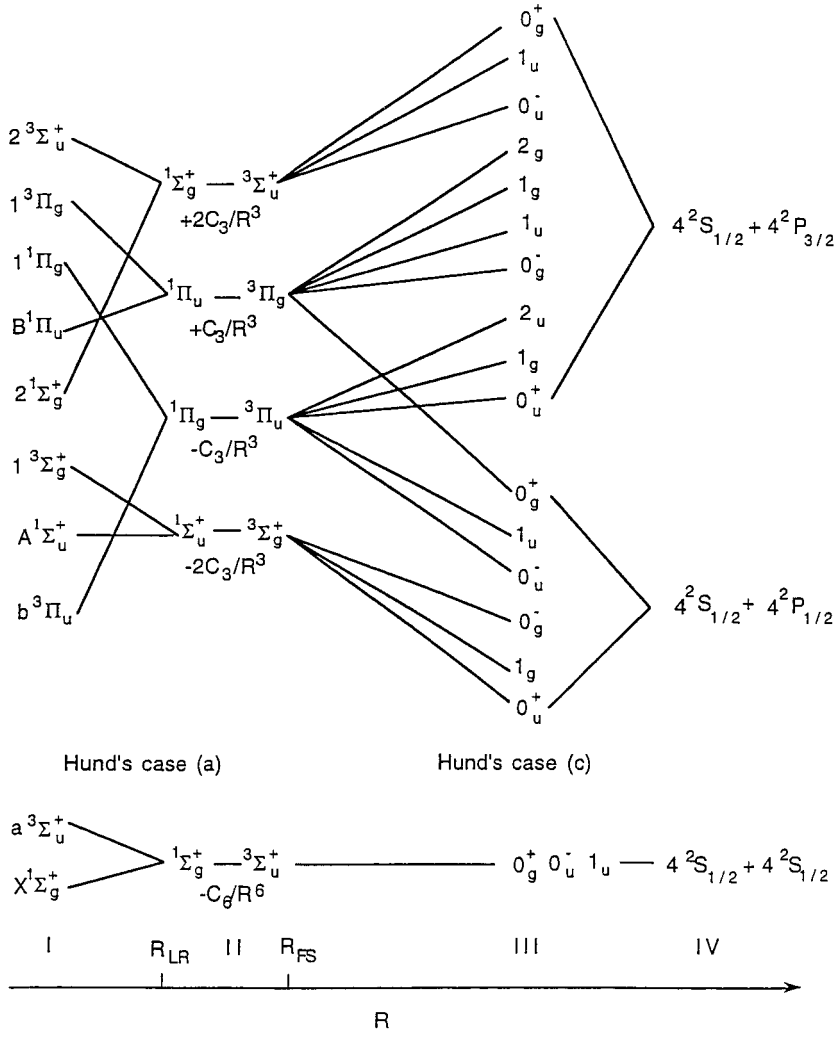


**FIG. 21.** Correlation diagram for electronic states dissociating to the lowest three asymptotes of $^{39}K_2(4s^2S_{1/2} + 4s^2S_{1/2}$, $4s^2S_{1/2} + 4p^2P_{1/2}$, and $4s^2S_{1/2} + 4p^2P_{3/2})$. States at short internuclear distances $R$ are described by Hund's case (a) quantum numbers. As $R$ increases, pairs of electronic states exponentially converge as exchange interactions decrease, with the pair's average interaction given by a sum over $n$ of $C_nR^{-n}$. At larger $R$, the various components of Hund's case (a) states split into a variety of Hund's case (c) states, especially as the spin–orbit splitting exceeds the magnitude of the interaction potential. The $g$–$u$ symmetry of the paired short-range states determines the corresponding long-range states (e.g., for the $^1\Pi_g$–$^3\Pi_u$ pair, $^1\Pi_g$ correlates to $1_g(4p_{3/2})$; $^3\Pi_u$ correlates to $2_u(4p_{3/2})$, $0_u^+(4p_{3/2})$, $1_u(4p_{1/2})$, and $0_u^-(4p_{1/2})$).

$Rb_2$: (*89*, *90*); $Cs_2$: (*67*, *68*)). The $Li_2$ state is predicted (*87*) to be extremely difficult to observe; because of the small spin–orbit splitting for Li ($2p$), the $0_g^-(2p_{3/2})$ state is only $\sim$0.037 $cm^{-1}$ deep at $\sim$134 Å.

The $1_u(4p_{3/2})$ state, as noted above, was accurately predicted using $C_n$ coefficients from the $0_g^-(4p_{3/2})$ state (Fig. 24) and subsequently observed (Fig. 11; (*88*)). The spectra are complicated by the fact that the hyperfine interaction is comparable to the rotational constant, so the rotation–hyperfine structure is quite complex for the low rotational quantum numbers accessible by ultracold photoassociation. Work is continuing to fully assign the spectrum (including relative intensities), but a preliminary analysis yields molecular constants in Table 12 in good agreement with those predicted using the potential in Fig. 24.

The other state near the $4s + 4p$ asymptotes that is potentially observable is the $1_u(4p_{1/2})$ state with a local maximum (pure long-range barrier) shown in Fig. 25. This state in principle could show quasibound resonances (blue-detuned from the $4s \rightarrow 4p_{1/2}$ resonance line) related to tunneling through the barrier, analogous, for example, to results on the $B\,^1\Pi_u$ state of $K_2$ (*12*, *133*) and the $3\,^1\Pi_g$ state of $Na_2$ (*134*). However, since the collisional pair density scales like $R^2$ (*3*, *135*), photoassociation inside the barrier may be relatively weak. Nevertheless, we expect to observe this state in future experiments (Section IV.G).

### *III.C. Other $n_{min}s + n_{min}p$ Asymptotic States*

As noted in Table 6, we have observed five attractive states [$0_u^+(4p_{3/2})$, $1_g(4p_{3/2})$, $0_u^+(4p_{1/2})$, $1_g(4p_{1/2})$, and $0_g^-(4p_{1/2})$] in

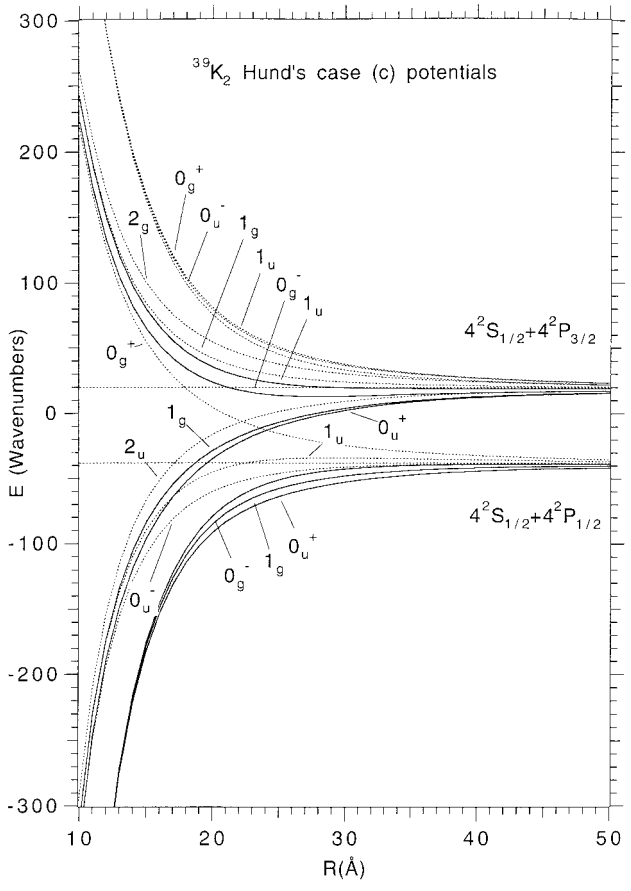


**FIG. 22.** The 16 adiabatic Hund's case (c) potential energy curves dissociating to the $4s + 4p_{3/2}$ and $4s + 4p_{1/2}$ asymptotes of $K_2$, based on the $C_3$, $C_6$, and $C_8$ values of (*37*). The solid curves are the seven observed states (Table 6) which support bound states and are accessible by dipole transitions from the $4s + 4s$ asymptote. The two uppermost of these seven are the $1_u(4p_{3/2})$ and $0_g^-(4p_{3/2})$ pure long-range states (wells of 0.5 and 6 $cm^{-1}$ at 39 and 28 Å, respectively) highlighted in Section III.B. The five lower of these seven are the $0_u^+(4p_{3/2})$, $1_g(4p_{3/2})$, $0_u^+(4p_{1/2})$, $0_g^-(4p_{1/2})$, and $1_g(4p_{1/2})$ states discussed in Section III.C. The other two long-range attractive states [$2_u(4p_{1/2})$; $0_u^-(4p_{1/2})$] are, in principle, observable by three-color experiments (all optical triple resonance), a future direction discussed in Section IV.C. The pure long-range barrier state ($1_u(4p_{1/2})$, with a barrier of 4 $cm^{-1}$ at 30 Å) and the six purely repulsive states are discussed briefly in Section IV.G. It should also be noted that bound and (blue-detuned from $4p_{1/2}$) quasibound resonances of the pure long-range barrier state may also be observable.

addition to the two pure long-range molecule states. These states are well described by their potential curves based on the $0_g^-(4p_{3/2})$ long-range coefficients in Table 11. Nevertheless, our long-term goal is a simultaneous "global" fit of all seven states (corrected for retardation and nonadiabaticity) to more precisely determine the long-range coefficients, e.g., $C_3$ in particular which determines the associated atomic radiative lifetime (*50*). However, these five states that penetrate to short range are sensitive to the short-range part of the potential as well as to the long-range part. While some properties such as $G(v)$, the vibrational energy, require only a "phase" or vibrational quantum number $v_{LR}$ out to the long-range region, other

**TABLE 8**
**Leading Long-Range Interaction Terms in the Alkali Dimers in the Absence of Spin–Orbit and Hyperfine Interactions**

| Asymptotic Atomic States | First Order Terms | Second Order Terms |
|---|---|---|
| S + S | -- | $C_6/R^6 + C_8/R^8 + C_{10}/R^{10}$ |
| S + P | $C_3/R^3$ | $C_6/R^6 + C_8/R^8 + C_{10}/R^{10}$ |
| S + D | $C_5/R^5$ | $C_6/R^6 + C_8/R^8 + C_{10}/R^{10}$ |
| P + P | $C_5/R^5$ | $C_6/R^6 + C_8/R^8 + C_{10}/R^{10}$ |

properties, e.g., short-range Franck–Condon factors for estimation of ground state molecule production (Sections II.A.4 and IV.D) require knowledge of the full short-range potential. For the case of the $1_g(4p_{3/2})$ state, the connection to short range is in very good shape (Section III.F), but the connections for the other states will require additional molecular spectroscopy. The other two long-range attractive states ($2_u(4p_{3/2})$ and $0_u^-(4p_{1/2})$) are, in principle, observable using three-color experiments (all optical triple resonance) as discussed in Section IV.C.

Evidence on the repulsive states can also be obtained. For example, the predissociation of the $1_g(4p_{3/2})$ state shown in Fig. 13 can be explained using the repulsive $0_g^+(4p_{1/2})$ state, as shown in Fig. 26. As noted in the figure, $v = 91$ of the $1_g(4p_{3/2})$ state is the lowest vibrational level above the $0_g^+(4p_{1/2})$/$1_g(4p_{3/2})$ crossing. The overlap between the $v = 91$ wavefunction and the $0_g^+$ continuum wavefunction at the same energy is large in the region of the crossing point. Vibrational levels $v < 91$ have at least an order of magnitude smaller overlap, corresponding to two orders of magnitude weaker predissociation, thus explaining the abrupt cutoff in $1_g$ predissociation below $v = 91$ (Fig. 13). Vibrational levels above $v = 91$ have somewhat smaller overlap than $v = 91$, the overlap decreasing with increasing $v$. By $v = 105$, shown in Fig. 26, the overlap is small and the predissociation is barely detectable in Fig. 13.

Likewise, the predissociation of the $0_u^+(4p_{3/2})$ state in Figs. 13 and 14 is even more complex as shown in Fig. 27. There is a purely long-range crossing of the $0_u^+(4p_{3/2})$ and $1_u(4p_{1/2})$ states near 17 Å; there is a second crossing at short range (~5

**TABLE 9**
**Calculation of the Modified Le Roy Radii ($R_{LRm}$) in Angstroms for the Various Observed Atomic Asymptotes of $K_2$ Discussed Herein**

| | $R_{LR-m}$ | | |
|---|---|---|---|
| Asymptote | $\Lambda = 0$ ($\Sigma$) | $\Lambda = 1$ ($\Pi$) | $\Lambda = 2$ ($\Delta$) |
| 4s + 4s | 11.29 | | |
| 4s + 4p | 16.24 | 11.76 | |
| 4s + 4d | 31.33 | 28.88 | 19.06 |
| 4s + 6s | 30.11 | | |
| 4s + 5d | 49.27 | 45.10 | 28.43 |
| 4s + 7s | 44.53 | | |
| 4s + 6d | 71.34 | 65.07 | 39.95 |

**TABLE 10**
**$D_0^0$ Values ($cm^{-1}$) for the Alkali Dimers**

| | | | | |
|---|---|---|---|---|
| $^6Li_2$ | 8344.10 | ± | 0.07 | (125) |
| $^7Li_2$ | 8341.55 | ± | 0.08 | (125) |
| $Na_2$ | 5942.6880 | ± | 0.0049 | (47) |
| $^{39}K_2$ | 4404.583 | ± | 0.072 | (39) |
| $Rb_2$ | 3965.6 | ± | 0.4 | (126) |
| $Cs_2$ | 3628.5 | ± | 0.8 | (127) |

Å) of the correlary $b^3\Pi_u$ and $A^1\Sigma_u^+$ states; and finally, there is fine-structure mixing of the components of the $b^3\Pi_u$ state at short range. As discussed in (*64*), we believe the fine-structure mixing is dominant, in accord with theoretical predictions that the low-temperature fine structure changing collisions ($K(4p_{3/2}) + K \rightarrow K(4p_{1/2}) + K$) are dominated by this mechanism as well (*136*). It is noteworthy that these collisions are an important trap-loss process.

A general method for the study of the repulsive curves ($0_g^+$, $0_u^-$, $1_u$, $2_g$, and $1_g$ states at $4s + 4p_{3/2}$ and $0_g^+(4p_{1/2})$) and the pure long-range barrier state ($1_u(4p_{1/2})$) is ultracold free–free spectroscopy (Section IV.G), although the analysis will not always be as simple as in ultracold photoassociation.

### *III.D. Ground State Atom Asymptote*

The asymptote corresponding to two ground state atoms is the simplest and best understood in $^{39}K_2$ (see (*39*) and references therein). Strictly speaking, there are three asymptotes corresponding to the three possible energy levels of the hyperfine states: $F_A = 1$, $F_B = 1(0)$; $F_A = 1$, $F_B = 2$ and $F_A = 2$, $F_B = 1$ (462 MHz); $F_A = 2$, $F_B = 2$ (924 MHz). However, as in the preceding sections, we will normally ignore hyperfine splittings if possible in our discussions.

In particular, the ground $X^1\Sigma_g^+$ and metastable $a^3\Sigma_u^+$ states have been extensively studied by conventional "short-range" molecular spectroscopy out to 15.23 Å (*5*) and 10.52 Å (*39*), respectively. While the latter distance is slightly inside the Le Roy radius (10.82 Å, as listed in Table 9), one can combine data on both states to obtain the exchange energy (from the splitting of the two potentials) and the Coulomb energy (from the average of the two potentials) (*39, 125, 137–139*). The exchange energy is approximately exponential in $R$, while the Coulomb energy is well fit by the long-range inverse power series in Table 8 ($C_6R^{-6} + C_8R^{-8} + C_{10}R^{-10}$). A further improvement in fitting the exchange energy (power of $R$ times an exponential) for $^{39}K_2$ is given in (*140*); see also (*141*).

An important motivation for studying the uppermost levels of the $X^1\Sigma_g^+(0_g^+)$ and $a^3\Sigma_u^+(0_u^-, 1_u)$ states is to determine the scattering lengths for atomic collisions on the appropriate potential energy curve. In particular, the triplet scattering length (with perhaps some singlet scattering length admixture depending on hyperfine state) determines the stability of a BEC and the magnitude of the elastic collision cross sections. A positive scattering length indicates the BEC of identical particles has a positive (repulsive) mean field interaction and it will not collapse; a negative scattering length indicates a negative (attractive) mean field interaction in the BEC, yielding collapse except for a very small number of particles (*142*). A large elastic scattering cross section (proportional to scattering length squared) implies rapid evaporative cooling to BEC, while a small cross section suggests that the cooling will be difficult (*143*).

Unfortunately, determination of an accurate scattering length requires an extremely accurate full potential (*144*). The scattering length goes to $-\infty$ and then to $+\infty$ as a potential well is slightly deepened to the point where a new bound vibrational level (for 0 rotation) appears at dissociation (*3, 144*). As the well is further deepened (or equivalently the reduced mass increased), the scattering length drops from $+\infty$ to small positive numbers, going through 0 at about $\frac{3}{4}$ of a vibrational quantum. For the next $\frac{1}{4}$ of a quantum, the scattering length drops from 0 to $-\infty$ again, where an additional vibrational level again appears. Thus an accurate value of scattering length requires an accurate value of $v_D$, the vibrational quantum number at dissociation, discussed in Section III.A, with a small uncertainty when compared to unity. (It is also possible that BEC-related experiments which accurately determine the scattering length will provide important "spectroscopic" information, e.g., an accurate value of $v_D$.) For the $a^3\Sigma_u^+$ state of $K_2$, there are 27 or 28 vibrational levels for the various (six) isotopic variants, so a very accurate potential well is required (extrapolated to $R = \infty$ as in (*39, 140*)). Thus a 1.78 $cm^{-1}$ error in the $a^3\Sigma_u^+$ well depth in (*138*) changed the early K scattering length calculations (negative) of (*145*) to positive (*39, 140*). The more recent work (*146, 147*) has found a value of $-17 \pm 25a_0$.

It is also worth noting that, since to a very good approxi-

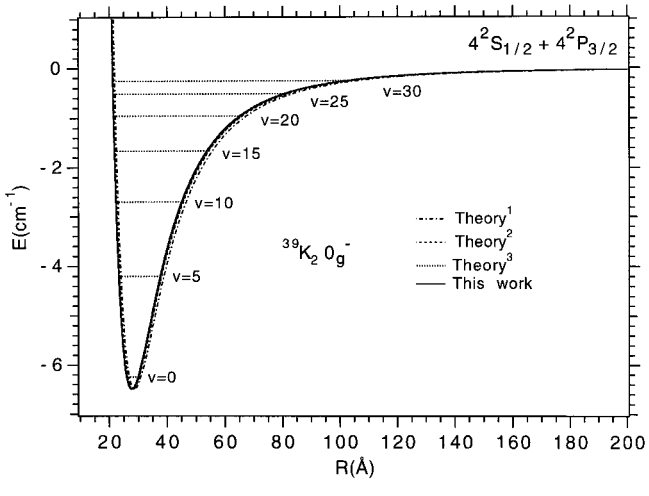


**FIG. 23.** Potential energy curves of the $0_g^-(4p_{3/2})$ pure long-range molecule state of $^{39}K_2$. Three theoretical curves (based on theoretical long-range coefficients given in 1 (*118, 119*), 2 (*129*), and 3 (*130, 131*)) are compared with an experimental curve based on a long-range coefficient fit to the 31 levels observed by ultracold photoassociation spectroscopy (*37, 50*). Every fifth observed vibrational level is also shown.

**TABLE 11**

**Results for Long-Range Coefficients (All in Atomic Units) at the 4*s* + 4*p* Asymptotes of $^{39}K_2$ from Ultracold Photoassociation, Conventional Molecular Spectroscopy, and Theory**

| $C_3^{\Pi}$ | $C_3^{\Sigma}$ | $C_6^{\Pi}$ | $C_6^{\Sigma}$ | $C_8^{\Pi}$ | $C_8^{\Sigma}$ | reference |
|---|---|---|---|---|---|---|
| Ultracold Photoassociation: | | | | | | |
| 8.445 (14) | 16.890 (28) | 6480 (94) | 9675 (141) | 762300[a] | 1975000[a] | (50) |
| 8.436 (14) | 16.872 (28) | 6272 (94) | 9365 (141) | 762300[a] | 1975000[a] | (37) |
| Molecular Spectroscopy: | | | | | | |
| 8.433 (9) | 16.866 (18) | 6840 (210) | 10213 (314) | 762300[a] | 1975000[a] | (15) |
| Theory: | | | | | | |
| 8.665 | 17.33 | 6291 | 9393 | 762300 | 1975000 | (130, 131) |
| 8.768 | 17.54 | 6465 | 9651 | 713200 | 1892000 | (129) |
| 9.340 | 18.68 | 6868 | 10130 | 581400 | 2454000 | (118, 119) |

[a] $C_8$ values from (*130, 131*) assumed in the fits to experimental data.

mation ($<0.1$ cm$^{-1}$), the potential energy curves of all isotopic variants of the same alkali dimer molecule (e.g., $K_2$) are the same, the determination of scattering length (or $v_D$) for any single isotopomer determines the scattering length for all others.

Particularly significant therefore were PUMP-DUMP experiments (Lambda-type two-color spectroscopy of Fig. 17) for $^7$Li (*70*), $^6$Li (*76*), Rb (*94*) and $^{39}$K (work in progress). In the first case, the last bound level of the $a^3\Sigma_u^+$ potential was observed and the corresponding scattering length accurately determined (confirming the early predictions of a negative sign (*148–150*)), establishing that a $^7$Li BEC was stable only for small numbers of atoms ($\leq$1200 (*142*)). In the last two cases, a variety of levels were observed, pinning down the scattering lengths. Very recently, in an important advance, the coherent version of the PUMP-DUMP process ("stimulated Raman pho-

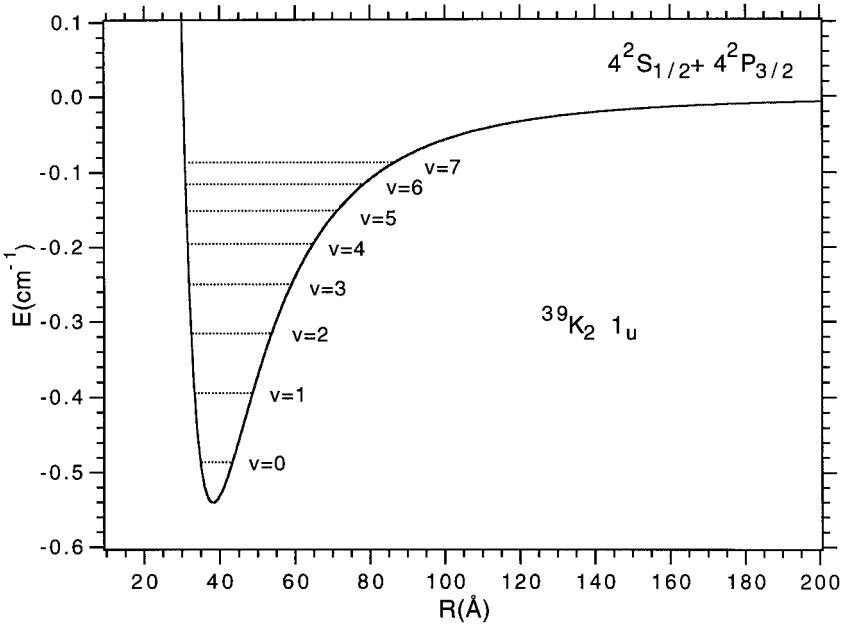


**FIG. 24.** Potential energy curve of the $1_u(4p_{3/2})$ pure long-range molecule state of $^{39}K_2$, based on the long-range coefficients obtained from analysis of the $0_g^-(4p_{3/2})$ pure long-range molecule state (*37*). Also shown are the vibrational levels observed by ultracold photoassociation ($v = 0$–7) (*88*).

**TABLE 12**

**Observed Major Molecular Constants (in $cm^{-1}$) of the $1_u(4p_{3/2})$ Pure Long-Range Molecule State Compared to Those Predicted Using the Potential of Fig. 24 (Based on Analysis of the $0_g^-(4p_{3/2})$ State))**

| | Observed | Predicted |
|---|---|---|
| $D_e$ | 0.5394 (20) | 0.5410 (4) |
| $\omega_e$ | 0.1046 (22) | 0.1071 (4) |
| $\omega_e x_e \times 10^2$ | 0.750 (64) | 0.788 (8) |
| $\omega_e y_e \times 10^3$ | 0.202 (52) | 0.216 (5) |
| $B_e \times 10^3$ | — | 0.5958 (5)[a] |
| $\alpha_e \times 10^4$ | — | 0.616 (2) |
| $\gamma_e \times 10^5$ | — | 0.166 (3) |

[a] Corresponds to $R_e = 38.15(2)$ Å.

toassociation") has been observed in a BEC (*98*), observing a single level slightly below dissociation. Work on laser-driven collisions in a BEC should also be noted (*46*).

### *III.E. Highly Excited Atomic Asymptotes*

The Hund's case (a) degenerate state pairs at large internuclear distance and the correlating case (c) components can also be readily calculated for higher asymptotes. For example, the spin–orbit splitting for the $4s + 4d$ asymptote is very small (1.10 $cm^{-1}$ compared to 57.71 $cm^{-1}$ for the $4s + 4p$ limit). The $4s + 5p$ limit has the same Hund's case (c) state symmetries at large $R$ as the $4s + 4p$ does. However, a smaller spin–orbit interaction (18.76 $cm^{-1}$) is involved. The doubly excited $4p + 4p$ atomic limit and the corresponding molecular states are important and have recently been calculated at long-range for the first time in our group. Of particular interest are extrema outside $30a_0$: $0_g^+$ minima at 33 and $34a_0$ at the (1/2, 1/2) asymptote and a $1_g$ maximum at $42a_0$ at the (1/2, 3/2) asymptote (the $Na_2$ states at the $3p + 3p$ asymptotes have also been discussed in detail (*81, 151*)).

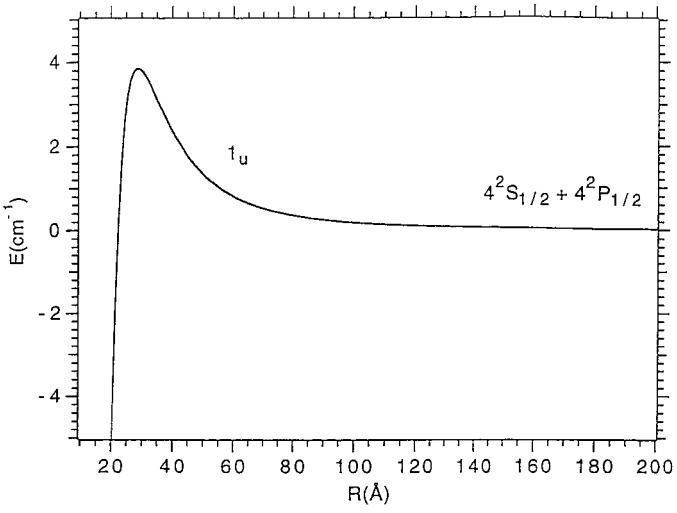


**FIG. 25.** Potential energy curve of the $1_u(4p_{1/2})$ pure long-range barrier state of $^{39}K_2$, based on the long-range coefficients obtained from analysis of the $0_g^-(4p_{3/2})$ pure long-range molecule state (*37*).

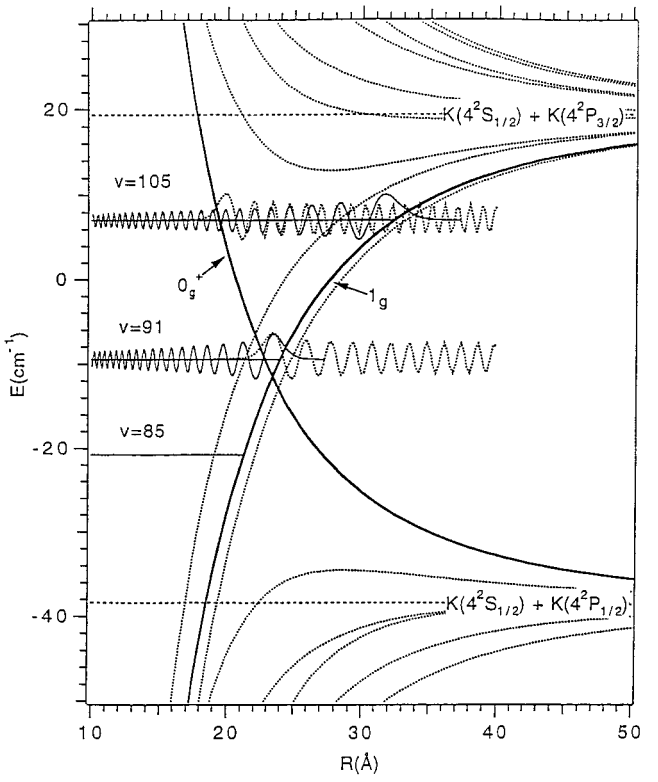


**FIG. 26.** The predissociation of vibrational levels $v = 91$–$105$ of the $1_g(4p_{3/2})$ state (solid line) of $^{39}K_2$ (shown in Fig. 13) is explained by the coupling to the $0_g^+(4p_{1/2})$ state (other solid line). The level $v = 91$ is the first level above the $1_g/0_g^+$ crossing and has a large vibrational overlap, corresponding to the strong predissociation for $v = 91$ in Figure 13. By $v = 105$, the vibrational overlap has become very weak, corresponding to the barely visible predissociation in Figure 13.

An additional complexity occurs at large $R$ when $V(R)$ is comparable to the hyperfine splitting, similar to the above situation where $V(R)$ becomes comparable to the fine-structure splitting. Full treatment is underway, e.g., for the shallow $1_u$ state at the $4s + 4p_{3/2}$ asymptote (*88*), but a discussion of hyperfine details is beyond the scope of this review and will not be given here.

For the $4s + nd$ asymptotes we have studied thus far by two-color ultracold photoassociation ($4s + 4d$, $5d$, $6d$; discussed in Section II.B), the long-range behavior is expected to include a $C_5R^{-5}$ first-order resonant quadrupole term plus dispersion ($C_6R^{-6} + C_8R^{-8} + C_{10}R^{-10}$) as listed in Table 8. However, the first-order term is negligible (*63*) and thus a linear relation between $v$ and binding energy ($D_e - G(v)$) to the $\frac{1}{3}$ power is predicted and observed, as shown in Fig. 28 for the state observed at the $4s + 5d$ asymptote (Fig. 20). The

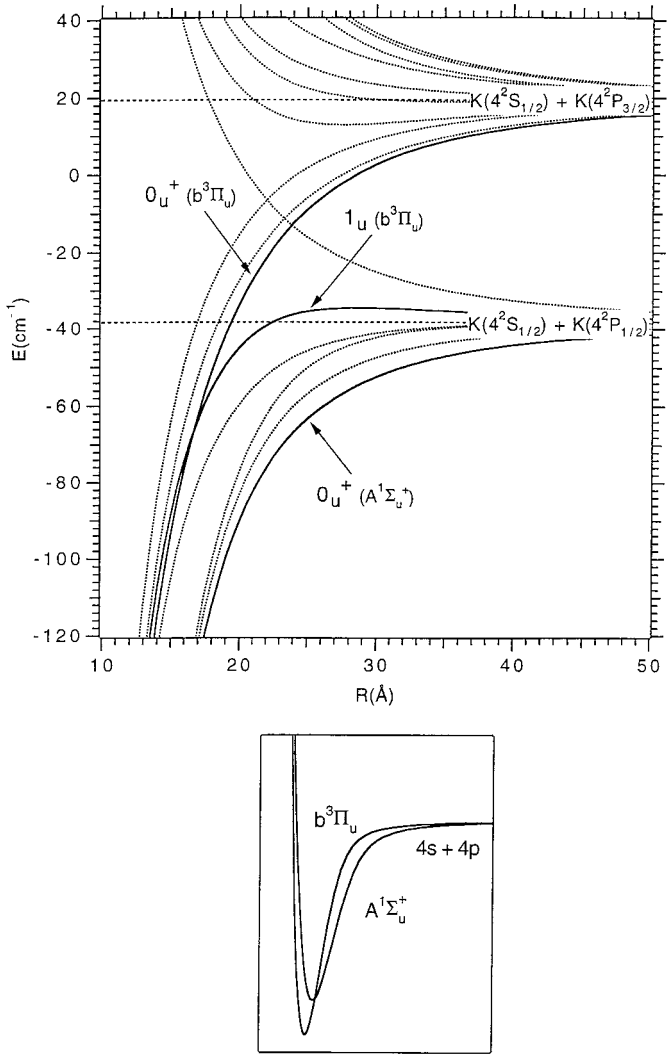


**FIG. 27.** The predissociation of the vibrational levels near dissociation of the $0_u^+(4p_{3/2})$ state includes three electronic contributions (*64*) involving the curves indicated with solid lines in the upper (long range) and lower (short range) part of the figure: the $0_u^+(4p_{3/2})$ state which is predissociated (a) crosses (upper figure) the $1_u(4p_{1/2})$ pure long-range barrier state at ~17 Å; (b) correlates with the $\Omega = 0^+$ component of the $b^3\Pi_u$ state which crosses the $A^1\Sigma_u^+$ state (correlated to the $0_u^+(4p_{1/2})$ state); and (c) mixes with the $\Omega = 1$ component (and indirectly the $0^-$ and 2 components) of the $b^3\Pi_u$ state at short range (which we believe is the most important mechanism (*64*)).

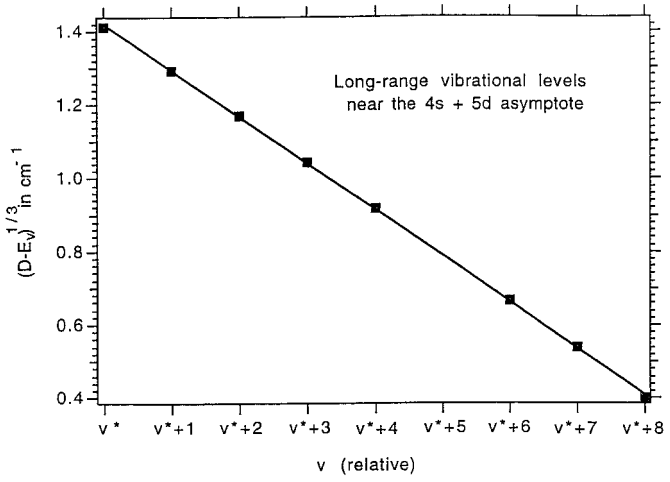


**FIG. 28.** Long-range plot of the one-third power of the binding energy (in $cm^{-1}$), $(D_e - E_v)^{1/3}$, versus the vibrational quantum number $v$ for levels of the $1_u$ state dissociating to the $4s + 5d_{3/2}$ asymptote of $^{39}K_2$. The $v^* + 5$ level is obscured by the $5d_{5/2}$ atomic feature. Three more levels are predicted ($v^* + 9$–11) with $v^* = 11.5 + 0.1$. The slope of this plot yields a $C_6$ value (see Table 13).

corresponding $C_6$ values for these states at $4s + nd$ asymptotes and also for states at the $4s + ns$ asymptotes are very large, roughly two orders of magnitude larger than the $4s + 4s$ $C_6$ coefficient of 3813 (*152*).

Finally we note a very interesting new calculation by Marinescu (*114*) for the $^3\Sigma_u^+$ state (correlating to $0_u^-$ and $1_u$) at the $4s + 6s$ asymptote. This calculation combines the accurate $C_6$ and higher order dispersion terms (*114, 130*) (tested in Table 13) with an asymptotic calculation of the repulsive exchange term to calculate the full long-range potential, but is all long range and much simpler than a full electronic structure calculation (this is the ninth state of $^3\Sigma_u^+$ symmetry (*155*)). A comparison of our measured vibrational eigenvalues and those predicted using Marinescu's potential is given in Table 14. The results are quite encouraging and we look forward to seeing further results of this type.

### *III.F. Connections to Short-Range States*

An important goal of our work is to bridge the gap between long-range interatomic potentials obtained from ultracold photoassociation and the shorter range interatomic potentials obtained from conventional molecular spectroscopy, e.g., OODR (*156*) and AOTR (*157*). There are a number of examples of such connections; e.g., the $A^1\Sigma_u^+ \sim 0_u^+(n_{\min} p_{1/2})$ correlation for $Li_2$ (*158–160*) and for $Na_2$ (*47*) and the $1^1\Pi_g \sim 1_g(n_{\min} p_{3/2})$ correlation for $Na_2$ (*161*) and for $^{39}K_2$ (*14, 15, 37*). We illustrate with this last $K_2$ example here. Figure 29 shows the potential curve of the $1^1\Pi_g$ state from (*14*) out to 16.2 Å and the $1_g(4p_{3/2})$ potential from (*37*) (as in Fig. 22) in to $R_{LRm} =$

**TABLE 13**

**Long-Range $C_6$ Coefficients (in atomic units) for Observed Electronic States (Most and Probably All Are $1_u$ Symmetry; See Section II.B), Obtained From Plots of Experimental Binding Energies Such as Fig. 28, Compared with Theoretical Values**

| Asymptote | $R_{LR-m}$ (Å) | $C_6$(a.u.) | | | |
|---|---|---|---|---|---|
| | | Expt | Theory | | |
| | | (63) | (153) | (130) | (154) |
| $4s + 6s_\sigma$ | 29.89 | 160 000 (5 000) | 155 100 | 146 300 | — |
| $4s + 7s_\sigma$ | 48.48 | 370 000 (20 000) | 393 700 | — | 391 950 |
| $4s + 4d_{3/2\Pi}$ | 29.34 | 123 000 (3 000) | — | 124 900 | — |
| $4s + 5d_{3/2\Pi}$ | 45.27 | 330 000 (3 000) | — | — | 356 200 |
| $4s + 6d_{3/2\Pi}$ | 65.03 | 1 010 000 (70 000) | — | — | 808 700 |

**TABLE 14**
**$^{39}K_2(4s + 6s)^3\Sigma_u^+$ Binding Energies ($cm^{-1}$) from Experiment and from a Theoretical Potential Combining Asymptotic Exchange and Dispersion**

| v | Expt. (63) | Thry. (114) |
|---|---|---|
| 0 | 4.726 | 3.929 |
| 1 | 3.765 | 2.911 |
| 2 | 2.908 | 2.070 |
| 3 | 2.169 | 1.399 |
| 4 | 1.538 | 0.885 |
| 5 | 1.030 | 0.514 |
| 6 | 0.638 | 0.264 |
| 7 | 0.358 | 0.113 |
| 8 | 0.174 | 0.0311 |

11.8 Å. On this scale the curves are virtually identical since the $D_e$ value for $^{39}K_2$ is accurately known to 0.07 $cm^{-1}$ (Table 10). However, if one blows up the scale and focuses on the region of overlap (Fig. 30), one sees that the $1_g(4p_{3/2})$ potential based on the theoretical $C_n$ coefficients of (*130, 131*) lies about 3 $cm^{-1}$ below the experimental RKR potential. However, if one simply uses the experimental $C_n$ coefficients of (*37*), one obtains an order of magnitude better agreement with the RKR. Ross and co-workers have recently extended their work (*14*), with a new potential out to 40.27 Å which would be indistinguishable from the prior RKR and our long-range (Exp) curve in Fig. 30. A careful joint analysis of data from both short-range molecular spectroscopy and long-range ultracold photoassociative spectroscopy is currently underway and should yield improved results for $C_3$, $D_e$, and other parameters (note that $C_3$ values already agree to 0.036%, less than their (*14*) and our (*37*) estimated uncertainties (0.11 and 0.17%, respectively)).

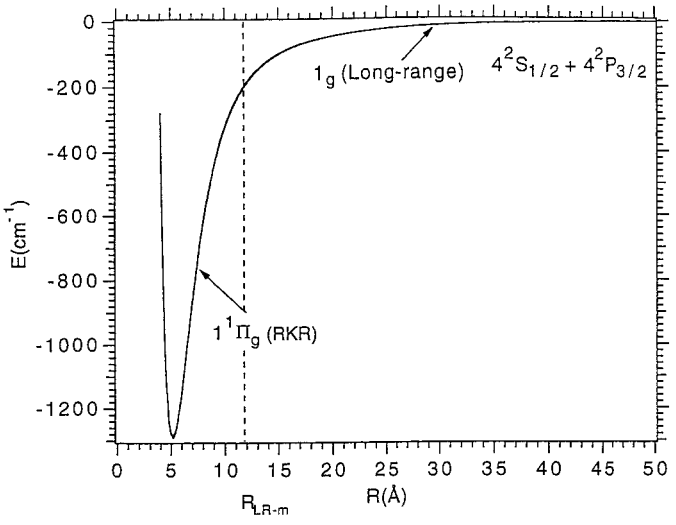


**FIG. 29.** The RKR potential energy curve of the $1\,^1\Pi_g$ state of $^{39}K_2$ to 16.2 Å (*14*) compared to the long-range potential into 11.8 Å predicted (*37*) for the $1_g(4p_{3/2})$ state which correlates to the $1\,^1\Pi_g$ state. A blow-up of the overlap region is Figure 30.

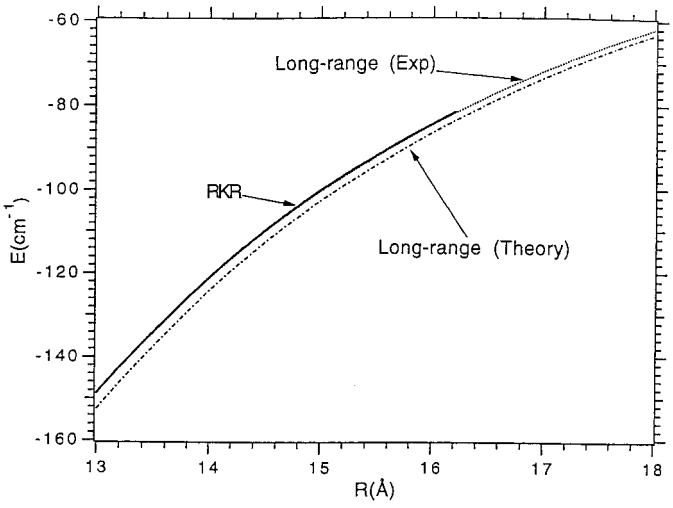


**FIG. 30.** Blow-up of the region of overlap in Figure 29 between the RKR potential of (*14*) and the long-range $1_u(4p_{3/2})$ potentials of (*37*) based on the theoretical $C_n$ coefficients of (*130, 131*) or on the experimental $C_n$ coefficients of (*37*) from ultracold photoassociation to the $0_g^-(4p_{3/2})$ state. On this scale, the other long-range (Exp) results of (*15, 50*) would be indistinguishable from those of (*37*).

Useful connections can also be made even when there are limited or no experimental short-range spectroscopic results available because of the high quality of electronic structure calculations for lighter alkali dimers, e.g., the work of Magnier et al. for $Na_2$, NaK, and $K_2$ (*6, 162, 163*). Using such calculations at short-range and ultracold photoassociation experiments (or asymptotic theory; e.g., (*130, 131, 154, 164*)), one can obtain approximate potentials which are very useful for experimental planning or interpretation (e.g., (*81, 85*)).

### *III.G. Other Scientific Significance*

Interatomic forces are fundamental to the understanding of atomic collisions and to the assembly of atoms into molecules, clusters, and solids. Traditionally, interatomic forces (actually potential energy curves) are derived from a variety of sources: perturbation theory of atom–atom interactions (long range), molecular electronic structure theory (short range), bulk and transport properties, scattering, and spectroscopy. The distance $R_{LRm}$ discussed in Section III.A represents the rough boundary between short and long range (*122*). Inside $R_{LRm}$ perturbation theory of atom–atom interactions becomes inaccurate; outside meaningfully precise molecular electronic structure theory becomes exceedingly difficult. It represents the distance at which the energy associated with the exchange of indistinguishable electrons between atoms becomes significant compared to the interaction ("coulombic") energy calculated assuming the electrons on the different atoms are distinguishable. This exchange contribution can be directly extracted from experiment if potential curves of the appropriate complementary symmetries are all observed. We have provided the first such direct observations of exchange (*39, 125, 137–139*) for two ground state

**TABLE 15**
**Selected Asymptotes of the $^{39}K_2$ Molecule**

| Asymptote | Observations | Section for discussion | Section for future directions |
|---|---|---|---|
| 4s + 4s | lower free state of all photoassociation | III.D. | IV.A. |
| 4s + 4p | upper bound state of one color photoassociation | III.B.,C. | IV.C.,G. |
| 4s + ns, n″d | upper bound state of two color photoassociation (observed for n = 6,7; n″= 4,5,6) | III.E. | IV.A. |
| 4s + n′p (n′≤5) | — | III.E. | IV.A. |
| 4s + n‴f,… | — | III.E. | IV.C. |
| 4p + 4p | — | III.E. | IV.A. |
| $K^+ + K^-$ | — | — | IV.B. |
| $K^+ + 4s + e^-$ | — | — | IV.B. |
| $K^+ + 4p + e^-$ | — | — | IV.B. |

alkali atoms and plan to extend them to excited asymptotes as well (*37*).

Moreover, at short range, the atomic interactions are large (on the order of 0.1–0.001 a.u.) and much greater than fine structure and hyperfine structure, as well as other small effects (retardation, Lamb shift, etc.). Such strong interactions dominate in ordinary collisions. However, cold collisions (both in traps and interstellar gas clouds) are far more subtle and depend exquisitely on details of the potential. For example, Feshbach resonances show a factor of $10^{10}$ enhancement in cross section in H + D collisions (*165*). (Such fine- and hyperfine-structure changing collisions often dominate trap loss.)

The clearly superior experimental technique for precise determination of interatomic potentials is high-resolution diatomic spectroscopy, starting in the molecular ground state. However, it is exceedingly difficult to obtain long-range data outside $R_{\mathrm{LR}m}$ for a variety of reasons, especially excruciatingly small Franck–Condon factors. One often requires the potential at *both* short and long range. The techniques of ultracold photoassociative spectroscopy described here represent the logical long-range complement to traditional short-range molecular spectroscopy. Indeed, the narrow energy and the narrow angular momentum distribution in the initial state largely obviates the need for an initial "pump" step in multiple resonance molecular spectroscopy to prepare an individual level. Such techniques also offer the future opportunity to prepare ultracold molecules (*19, 65, 67, 68, 103, 104, 166–169*) and explore an entirely new range of reaction dynamics, dominated by resonances and other quantum phenomena.

We note that there are close relationships between the long-range atom–atom interactions and atomic properties. The ability to extract a precise value of $C_3$ from photoassociative spectroscopy (e.g., for Li (*48, 72*), Na (*49*), K (*50*), and Rb (*51*)) allows determination of the atomic radiative lifetime to high precision. Such atomic radiative lifetimes, based on ultracold photoassociative spectroscopy, are the most precise determinations available for all alkali atoms except Cs (*170*). Such information provides valuable tests for atomic structure calculations, for example in conjunction with atomic parity nonconservation experiments, to test theories of the weak interaction. More generally, not only does the long-range $C_3$ coefficient depend on $|\langle ns|\bar{\mu}|np\rangle|^2$, but so do other long-range molecular properties: the static polarizability of the alkalis is predominantly determined by this quantity and is found in the $M_2^+$ long-range potential coefficient $C_4$; the $C_6$ coefficient between ground state atoms is likewise dominated by $|\langle ns|\bar{\mu}|np\rangle|^2$; the "retarded" long-range coefficients and long-range electric dipole strength functions likewise depend on this atomic quantity. Note also that evidence for the effects of retardation has been obtained from ultracold photoassociative spectroscopy (*48–50, 160*). In a similar way, the long-range ion pair potential curves should provide accurate determinations of atomic electron affinity and negative ion polarizabilities, competitive with the current best "atomic" values. We also note that photoassociative spectroscopy may be useful as a probe of the short-range approach of cold atoms. Such a probe may also allow more detailed studies of optical "shielding" of collisions (*3, 171–174*), where close approach is suppressed by excitation to a repulsive potential.

## IV. FUTURE DIRECTIONS

The authors feel that the potential for scientific advances based on ultracold photoassociative spectroscopy is extremely high and thus far barely tapped.

We first examine possible directions in which to go for our illustrative case of $^{39}K$, i.e., to other asymptotes (Section IV.A), to photoassociative ionization (Section IV.B), to three-color spectra (Section IV.C), and to formation of ultracold alkali

dimer molecules (Section IV.D). We then look beyond the alkalis to other atoms which might be cooled, trapped, and photoassociated (Section IV.E). In Section IV.F we discuss the possibility of atom–molecule and molecule–molecule photoassociation, while in Section IV.G we discuss the possibility of ultracold free–free spectroscopy. Finally, in Section IV.H we briefly discuss the effects of electromagnetic fields. As an aid, we include a list of asymptotes in Table 15.

### *IV.A. Other Asymptotes*

As summarized in Table 4, all ultracold photoassociation begins in the free states of two colliding atoms, i.e., the $X^1\Sigma_g^+$ and $a^3\Sigma_u^+$ states at short range which correlate with the $0_g^+$ and the $0_u^-$ and $1_u$ states at long-range (Fig. 21). With spin–polarization it is possible to change the nominal 1:3 ratio of singlet to triplet collisions, e.g., (*91*) where only ungerade state collisions contribute. Nevertheless, it is clear that careful studies of intensities as opposed to simply energies of photoassociative transitions will require quantitative understanding of the lower state potentials at a level which predicts accurate scattering lengths, as discussed in Section III.D. Thus two-color PUMP-DUMP studies of $K_2$ analogous to those for other alkalis (e.g., (*70, 94*)) are now underway at the University of Connecticut.

The $4s + 4p$ asymptote has been extensively studied, but new possibilities will be discussed in Sections IV.C and IV.G.

The $4s + ns$ ($n > 4$) asymptotes have been studied only for $n = 6$ and 7. An interesting question is the scaling with $n$ (or $n^* = n - \delta$, where $\delta$ is the quantum defect). The situation is particularly simple for these asymptotes since there is no spin–orbit splitting. The four short-range states are now $^1\Sigma_g^+$, $^1\Sigma_u^+$, $^3\Sigma_g^+$, and $^3\Sigma_u^+$ with six unique correlating long-range states $0_g^+$, $0_u^+$, $0_g^-$ and $1_g$, and $0_u^-$ and $1_u$, respectively. Thus there is no mixing in the absence of hyperfine interactions. It is clear that such states (e.g., $1_u$) can be readily observed (*63*) for $n = 6$ and 7; going to higher $n$ ($8 \leq n < \infty$) is possible by using a range of visible laser dyes. The scaling of $C_6$ (and $C_8$ and $C_{10}$) coefficients with $n^*$ was predicted long ago (*153, 175*) and has been verified for $n = 6$ and 7. Note also that $R_{\mathrm{LR}m}$, the distance outside which the inverse power expansion is accurate, scales like $(n^*)^2$. Likewise there is a distance $R_{\mathrm{CRIT}}$ (*175*) at which

$$C_8 R_{\mathrm{CRIT}}^{-8} = C_6 R_{\mathrm{CRIT}}^{-6};$$

that is, where

$$R_{\mathrm{CRIT}} = (C_8/C_6)^{1/2}$$

and inside which the long-range inverse power expansion clearly diverges. $R_{\mathrm{CRIT}}$ also scales as $(n^*)^2$ (*175*). Fortunately, $R_{\mathrm{CRIT}}$ seems always to be significantly less than $R_{\mathrm{LR}m}$, e.g., the $n = 6$ values of $R_{\mathrm{CRIT}}$ and $R_{\mathrm{LR}m}$ are 17.53 and 39.89 Å, respectively.

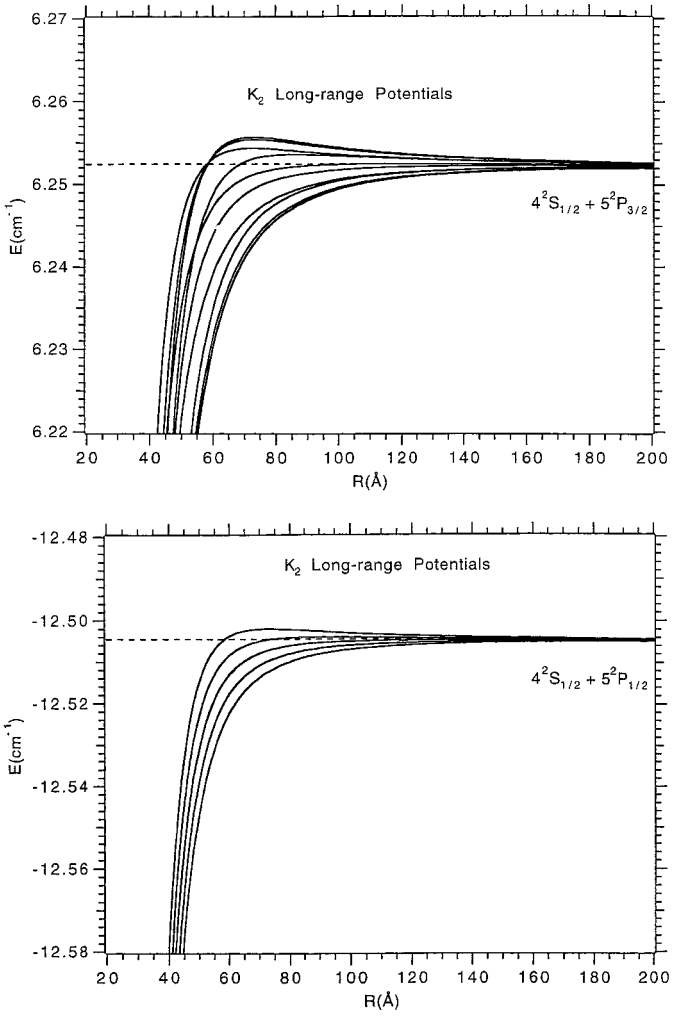


**FIG. 31.** The long-range potential energy curves of $K_2$ near the $4s + 5p_{3/2}$ (upper figure) and $4s + 5p_{1/2}$ (lower figure) asymptotes. Note the structure is very different from the $4s + 4p$ asymptotes (Figure 22). In particular, there are now no states with minima (pure long-range molecules) and many states with maxima (pure long-range barriers).

The $4s + nl$ asymptotes ($l > 0$) are also of interest, although only the $4s + n''d$ ($n'' = 4, 5, 6$) asymptotes have been studied. The $4s + n'p$ asymptotes ($n' \geq 5$) have quite different structure from the $4s + 4p$ asymptotes in Fig. 22. For example, the curves for $n' = 5$ are given in Fig. 31. The atomic oscillator strength of the $4s \rightarrow 4p$ transition is nearly the Thomas–Reiche–Kuhn sum rule value of unity, leaving little oscillator strength for the other $n'p$ levels ($n' \geq 5$). The NBS (now NIST) compilation (*176*) lists the oscillator strengths for $4s \rightarrow 5p$ to $13p$ as $9.1 \times 10^{-3}$ to $6.7 \times 10^{-6}$ compared to 1.02 for $4s \rightarrow 4p$. Consequently, the $C_3$ coefficients (proportional to the oscillator strengths) for the $4s + n'p$ asymptotes are at least two orders of magnitude smaller than the $C_3$ coefficient for $4s + 4p$ given in Table 11. As a result, the $4s + n'p$ asymptotes are highly influenced by their

(larger) $C_6$ values, and the structure does not include any accessible states with minima, such as the pure long-range molecule states which are described in Section III.B.

Observation of the $4s + n''d$, $n'''f$, . . . , levels appears to be primarily of purely academic interest, although the near degeneracy of high-$l$ levels might complicate the structure in interesting ways.

The $4p + 4p$ asymptotes are of major interest in quantitative understanding of intensities, since all "one-color" experiments (often saturated) have a reasonable probability of two-photon excitation to the $4p + 4p$ asymptotes. We have preliminary and fascinating calculations of the 23 Hund's case c states at the $4p + 4p$ asymptotes: $4(0_g^+)$, $1(0_g^-)$, $3(1_g)$, $2(2_g)$, $2(0_u^+)$, $3(0_u^-)$, $5(1_u)$, $2(2_u)$, and $1(3_u)$. Fortunately, the complex correlation diagram was worked out (*120*) for the analogous case of $B(2p) + B(2p)$; see also the calculations for Na($3p$) + Na($3p$) (*81, 151*). Moreover, accurate $C_n$ coefficients are now available (*164*). The situation is much simpler in $K_2$ (where the $4s + 5p$ and $4s + 4d$ asymptotes are over 1000 $cm^{-1}$ away) than in the most studied case of $Na_2$ (where the $3s + 5s$ and $3s + 4d$ asymptotes are close to the $3p + 3p$ asymptotes, as is the ion pair curve ($Na^+ + Na^-$) and the $Na_2^+$ potential minimum). As noted in Section III.E, there are several predicted extrema in potential curves near the $4p + 4p$ asymptotes. More importantly, a quantitative understanding (including intensities) of the trap and its interaction with light of near resonant wavelengths requires the understanding of $4s + 4p \rightarrow 4p + 4p$ excitation as well as $4s + 4s \rightarrow 4s + 4p$. Potassium, with its larger spin–orbit splitting and accurate electronic structure and long-range calculations, is the ideal test case. For example, we believe the large and somewhat frequency-dependent background of $4p_{1/2}$ atoms in Fig. 14 includes $4s + 4p \rightarrow 4p + 4p$ processes.

It might also be noted that the fragmentation spectroscopy technique (Section II.A.3) might be particularly useful in the case of "interacting asymptotes." For example, the $6s$ level of $^{39}K$ is only 53 $cm^{-1}$ above the $4d$ levels. Thus bound states below the $4s + 6s$ limit may predissociate to the $4s + 4d$ asymptotes (the "negative energy" bound-state analog of $6s \rightarrow 4d$ ultracold energy transfer). Such processes could be monitored by $4d$ resonance-enhanced multiphoton ionization or fluorescence.

Finally, it should be noted that photoassociation can allow one to access intermediate range (6–20 Å) features that are not readily accessed from $R_e$ of the ground state of the molecule. For example, the $3^1\Pi_g$ state of $Na_2$ has a short distance "Rydberg" potential, an intermediate barrier above dissociation, and an unobserved outer well (*134*). To observe the outer well starting from the $Na_2$ $X^1\Sigma_g^+$ equilibrium distance, it is proposed that one use all-optical quadruple resonance (*134*) (which has not yet been achieved) as illustrated in Fig. 32. However, as also shown in Fig. 32, a two-color photoassociation may also be used to access the well (the first step $L_1'$ is well known).

### *IV.B. Photoassociative Ionization*

The topic of ultracold photoassociative ionization has a considerable history (*3*), not really covered in this review, particularly for Na. This is because collisions of two Na($3p$) atoms yield $Na_2^+$ by associative ionization (*177*). In contrast, for the other alkalis, collisions of two excited atoms in their lowest $n_{\min}p$ excited states do not yield ionization.

For K we envisage several kinds of experiments that would yield important information on the $K^+ + K^-$ asymptote, on $K^+ + K + e^-$ formation, on $K^+ + K(4p) + e^-$, and on $K_2^+ + e^-$ formation. Since the outgoing $e^-$ can be in a $g$ or a $u$ state, the selection rule constraints are significantly reduced. Attractive experiments to produce $K_2^+$ in its ground $1^2\Sigma_g^+$ state, for example, might start with photoassociation to the $1_g(4p_{3/2})$ or to the $0_u^+(4p_{1/2})$ long-range states; the short-range correlates of these states, the $1^1\Pi_g$ and $A^1\Sigma_u^+$ states, could easily be Franck–Condon state-selectively excited to the $K_2^+$ ground state. An analogous procedure for $Na_2$ is shown in Fig. 33, since in that case an autoionization resonance which can yield only $v = 0$, $N = 0$ of the ground state $Na_2^+$ ion is known (*178*). Similarly, the weakly bound $1^2\Sigma_u^+$ $K_2^+$ state might easily be produced via the pure long-range molecular $0_g^-(4p_{3/2})$ and $1_u(4p_{3/2})$ states.

The prospects for direct photoassociation from colliding neutral atoms to an ion pair are poor as $R$ increases. However, it is certainly possible to access the asymptotes which interact with the ion pair curve, as shown in Fig. 34 for $K_2$. Indeed, in $Na_2$ the $3^1\Sigma_g^+$–$4^1\Sigma_g^+$, $4^1\Sigma_g^+$–$5^1\Sigma_g^+$, and $5^1\Sigma_g^+$–$6^1\Sigma_g^+$ crossings have been thoroughly studied and found to be adiabatic (*106–110*). It is expected that $K_2$ will show similar behavior at least for the lower crossings.

### *IV.C. Three-Color Spectra*

The use of AOTR (*157, 179*) in the ultracold photoassociative domain should definitely be feasible. Such three-color spectra could offer important advantages. For example, one could then reach symmetry states previously forbidden. The $2_u$ and $0_u^-$ attractive states at the $4s + 4p$ asymptotes (Fig. 22) can be reached by using a DUMP laser from previously observed two-color-excited $g$ levels near the $4s + 4d$, $4s + 6s$ and $4s + 5d$ asymptotes. Likewise, these two-color excited levels could be used to access states near $4s + n'''f$ asymptotes.

More importantly, the DUMP laser just mentioned from, for example, the $4s + 5d$ asymptote to the $4s + 4p$ asymptote can provide resolved spectra right through the dissociation thresholds at the $4s + 4p_{3/2}$ (and also at the $4s + 4p_{1/2}$) asymptote. This is not possible in one-color experiments where the near resonant light interferes with the trap and where a variety of colliding pairs ($0_g^+$, $0_u^-$, and $1_u \otimes J = 0, 1, 2$) are excited.

### *IV.D. Formation of Ultracold Molecules*

Ultracold photoassociation is a leading technique for producing ultracold molecules (reviewed in (*19*)) and has been

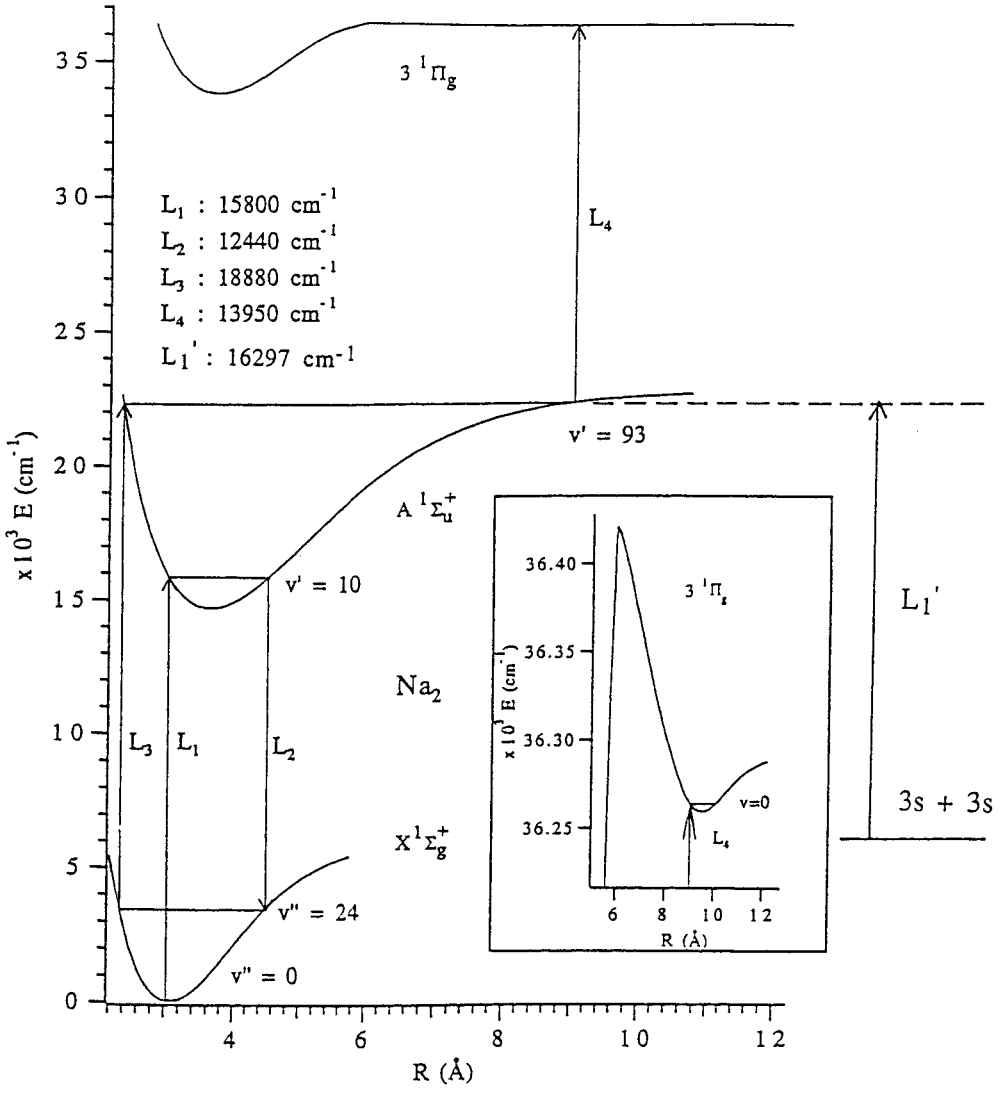


**FIG. 32.** Proposed schemes to access the outer well of the $3^1\Pi_g$ state of $Na_2$ (*134*). Scheme $L_1$-$L_2$-$L_3$-$L_4$ (*134*) corresponds to as yet unachieved all-optical quadruple resonance. Scheme $L_1'$–$L_4$, where $L_1'$ is a known photoassociation, is an attractive alternative.

used to produce translationally ultracold $K_2$ (*65*) and $Cs_2$ (*67, 68, 103, 104*) molecules.

The first results (*67*) on $Cs_2$ produced unspecified levels clearly in the metastable $a^3\Sigma_u^+$ state, which were detected by resonance-enhanced multiphoton ionization. Subsequent experiments (*68*) have partly assigned the spectra and provided evidence that some $X^1\Sigma_g^+$ ground state $Cs_2$ molecules are also being formed.

Our results on $K_2$ (*65*) clearly indicate that we are producing $v = 36$ of the $X^1\Sigma_g^+$ ground state of $^{39}K_2$ via photoassociation to a specific level (tentatively $v = 191$) of $A^1\Sigma_u^+ \sim 0_u^+$ $(4p_{1/2})$ state (Fig. 16). Level $v = 36$ is then resonance-enhanced two-photon ionized through various levels of the $B^1\Pi_u$ state (e.g., $v = 26$). The photoassociative spectrum detected by trap loss for the $0_u^+(4p_{1/2})$ state agrees with that detected by molecule formation (Fig. 8).

Other results (*103, 104*), where the trap laser does the photoassociation, produce an unspecified distribution of vibrational levels (probably near dissociation) in the $a^3\Sigma_u^+$ and possibly the $X^1\Sigma_g^+$ state of $Cs_2$. These results (*104*) include clear evidence of trapping $Cs_2$ molecules in an optical trap.

It is likely that future efforts will focus on finding more efficient and selective methods for production of translationally ultracold molecules and on employing methods giving narrower distributions involving only low vibrational levels of the ground $X^1\Sigma_g^+$ state for which an internal cooling scheme is available (*167*). Interesting suggestions include the two-color excitation scheme of (*166*) and the triplet state formation schemes of (*168, 169*). Of particular significance, in our opinion, are the stimulated Raman proposals (*180, 181*), which could directly produce state-selected molecules (perhaps even $v = 0$, $J = 0$ (*180*), and even a "molecule laser" from an atomic BEC (*181*)). Such a stimulated Raman process has been observed very recently in a BEC (98).

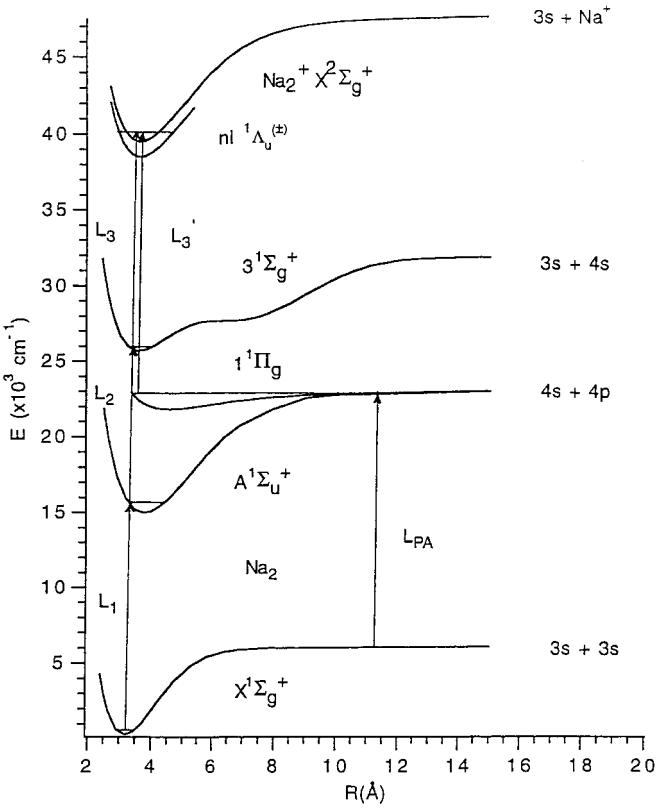


**FIG. 33.** Three color ($L_1$-$L_2$-$L_3$) doubly resonant photoionization of $Na_2$ (*178*) and proposed photoassociative ionization ($L_{PA}$–$L_3'$) of ultracold Na atoms via the $1_g(4p_{3/2})$ state, correlated with the $1^1\Pi_g$ state at short range. Both processes should access the same autoionization resonance (*178*) which energetically can produce only $v = 0$, $N = 0$ $Na_2^+$.

### *IV.E. Extension to Other Atoms*

An interesting question is how far beyond the homonuclear alkali metals one can extend the extraordinary spectroscopic results achieved with them. This is clearly an unanswered question since no ultracold photoassociative results have yet appeared for a nonalkali species except for a very recent result for H (*20*). In our opinion, we expect that results on other atoms will proliferate in the next decade, limited primarily by laser technology.

The simplest extension would be study of heteronuclear, homopolar species such as $^6Li^7Li$, $^{39}K^{41}K$, and $^{85}Rb^{87}Rb$. The spectroscopy of such species involves dual species traps and full understanding of single species spectra, but that is certainly feasible. Moreover, it is certain that interesting energy transfer processes between isotopes $M$ and $M'$ will occur because of the small splittings between isotopes. For example, excitation of $^{39}K^{41}K$ near the $^{39}K(4p_{3/2})$ level will produce $^{41}K(4p_{3/2})$ atoms detectable by REMPI.

The next simplest extension would be to truly heteronuclear species, e.g., $^{39}K^{85}Rb$. We have recently discussed the various aspects of such a study, e.g., photoassociation would occur to the $Rb(5p_{3/2}) + K(4s)$ and $Rb(5p_{1/2}) + K(4s)$ asymptotes, but not to the $Rb(5s) + K(4p_{3/2})$ and $Rb(5s) + K(4p_{1/2})$ asymptotes (*182*). We have also estimated the relative probabilities of photoassociation to Rb* + Rb versus Rb* + K (*182*) and are convinced one can obtain the KRb spectrum.

A further extension is to photoassociation of an alkali atom with a rare gas atom (e.g., $^4He$). From the considerations in (*182*) we expect to be able to distinguish an alkali metal–rare gas photoassociation. In particular, for the heavier alkalis ($M$ = K, Rb, Cs), the linewidth will be significantly broader for a $M$–He line than for an $M_2$ line.

Work on trapping of other atoms has been successful in many cases, including the alkaline earths (Mg, Ca, Sr), yttrium, and the metastable rare gases (*3*). For many other atoms, the question is what investment in cw laser technology can be provided to allow for cooling and trapping of a given atom. For example, the boron atom has transitions near 250 nm that could be used for cooling and trapping, which could be provided by doubling a dye laser or tripling a titanium:sapphire or Alexandrite laser into the UV.

### *IV.F. Extension to Atom–Molecule and Molecule–Molecule Collisions*

Since we expect alkali atom–rare gas atom photoassociative spectra to be observable (Section IV.E), alkali metal–$H_2$ spectra (ideally para-$H_2$ in $v = 0$, $J = 0$) should also be observable. Such an experiment (for Cs + $H_2$) is currently being assembled at the University of Connecticut.

There is already clear evidence for the existence of such excited states of metal–$H_2$ systems. For example, coherent anti-Stokes–Raman scattering of the $Na(3p)H_2$ complex has been carried out and modeled (*183*). Likewise, similar states have been observed in the photoexcitation of $MgD_2^+$ to the red of the $Mg^+(3p) + D_2$ dissociation limit (*184*).

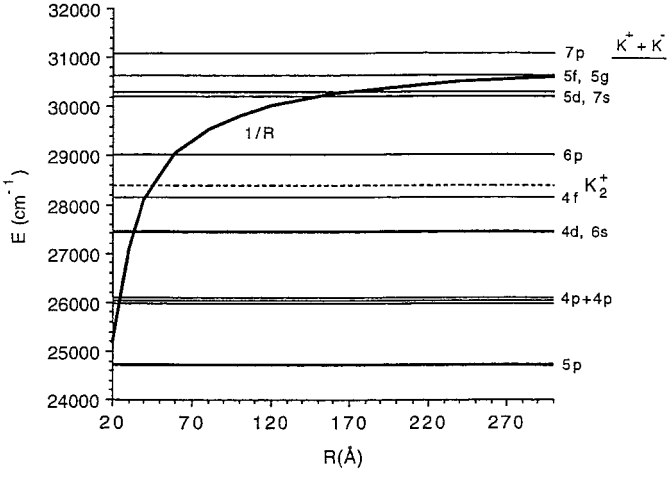


**FIG. 34.** The diabatic ion pair potential curve of $^{39}K_2$ compared to the various asymptotic diabatic potential energy curves (flat on this scale). While the lower crossings of these diabatic curves will yield widely separated adiabatic curves with predominantly adiabatic dynamics, the upper curves will yield predominantly diabatic dynamics. These crossings are in the region (20–200 Å) where ultracold photoassociation is particularly sensitive.

Alkali atom–alkali molecule photoassociation (to known short-range trimer states) should be attempted when a trap containing both at respectable densities ($>10^{10}$ cm$^3$) is available.

It is speculative to consider the possibility of molecule–molecule photoassociation. Nevertheless, if one can achieve a trap with reasonable density ($10^{10}$ cm$^3$) containing exclusively a ground state alkali dimer in $v = 0$, $J = 0$ (or possibly in $v = 0$, $J = 1$), it is likely that molecule–molecule photoassociation (and perhaps determination of the molecule–molecule scattering length) can be achieved.

### *IV.G. Extension to Free–Free Spectra*

One of the more difficult calculations of ultracold spectroscopy of alkali atoms is the free–free radiative transition probability. Indeed, this is the core for calculation of self-line broadening of alkali atoms in the limit when $T \rightarrow 0$ K. Such a calculation can certainly be made for blue-detuned laser frequencies for the $4s + 4p$ asymptotes of $^{39}K_2$. The fragmentation spectroscopy technique pioneered by (*64*) could in principle be used to detect the continuous free $\rightarrow$ free photoabsorption. However, the continuous photoabsorption does involve a sum over many electronic states and will not be as high in information content as a photoassociation spectrum. Nevertheless, the fragmentation spectra should reveal interesting results (e.g., the height of the barrier of the $1_u(4p_{1/2})$ pure long-range barrier state). In addition, blue-detuned quasibound levels may also be of considerable interest (*85, 185*).

More generally, the photoassociative spectra offer the opportunity to model *all* the potential curves which contribute to the broadening of an atomic spectral line. We anticipate that such broadening will be measured at very low temperatures and simultaneously accurately calculated from ultracold photoassociative spectroscopy.

### *IV.H. Influence of Electromagnetic Fields*

The AC and DC Stark and Zeeman effects of electromagnetic fields are clearly comparable to the collision energies important in a variety of experiments. To survey all possibilities is well beyond the scope of this review and is complicated by the fact that the trap itself imposes its own electromagnetic field on the problem. Nevertheless, it is clear that there are a great many opportunities to drastically modify the ultracold collisions and, therefore, the photoassociative spectra by tuning a field knob (e.g., (*186*)). For example, dramatic effects of tuning Feshbach resonances near dissociation with a magnetic field were presented in 1976 (*187*). In particular, an important spin–flip cross section was shown to increase from $10^{-8}\ a_0^2$ to $10\ a_0^2$ because of such a tunable resonance (*165*). Similar resonances were predicted in $Li_2$ (*188*). Recently, Feshbach resonances have been observed in a BEC of $^{23}$Na (*189*) and in trapped ultracold Rb (*95, 190*). Light or electric fields could similarly be used, e.g., (*191*).

## V. ACKNOWLEDGMENTS

The authors particularly acknowledge their experimental and theoretical collaborators on ultracold photoassociation: John Bahns, Ed Eyler, Phil Gould, Paul Julienne, Jing Li, Anguel Nikolov, Marin Pichler, Eite Tiesinga, Xiaotian Wang, Carl Williams, and Guoxing Zhao. The authors also acknowledge helpful discussions with a great many individuals including Claude Amiot, Mike Andrews, Vanderlei Bagnato, Yehuda Band, Klaas Bergmann, John Bohn, Jim Burke, Keith Burnett, Robin Côté, Alex Dalgarno, John Doyle, Oliver Dulieu, Bob Gordon, Chris Greene, Dan Heinzen, Randy Hulet, Juha Javanainen, Gwang-Hi Jeung, Paul Lett, Li Li, Marjatta Lyyra, Matt Mackie, Mircea Marinescu, Francoise Masnou-Seeuws, Fred Mies, Bill Phillips, Goran Pichler, Pierre Pillet, Amanda Ross, Tamar Seideman, Moshe Shapiro, Win Smith, Tony Starace, Boudewijn Verhaar, Udo Volz, John Weiner, Alexandra Yiannopoulou, and Warren Zemke. This work was supported in part by NSF CHE96-12207 and CHE 97-32467.

## REFERENCES

1. P. D. Lett, P. S. Julienne, and W. D. Phillips, Photoassociative spectroscopy of laser cooled atoms, *Ann. Rev. Phys. Chem.* **46,** 423–452 (1995).
2. D. J. Heinzen, Collisions of ultracold atoms in optical fields, *in* "Atomic Physics 14," (D. J. Wineland, C. E. Wieman, and S. J. Smith, Eds.), pp. 369–388, AIP Press, New York, 1995.
3. J. Weiner, V. S. Bagnato, S. C. Zilio, and P. S. Julienne, Experiments and theory in cold and ultracold collisions, *Rev. Mod. Phys.* **71,** 1–86 (1999).
4. W. C. Stwalley, Laser manipulation of metallic vapors, *in* "Radiation Energy Conversion in Space," (K. W. Billman, Ed.), Progress in Astronautics and Aeronautics, Vol. 61, pp. 593–601, 1978.
5. C. Amiot, J. Verges, and C. E. Fellows, The long-range potential of the $K_2X^1\Sigma_g^+$ ground electronic state up to 15 Å, *J. Chem. Phys.* **103,** 3350 (1995).
6. S. Magnier and Ph. Millie, Potential curves for the ground and numerous highly excited electronic states of $K_2$ and NaK, *Phys. Rev. A* **54,** 204–218 (1996); S. Magnier, Ph.D. thesis, University of Paris-Sud (Orsay), 1993.
7. H. E. Roscoe and A. Schuster, Note on the absorption spectra of potassium and sodium at low temperatures, *Proc. R. Soc. Lond.* **22,** 362–364 (1874).
8. J. Heinze and F. Engelke, The $B^1\Pi_u$ potential energy curve and dissociation energy of $^{39}K_2$, *J. Chem. Phys.* **89,** 42–50 (1988).
9. J. T. Kim, H. Wang, J. T. Bahns, and W. C. Stwalley, The $3^1\Pi_g$ and $3^1\Delta_g$ states of $^{39}K_2$ studied by optical–optical double resonance spectroscopy, *J. Chem. Phys.* **102,** 6966–6974 (1995).
10. J. T. Kim, H. Wang, C. C. Tsai, J. T. Bahns, W. C. Stwalley, G. Jong, and A. M. Lyyra, The $4^3\Sigma_g^+$, $3^3\Pi_g$, $2^3\Delta_g$ and $b^3\Pi_u$ states of $^{39}K_2$ studied by perturbation-facilitated optical–optical double resonance spectroscopy, *J. Chem. Phys.* **102,** 6646–6652 (1995); Erratum, **103,** 9891 (1995).
11. G. Jong, L. Li, T. J. Whang, A. M. Lyyra, W. C. Stwalley, M. Li, and J. Coxon, CW all optical triple resonance spectroscopy of $K_2$: deperturbation analysis of the $A^1\Sigma_u^+$ state ($v \leq 12$) and $b^3\Pi_u$ ($13 \leq v \leq 24$) states, *J. Mol. Spectrosc.* **155,** 115–135 (1992).
12. B. Ji, P. D. Kleiber, W. C. Stwalley, A. Yiannopoulou, A. M. Lyyra, and P. S. Julienne, Quantum state-selected photodissociation of $K_2$ ($B^1\Pi_u \leftarrow X^1\Sigma_g^+$): a case study of final state alignment in all-optical multiple resonance photodissociation, *J. Chem. Phys.* **102,** 2440–2451 (1995).
13. J. Higgins, C. Callegari, J. Reno, F. Stienkemeier, W. E. Ernst, M. Gutowski, and G. Scoles, Helium cluster isolation spectroscopy of alkali dimers in the triplet manifold, *J. Phys. Chem. A* **102,** 4952–4965 (1998).
14. A. J. Ross, C. Effantin, J. D'Incan, R. F. Barrow, and J. Vergès, The (1) $^1\Pi_g$ state of $K_2$ studied by infrared Fourier-transform spectroscopy, *Indian J. Phys. B* **60,** 309–317 (1986).
15. I. Russier, M. Aubert-Frécon, A. J. Ross, F. Martin, A. Yiannopoulou, and P. Crozet, The (1) $^1\Pi_g$ state of $^{39}K_2$ revisited, *J. Chem. Phys.* **109,** 2717–2726 (1998).
16. H. R. Thorsheim, J. Weiner, and P. S. Julienne, Laser-induced photoas-

sociation of ultracold sodium atoms, *Phys. Rev. Lett.* **58,** 2420–2423 (1987).
17. P. D. Lett, K. Helmerson, W. D. Phillips, L. P. Ratcliff, S. L. Rolston, and M. E. Wagshul, Spectroscopy of $Na_2$ by photoassociation of laser-cooled Na, *Phys. Rev. Lett.* **71,** 2200–2203 (1993).
18. J. D. Miller, R. A. Cline, and D. J. Heinzen, Photoassociation spectrum of ultracold rubidium atoms, *Phys. Rev. Lett.* **71,** 2204–2207 (1993).
19. J. T. Bahns, P. L. Gould, and W. C. Stwalley, Formation of cold ($T = 1$ K) molecules, submitted for publication.
20. A. P. Mosk, M. W. Reynolds, T. J. Hijmans, and J. T. M. Walraven, Photoassociation of spin-polarized hydrogen, *Phys. Rev. Lett.* **82,** 307–310 (1999).
21. W. Finkelnburg, "Kontinuerliche Spektren," Springer-Verlag, Berlin, 1938.
22. G. Herzberg, "Molecular Spectra and Molecular Structure. I. Spectra of Diatomic Molecules," Van Nostrand, Princeton, NJ 1950.
23. W. Finkelnburg and T. Peters, Kontinuerliche spektren *in* "Spektroskopie II," (S. Flugge, Ed.), Handbuch der Physik, Vol. 28, pp. 79–204, Springer-Verlag, Berlin, 1957.
24. J. M. Walter and S. Barratt, The existence of intermetallic compounds in the vapour state. The spectra of the alkali metals, and their alloys with each other, *Proc. R. Soc. Lond.* **119,** 257–275 (1928).
25. G. Pichler, S. Milosevic, D. Veza, and R. Beuc, Diffuse bands in the visible absorption spectra of dense alkali vapours, *J. Phys. B* **16,** 4619–4631 (1983).
26. D. E. Johnson and J. G. Eden, Continua in the visible absorption spectrum of $K_2$, *J. Opt. Soc. Am. B* **2,** 721–728 (1985).
27. W. T. Luh, K. M. Sando, A. M. Lyyra, and W. C. Stwalley, Free-bound–free resonance fluorescence in the $K_2$ yellow diffuse band: Theory and experiment, *Chem. Phys. Lett.* **144,** 221–225 (1988).
28. W. T. Luh, J. T. Bahns, A. M. Lyyra, K. M. Sando, P. D. Kleiber, and W. C. Stwalley, Direct excitation studies of the diffuse bands of alkali metal dimers, *J. Chem. Phys.* **88,** 2235–2241 (1988).
29. C. S. Adams and E. Riis, Laser cooling and trapping of neutral atoms, *Prog. Quant. Electr.* **21,** 1–79 (1997).
30. S. Chu, The manipulation of neutral particles, *Rev. Mod. Phys.* **70,** 685–706 (1998).
31. C. N. Cohen-Tannoudji, Manipulating atoms with photons, *Rev. Mod. Phys.* **70,** 707–720 (1998).
32. W. D. Phillips, Laser cooling and trapping of neutral atoms, *Rev. Mod. Phys.* **70,** 721–742 (1998).
33. H. Metcalf and P. van der Straten, Cooling and trapping of neutral atoms, *Phys. Rep.* **244,** 203–286 (1994).
34. T. Walker and P. Feng, Measurements of collisions between laser-cooled atoms, *Adv. At. Mol. Opt. Phys.* **34,** 125–170 (1994).
35. J. Weiner, Advances in ultracold collisions: experimentation and theory, *Adv. At. Mol. Opt. Phys.* **35,** 45–78 (1995).
36. H. Wang, P. L. Gould, and W. C. Stwalley, Photoassociative spectroscopy of ultracold $^{39}$K atoms in a high-density vapor cell magneto-optical trap, *Phys. Rev. A* **53,** R1216-R1219 (1996).
37. H. Wang, P. L. Gould, and W. C. Stwalley, The long-range interaction of $^{39}K(4s) + {}^{39}K(4p)$ asymptote by photoassociative spectroscopy: Part I: The $O_g^-$ pure long-range state and the long-range potential constants, *J. Chem. Phys.* **106,** 7899–7912 (1997).
38. W. Ketterle, K. Davis, M. Joffe, A. Martin, and D. E. Pritchard, High densities of cold atoms in a dark spontaneous-force optical trap, *Phys. Rev. Lett.* **70,** 2253–2256 (1993).
39. G. Zhao, W. T. Zemke, J. T. Kim, B. Ji, H. Wang, J. T. Bahns, W. C. Stwalley, Li Li, A. M. Lyyra, and C. Amiot, New measurements of the $a^3\Sigma_u^+$ state of $K_2$ and analysis of long-range dispersion and exchange interactions between two K atoms, *J. Chem. Phys.* **105,** 7976–7985 (1996).
40. C. J. Williams and P. S. Julienne, Molecular hyperfine structure in the photoassociation spectroscopy of laser cooled atoms, *J. Chem. Phys.* **101,** 2634–2637 (1994).
41. C. J. Williams, E. Tiesinga, and P. S. Julienne, Hyperfine structure of the $Na_2$ $O_g^-$ long-range molecular state, *Phys. Rev. A* **53,** R1939-R1942 (1996).
42. E. Tiesinga, C. J. Williams, and P. S. Julienne, Photoassociation spectroscopy of highly excited vibrational levels of alkali dimers: Greens function approach for eigenvalue solvers, *Phys. Rev. A* **57,** 4257–4267 (1997).
43. R. Napolitano, J. Weiner, C. J. Williams, and P. S. Julienne, Line shapes of high resolution photoassociation spectra of optically cooled atoms, *Phys. Rev. Lett.* **73,** 1352–1355 (1994).
44. O. Dulieu and P. S. Julienne, Coupled channel bound states calculations for alkali dimers using the Fourier grid method, *J. Chem. Phys.* **103,** 60–66 (1995).
45. J. L. Bohn and P. S. Julienne, Semianalytic treatment of two-color photoassociation spectroscopy and control of cold atoms, *Phys. Rev. A* **54,** R4637–R4640 (1996).
46. K. Burnett, P. S. Julienne, and K.-A. Souminen, Laser driven collisions between atoms in a Bose–Einstein condensed gas, *Phys. Rev. Lett.* **77,** 1416–1419 (1996).
47. K. M. Jones, S. Maleki, S. Bize, P. D. Lett, C. J. Williams, H. Richling, H. Knöckel, E. Tiemann, H. Wang, P. L. Gould, and W. C. Stwalley, Direct measurement of the ground state dissociation energy of $Na_2$, *Phys. Rev. A* **54,** R1006–R1009 (1996).
48. W. I. McAlexander, E. R. I. Abraham, and R. G. Hulet, Radiative lifetime of the $2P$ state of lithium, *Phys. Rev. A* **54,** R5–R8 (1996).
49. K. M. Jones, P. S. Julienne, P. D. Lett, W. D. Phillips, E. Tiesinga, and C. J. Williams, Observation of retardation in the interaction between two Na atoms bound in a molecule and a determination of the atomic $3p$ lifetime, *Europhys. Lett.* **35,** 85–90 (1996).
50. H. Wang, J. Li, X. T. Wang, C. J. Williams, P. L. Gould, and W. C. Stwalley, Precise determination of the dipole matrix element and radiative lifetimes of the $^{39}$K $4p$ states by photoassociative spectroscopy, *Phys. Rev. A* **55,** R1569–R1572 (1997).
51. R. S. Freeland, C. C. Tsai, R. A. Cline, J. D. Miller, D. J. Heinzen, M. Marinescu, and A. Dalgarno, Precise Rb $5p$ state radiative lifetime, submitted for publication.
52. J. D. Miller, R. A. Cline, and D. J. Heinzen, Far-off-resonance trapping of atoms, *Phys. Rev. A* **47,** R4567-R4570 (1993).
53. C. J. Lorenzen and K. Niemax, Quantum defects of the $n^2P_{1/2,3/2}$ levels in $^{39}$KI and $^{85}$RbI, *Phys. Scr.* **27,** 300–305 (1983).
54. M. Broyer, J. Chevaleyre, G. Delacretaz, S. Martin, and L. Wöste, $K_2$ Rydberg state analysis by two- and three-photon ionization, *Chem. Phys. Lett.* **99,** 206–212 (1983).
55. C. Corliss and J. Sugar, Energy levels of potassium, KI through KXIX, *J. Phys. Chem. Ref. Data* **8,** 1109–1145 (1979).
56. C. E. Moore, "Atomic Energy Levels, Vol. I," NSRDS-35 U.S. Government Printing Office, Washington, DC, 1971.
57. C. J. Lorenzen, K. Niemax, and L. R. Pendrill, Precise measurements of $^{39}$K $ns$ and $nd$ energy levels with an evacuated wavemeter, *Opt. Commun.* **39,** 370–374 (1981).
58. C. Amiot, The $X^1\Sigma_g^+$ electronic state of $K_2$, *J. Mol. Spectrosc.* **146,** 370–382 (1991).
59. L. Li, A. M. Lyyra, W. T. Luh, and W. C. Stwalley, Observation of the $^{39}K_2$ $a^3\Sigma_u^+$ state by perturbation facilitated optical–optical double resonance resolved fluorescence spectroscopy, *J. Chem. Phys.* **93,** 8452–8463 (1990).
60. W. Mueller and W. Meyer, Ground state properties of alkali dimers and their cations (including the elements Li, Na, and K) from ab initio calculations with effective core polarization potentials, *J. Chem. Phys.* **80,** 3311–3320 (1984).
61. E. Ilyabaev and U. Kaldor, Ground and excited states of $K_2$ and $K_2^+$ by the open shell coupled-cluster method, *J. Chem. Phys.* **98,** 7126–7131 (1993).
62. J. Slater, F. H. Read, S. E. Novick, and W. C. Lineberger, Alkali negative ions. III. Multichannel photodetachment study of $Cs^-$ and $K^-$, *Phys. Rev. A* **17,** 201–213 (1978).

63. H. Wang, X. T. Wang, P. L. Gould, and W. C. Stwalley, Optical–optical double resonance photoassociative spectroscopy of ultracold $^{39}K$ atoms near highly-excited asymptotes, *Phys. Rev. Lett.* **78,** 4173–4176 (1997).
64. H. Wang, P. L. Gould, and W. C. Stwalley, Fine structure predissociation of ultracold photoassociated $^{39}K_2$ molecules observed by fragmentation spectroscopy, *Phys. Rev. Lett.* **80,** 476–479 (1998).
65. A. N. Nikolov, E. E. Eyler, X. Wang, J. Li, H. Wang, W. C. Stwalley, and P. L. Gould, Observation of translationally ultracold ground state potassium molecules, *Phys. Rev. Lett.* **82,** 703–706 (1999).
66. R. Côté and A. Dalgarno, Photoassociation intensities and radiative trap loss in lithium, *Phys. Rev. A* **58,** 498–508 (1998).
67. A. Fioretti, D. Comparat, A. Crubellier, O. Dulieu, F. Masnou-Seeuws, and P. Pillet, $Cs_2$ cold molecules formation through photoassociative scheme in a Cs vapor-cell magneto–optical trap, *Phys. Rev. Lett.* **80,** 4402–4405 (1998).
68. A. Fioretti, D. Comparat, C. Drag, C. Amiot, O. Dulieu, F. Masnou-Seeuws, and P. Pillet, Photoassociative spectroscopy of the $Cs_2$ $O_g^-$ long-range state, *Eur. Phys. J.* in press.
69. E. R. I. Abraham, N. W. M. Ritchie, W. I. McAlexander, and R. G. Hulet, Photoassociative spectroscopy of long-range states of ultracold $^6Li_2$ and $^7Li_2$, *J. Chem. Phys.* **103,** 7773–7778 (1995).
70. E. R. I. Abraham, W. I. McAlexander, C. A. Sackett, and R. G. Hulet, Spectroscopic determination of the *s*-wave scattering length of lithium, *Phys. Rev. Lett.* **74,** 1315–1318 (1995).
71. R. Côté, A. Dalgarno, Y. Sun, and R. G. Hulet, Photoabsorption by ultracold atoms and the scattering length, *Phys. Rev. Lett.* **74,** 3581–3583 (1995).
72. W. I. McAlexander, E. R. I. Abraham, N. W. M. Ritchie, C. J. Williams, H. T. C. Stoof, and R. G. Hulet, Precise atomic radiative lifetime via photoassociative spectroscopy of ultracold lithium, *Phys. Rev. A* **51,** R871–R874 (1995).
73. N. W. M. Ritchie, E. R. I. Abraham, Y. Y. Xiao, C. C. Bradley, R. G. Hulet, and P. S. Julienne, Trap-loss collisions of ultracold lithium atoms, *Phys. Rev. A* **51,** R890–R893 (1995).
74. E. R. I. Abraham, W. I. McAlexander, H. T. C. Stoof, and R. G. Hulet, Hyperfine structure in photoassociative spectra of $^6Li_2$ and $^7Li_2$, *Phys. Rev. A* **53,** 3092–3097 (1996).
75. E. R. I. Abraham, W. I. McAlexander, J. M. Gerton, R. G. Hulet, R Côté, and A. Dalgarno, Singlet *s*-wave scattering lengths of $^6$Li and $^7$Li, *Phys. Rev. A* **53,** R3713-R3715 (1996).
76. E. R. I. Abraham, W. I. McAlexander, J. M. Gerton, R. G. Hulet, R Côté, and A. Dalgarno, Triplet *s*-wave resonance in $^6$Li collisions and scattering lengths of $^6$Li and $^7$Li, *Phys. Rev. A* **55,** R3299-R3302 (1997).
77. V. Bagnato, L. Marcassa, C. Tsao, Y. Wang, and J. Weiner, Two-color spectroscopy of colliding ultracold atoms, *Phys. Rev. Lett.* **70,** 3225–3228 (1993).
78. V. Bagnato, L. Marcassa, Y. Wang, J. Weiner, P. S. Julienne, and Y. B. Band, Ultracold photoassociative ionization collisions in a magneto-optical trap: the optical-field-intensity dependence in a radiatively dissipative environment, *Phys. Rev. A* **48,** R2523–R2526 (1993).
79. V. Bagnato, J. Weiner, P. S. Julienne, and C. J. Williams, Long-range molecular states and ultracold photoassociative ionization collisions, *Laser Phy.* **4,** 1062–1065 (1994).
80. L. P. Ratliff, M. E. Wagshul, P. D. Lett, S. L. Rolston, and W. D. Phillips, Photoassociative spectroscopy of $1_g$, $O_u^+$, and $O_g^-$ states of $Na_2$, *J. Chem. Phys.* **101,** 2638–2641 (1994).
81. O. Dulieu, B. Levy, S. Magnier, F. Masnou-Seeuws, and Ph. Millie, Long-range potentials for two Na(3*p*) atoms including ionic-covalent interaction and fine structure: application to two-color photoassociation spectroscopy, *Phys. Rev. Lett.* **76,** 2858–2861 (1996).
82. P. D. Lett, K. Molmer, S. D. Gensemer, K. Y. N. Tan, A. Kumarakrishnan, C. D. Wallace, and P. L. Gould, Hyperfine structure modifications of collisional losses from light-force atomic traps, *J. Phys. B* **28,** 65–81 (1995).
83. P. A. Molenaar, P. van der Straten, and H. G. M. Heideman, Long-range predissociation in two-color photoassociation of ultracold Na atoms, *Phys. Rev. Lett.* **77,** 1460–1463 (1996).
84. E. Tiesinga, C. J. Williams, P. S. Julienne, K. M. Jones, P. D. Lett, and W. D. Phillips, A spectroscopic determination of scattering lengths for sodium atom collisions, *J. Res. Natl. Inst. Stand. Technol.* **101,** 505–520 (1996).
85. O. Dulieu, R. Kosloff, F. Masnou-Seeuws, and G. Pichler, Quasibound states in long-range alkali dimers: grid method calculations, *J. Chem. Phys.* **107,** 10633–10642 (1997).
86. K. M. Jones, S. Maleki, L. P. Ratliff, and P. D. Lett, Two-colour photoassociation of ultracold sodium, *J. Phys. B* **30,** 289–308 (1997).
87. H. Wang, P. L. Gould, and W. C. Stwalley, Photoassociative spectroscopy of pure long-range molecules, *Z. Phys. D* **36,** 317–323 (1996).
88. X. T. Wang, H. Wang, P. L. Gould, and W. C. Stwalley, Observation of the pure long-range $1_u$ state of an alkali–metal dimer by photoassociative spectroscopy, *Phys. Rev. A* **57,** 4600–4603 (1998).
89. R. A. Cline, J. D. Miller, and D. J. Heinzen, Study of $Rb_2$ long-range states by high-resolution photoassociation spectroscopy, *Phys. Rev. Lett.* **73,** 632–635 (1994); Erratum, **73,** 2636 (1994).
90. C. Amiot, Analysis of spectra obtained by cold-atom photoassociation spectroscopy: the $Rb_2 1_g$ and $0_g^-$ electronic states up to 100 Å, *Chem. Phys. Lett.* **241,** 133 (1995).
91. J. R. Gardner, R. A. Cline, J. D. Miller, D. J. Heinzen, H. M. J. M. Boesten, and B. J. Verhaar, Collisions of doubly spin-polarized, ultracold $^{85}$Rb Atoms, *Phys. Rev. Lett.* **74,** 3764–3767 (1995).
92. D. Leonhardt and J. Weiner, Direct two-color photoassociative ionization in a rubidium magneto-optic trap, *Phys. Rev. A* **52,** R4332–4335 (1995); Erratum, **53,** 2904 (1996).
93. H. M. J. M. Boesten, C. C. Tsai, B. J. Verhaar, and D. J. Heinzen, Observation of a shape resonance in cold-atom scattering by pulsed photoassociation, *Phys. Rev. Lett.* **77,** 5194–5197 (1996).
94. C. C. Tsai, R. S. Freeland, J. M. Vogels, H. M. J. M. Boesten, B. J. Verhaar, and D. J. Heinzen, Two-color photoassociation spectroscopy of ground state $Rb_2$, *Phys. Rev. Lett.* **79,** 1245–1248 (1997).
95. P. Courteille, R. S. Freeland, D. J. Heinzen, F. A. van Abeelen, and B. J. Verhaar, Observation of a Feshbach resonance in cold atom scattering, *Phys. Rev. Lett.* **81,** 69–72 (1998).
96. E. Tiesinga, P. S. Julienne, Y. Huang, D. Hoffman, C. C. Tsai, and D. J. Heinzen, Hyperfine structure of Rb photoassociation spectra, submitted for publication.
97. C. C. Tsai, J. D. Miller, R. A. Cline, D. J. Heinzen, and C. Amiot, Accurate dissociation energy of the $Rb_2$ ground state $X^1\Sigma_g^+$ from photoassociation spectroscopy of the $1^1\Pi_g$ state, submitted for publication.
98. R. H. Wynar, R. S. Freeland, D. J. Han, and D. J. Heinzen, Stimulated Raman atom–molecule resonance in a Bose–Einstein condensate, submitted for publication.
99. D. Comparat, C. Drag, A. Fieretti, O. Dulieu, and P. Pillet, Photoassociative spectroscopy and formation of cold molecules in cold cesium vapor: trap-loss spectrum versus ion spectrum, submitted for publication.
100. A. Fioretti, D. Comparat, C. Drag, C. Amiot, O. Dulieu, F. Masnou-Seeuws, and P. Pillet, Long-range forces between cold atoms, submitted for publication.
101. C. B. Collins, F. W. Lee, P. A. Vicharelli, D. Popescu, and I. Popescu, Selective photolysis and photoionization of alkali metal dimers, *in* "Metal Bonding and Interactions in High Temperature Systems," (J. L. Gole and W. C. Stwalley, Eds.), ACS Symposium Series 179, American Chemical Society, p. 19–32, Washington, DC 1982.
102. J. X. Wang, H. Wang, P. D. Kleiber, A. M. Lyyra, and W. C. Stwalley, State-selected photodissociation of the $B^1\Pi_u$ state of $K_2$ by all-optical triple resonance spectroscopy, *J. Phys. Chem.* **95,** 8040–8044 (1991).
103. T. Takekoshi, B. M. Patterson, and R. J. Knize, Observation of cold ground state cesium molecules produced in a magneto-optical trap, *Phys. Rev. A* **51,** R5–R7 (1999).

*104.* T. Takekoshi, B. M. Paterson, and R. J. Knize, Observation of optically trapped cold cesium molecules, *Phys. Rev. Lett.* **81,** 5105–5108 (1998).

*105.* O. Dulieu, P. D. Lett, K. Jones, U. Volz, C. Amiot, and F. Masnou-Seeuws, Interpretation of two-color photoassociation spectroscopy experiments in a cold sodium sample: evidence for a $^1\Pi_u$ doubly-excited autoionizing state, *in* "Abstracts of Contributed Papers of the 20th International Conference on the Physics of Electronic and Atomic Collisions, Vienna, 1997," (F. Aumayr, G. Getz, and H. P. Winter, Eds.).

*106.* C. C. Tsai, J. T. Bahns, T. J. Whang, H. Wang, and W. C. Stwalley, Optical–optical double resonance spectroscopy of the $^1\Sigma_g^+$ "shelf" states and $^1\Pi_g$ states of $Na_2$ using an ultrasensitive ionization detector, *Phys. Rev. Lett.* **71,** 1152–1155 (1993).

*107.* C. C. Tsai, T. J. Whang, J. T. Bahns, and W. C. Stwalley, The $3^1\Sigma_g^+$ "shelf" state of $Na_2$, *J. Chem. Phys.* **99,** 8480–8488 (1993).

*108.* C. C. Tsai, J. T. Bahns, H. Wang, and W. C. Stwalley, Optical–optical double resonance spectroscopy of the $4^1\Sigma_g^+$ "shelf" state of $Na_2$ using an ultrasensitive ionization detector, *J. Chem. Phys.* **101,** 25–30 (1994).

*109.* C. C. Tsai, J. T. Bahns, and W. C. Stwalley, Optical–optical double resonance spectroscopy of the $6^1\Sigma_g^+$ "shelf" state of $Na_2$ using an ultrasensitive ionization detector, *J. Mol. Spectrosc.* **167,** 429–436 (1994).

*110.* C. C. Tsai, J. T. Bahns, and W. C. Stwalley, Optical–optical double resonance spectroscopy of the $5^1\Sigma_g^+$ "shelf" state of $Na_2$ using an ultrasensitive ionization detector, *J. Chem. Phys.* **100,** 768–774 (1994).

*111.* J. Li, J. Zhang, H. Wang, and W. C. Stwalley, Observation of the $5^1\Pi_u$, $6^1\Sigma_u^+$ and $7^1\Sigma_u^+$ states of $Na_2$ through a Franck–Condon window by all-optical triple resonance spectroscopy, *J. Chem. Phys.* **109,** 102–107 (1998).

*112.* R. J. Le Roy, *in* "Molecular Spectroscopy 1," (R. F. Barrow et al., Eds.), p. 113–176, Chemical Society, London, 1973.

*113.* W. C. Stwalley, Long-range molecules, *Contemp. Phys.* **19,** 65–80 (1978).

*114.* M. Marinescu, private communication.

*115.* E. I. Dashevskaya, V. I. Voronin, and E. E. Nikitin, Theory of excitation transfer in collisions between alkali atoms. I. Identical partners, *Can. J. Phys.* **47,** 1237–1248 (1969).

*116.* M. Movre and G. Pichler, Resonance interaction and self-broadening of alkali resonance lines. I. Adiabatic potential curves, *J. Phys. B* **10,** 2631–2638 (1977).

*117.* W. C. Stwalley, Y. H. Uang, and G. Pichler, Pure long-range molecules, *Phys. Rev. Lett.* **41,** 1164–1167 (1978).

*118.* B. Bussery and M. Aubert-Frécon, Multipolar long-range electrostatic, dispersion, and induction energy terms for the interaction between two identical alkali atoms Li, Na, K, Rb, and Cs in various electronic states, *J. Chem. Phys.* **82,** 3224–3234 (1985).

*119.* B. Bussery and M. Aubert-Frécon, Potential energy curves and vibration-rotation energies for the two purely long-range bound states $1_u$ and $O_g^-$ of the alkali dimers $M_2$ dissociating to $M(ns^2S_{1/2}) + M(np^2P_{3/2})$ with $M$ = Li, Na, K, Rb, and Cs *J. Mol. Spectrosc.* **113,** 21–27 (1985).

*120.* T. Y. Chang, Moderately long-range interatomic forces, *Rev. Mod. Phys.* **39,** 911–942 (1967).

*121.* A. Dalgarno, New methods for calculating long-range intermolecular forces, *Adv. Chem. Phys.* **12,** 143–166 (1967).

*122.* B. Ji, C.-C. Tsai, and W. C. Stwalley, Proposed modification of the criterion for the region of validity of the inverse-power expansion in diatomic long-range potentials, *Chem. Phys. Lett.* **236,** 242–246 (1995).

*123.* R. J. Le Roy and R. B. Bernstein, Dissociation energy and long-range potential of diatomic molecules from vibration spacings of higher levels, *J. Chem. Phys.* **52,** 3869–3879 (1970).

*124.* W. C. Stwalley, The dissociation energy of the hydrogen molecule using long-range forces, *Chem. Phys. Lett.* **6,** 241–244 (1970).

*125.* W. T. Zemke and W. C. Stwalley, Analysis of long-range dispersion and exchange interactions of two Li atoms, *J. Phys. Chem.* **97,** 2053–2058 (1993).

*126.* C. Amiot, Laser-induced fluorescence of $Rb_2$: The (1) $^1\Sigma_g^+$ $(X)$, (2) $^1\Sigma_u^+$, (1) $^1\Pi_u(B)$, and (1) $^1\Pi_u(C)$ electronic states, *J. Chem. Phys.* **93,** 8591–8604 (1990).

*127.* H. Weickenmeier, U. Diemer, M. Wahl, M. Raab, and W. Demtroeder, Accurate Ground state potential of $Cs_2$ up to the dissociation limit, *J. Chem. Phys.* **82,** 5354–5363 (1985).

*128.* E. A. Power, Very long-range (retardation effect) intermolecular forces, *Adv. Chem. Phys.* **12,** 167–224 (1967).

*129.* F. Vignemaeder, Excited alkali atoms: polarizabilities and van der Waals coefficients for resonant interactions, *Chem. Phys.* **85,** 139–148 (1984).

*130.* M. Marinescu and A. Dalgarno, Dispersion forces and long-range electronic transition dipole moments of alkali metal dimer excited states, *Phys. Rev. A* **52,** 311–328 (1995).

*131.* M. Marinescu and A. Dalgarno, Analytical interaction potentials of the long-range alkali metal dimers, *Z. Phys. D.* **36,** 239–248 (1996).

*132.* D. Kleppner, "Phys. Today," July 1995, p. 11.

*133.* B. Ji, A. Yiannopoulou, P. D. Kleiber, A. M. Lyyra, and W. C. Stwalley, Final state alignment from the quantum state-selected photodissociation of $K_2$ by all-optical triple resonance spectroscopy, *Phys. Rev. A* **49,** R1535–R1538 (1994).

*134.* C. C. Tsai, J. T. Bahns, and W. C. Stwalley, First observation of the quasibound levels and tunneling line broadening in the $3^1\Pi_g$ state of $Na_2$ using an ultrasensitive ionization detector, *J. Chem. Phys.* **99,** 7417–7423 (1993).

*135.* P. S. Julienne, Cold binary atomic collisions in a light field, *J. Res. Natl. Inst. Stand. Technol.* **101,** 487–503 (1996).

*136.* P. S. Julienne and J. Vigue, Cold collisions of ground- and excited-state alkali metal atoms, *Phys. Rev. A* **44,** 4464–4485 (1991).

*137.* W. T. Zemke and W. C. Stwalley, Analysis of long-range dispersion and exchange interactions between two Na atoms, *J. Chem. Phys.* **100,** 2661–2670 (1994).

*138.* W. T. Zemke, C.-C. Tsai, and W. C. Stwalley, Analysis of long-range dispersion and exchange interactions between two K atoms, *J. Chem. Phys.* **101,** 10382–10387 (1994).

*139.* W. T. Zemke and W. C. Stwalley, Analysis of long-range dispersion and exchange interactions between one Na atom and one K atom, submitted for publication.

*140.* R. Côté, A. Dalgarno, H. Wang, and W. C. Stwalley, Potassium scattering lengths and prospects for Bose–Einstein condensation and sympathetic cooling, *Phys. Rev. A* **57,** R4118–R4121 (1998).

*141.* W. T. Zemke and W. C. Stwalley, Analysis of exchange energy at long-range for states of alkali diatomic molecules correlating to two ground state atoms, submitted for publication.

*142.* C. C. Bradley, C. A. Sackett, and R. G. Hulet, Bose–Einstein condensation of lithium: observation of limited condensate number, *Phys. Rev. Lett.* **78,** 985–988 (1997).

*143.* W. Ketterle and N. J. van Druten, Evaporative cooling of trapped atoms, *Adv. At. Mol. Opt. Phys.* **37,** 181–236 (1996).

*144.* G. F. Gribakin and V. V. Flaumbaum, Calculation of the scattering length in atomic collisions using the semiclassical approximation, *Phys. Rev. A* **48,** 546–553 (1993).

*145.* H.M.J.M. Boesten, J. M. Vogels, J. G. C. Tempelaars, and B. J. Verhaar, Properties of cold collisions of $^{39}K$ atoms and of $^{41}K$ atoms in relation to Bose–Einstein condensation, *Phys. Rev. A.* **54,** R3726–R3729 (1996).

*146.* J. L. Bohn, J. P. Burke, C. H. Greene, H. Wang, P. L. Gould, and W. C. Stwalley, Collisional Properties of ultracold potassium: consequences for degenerate Bose and Fermi gases, *Phys. Rev. A,* in press.

*147.* J. P. Burke, C. H. Greene, J. L. Bohn, H. Wang, P. L. Gould, and W. C. Stwalley, Determination of $^{39}K$ scattering lengths using photoassociation spectroscopy of the $0_g^-$ state, submitted for publication.

*148.* R. Côté and A. Dalgarno, Elastic scattering of two $^7Li$ atoms, *Phys. Rev. A* **50,** 399–404 (1994).

*149.* A. J. Moerdijk and B. J. Verhaar, Prospects for Bose–Einstein condensation in atomic $^7Li$ and $^{23}Na$, *Phys. Rev. Lett.* **73,** 518–521 (1994).

*150.* A. J. Moerdijk, W. C. Stwalley, R. G. Hulet, and B. J. Verhaar, Negative scattering length of ultracold $^7Li$ gas, *Phys. Rev. Lett.* **72,** 40–43 (1994).

151. R. W. Heather and P. S. Julienne, Theory of laser-induced associative ionization of ultracold Na, *Phys. Rev. A* **47,** 1887–1906 (1993).
152. M. Marinescu, H. R. Sadeghpour, and A. Dalgarno, Dispersion coefficients for alkali metal dimers, *Phys. Rev. A* **49,** 982–988 (1994).
153. T. R. Proctor and W. C. Stwalley, The long-range interactions of s-state alkali atoms with rare gas and hydrogen atoms, *J. Chem. Phys.* **66,** 2063–2073 (1977).
154. M. Marinescu and A. F. Starace, Dispersion coefficients for highly excited molecular states of $K_2$, *Phys. Rev. A* **56,** 4321–4323 (1997).
155. H. Wang, W. C. Stwalley, and A. M. Lyyra, Assignment of the diabatic and adiabatic atomic asymptotic limits of the $K_2$ Rydberg states, *J. Chem. Phys.* **96,** 7965–7972 (1992).
156. L. Li and R. W. Field, CW perturbation facilitated optical–optical double resonance (PFOODR) spectroscopy of $Na_2$ and $Li_2$, *in* "Molecular Spectroscopy and Dynamics by Stimulated Emission Pumping" (H. L. Dai and R. W. Field, Eds.), p. 251–277, World Scientific, Singapore, 1995.
157. A. M. Lyyra, P. D. Kleiber, and W. C. Stwalley, All-optical triple resonance: spectroscopy and state-selected photodissociation dynamics, *in* "Stimulated Emission Pumping," (H. L. Dai and R. W. Field, Eds.), pp. 459–490, World Scientific, Singapore, 1995.
158. K. Urbanski, S. Antonova, A. M. Lyyra, A. Yiannopoulou, and W. C. Stwalley, All optical triple resonance spectroscopy of the $A^1\Sigma_u^+$ state of $^7Li_2$, *J. Chem. Phys.* **104,** 2813–2817 (1996).
159. C. Linton, F. Martin, I. Russier, A. J. Ross, P. Crozet, S. Churassy, and R. Bacis, Observation and analysis of the $A^1\Sigma_u^+$ state of $^6Li_2$ from $v = 0$ to the dissociation limit, *J. Mol. Spectrosc.* **175,** 340–353 (1996).
160. F. Martin, M. Aubert-Frecon, R. Bacis, P. Crozet, C. Linton, S. Magnier, A. J. Ross, and I. Russier, General analytical form for the long-range potential of the $(ns + np_J)$ $O_u^+$ States of alkali dimers applied to $^6Li_2$, *Phys. Rev. A* **55,** 3458–3464 (1997).
161. H. Wang, The connection between the $1^1\Pi_g$ short range potential and the $1_g(3p_{3/2})$ long-range potential of $Na_2$, unpublished data.
162. S. Magnier, Ph. Millie, O. Dulieu, and F. Masnou-Seeuws, Potential curves for the ground and excited states of the $Na_2$ molecule up to the $(3s + 5p)$ dissociation limit: results of two different effective potential calculations, *J. Chem. Phys.* **98,** 7113–7125 (1993); S. Magnier, Ph.D. Thesis, University of Paris-Sud (Orsay), 1993.
163. S. Magnier, M. Aubert-Frecon, O. Bouty, F. Masnou-Seeuws, Ph. Millie, and V. N. Ostrovsky, Structures in the long-range potential curves of the $Na_2$ molecule: comparison between ab initio and asymptotic calculations, *J. Phys. B.* **27,** 1723–1741 (1994).
164. M. Marinescu, Dispersion coefficiencies for the *n*P–nP asymptote of homonuclear alkali metal dimers, *Phys. Rev. A* **56,** 4764–4773 (1997).
165. Y.-H. Uang and W. C. Stwalley, Close-coupling calculations of spin-polarized hydrogen–deuterium collisions, *Phys. Rev. Lett.* **45,** 627–630 (1980).
166. Y. B. Band and P. S. Julienne, Ultracold molecule production by laser-cooled atom photoassociation, *Phys. Rev. A* **51,** R4317–R4320 (1995).
167. J. T. Bahns, W. C. Stwalley, and P. L. Gould, Laser cooling of molecules: a sequential scheme for rotation, translation and vibration, *J. Chem. Phys.*, **104,** 9689–9697 (1996).
168. R. Côté and A. Dalgarno, Mechanism for the production of vibrationally excited ultracold molecules of $^7Li_2$, *Chem. Phys. Letters*, **279,** 50–54 (1997).
169. R. Côté and A. Dalgarno, Mechanism for the production of $^6Li_2$ and $^7Li_2$ ultracold molecules, *J. Mol. Spectrosc.*, in press.
170. R. J. Rafac, C. E. Tanner, A. E. Livingston, K. W. Kukla, H. G. Berry, and C. A. Kurtz, Precision lifetime measurements of the $6p^2P_{1/2,\,3/2}$ states in atomic cesium, *Phys. Rev. A* **50,** R1976–R1979 (1994).
171. L. Marcassa, S. Muniz, E. de Queiroz, S. Zilio, V. Bagnato, J. Weiner, P. S. Julienne, and K. A. Suominen, Optical suppression of photoassociative ionization in a magneto–optical trap, *Phys. Rev. Lett.* **73,** 1911–1914 (1994).
172. H. Katori and F. Shimizu, Laser-induced ionizing collisions of ultracold krypton Gas in the metastable $1s_5$ state, *Phys. Rev. Lett.* **73,** 2555–2558 (1994).
173. M. Walkout, U. Sterr, C. Orzel, M. Hoogerland, and S. L. Rolston, Optical control of ultracold collisions in metastable xenon, *Phys. Rev. Lett.* **74,** 506–509 (1995).
174. V. Sanchez-Villicana, S. D. Gensemer, K. Y. N. Tan, A. Kumarakrishnan, T. P. Dinneen, W. Sueptitz, and P. L. Gould, Suppression of ultracold ground-state hyperfine-changing collisions with laser light, *Phys. Rev. Lett.* **74,** 4619–4622 (1995).
175. T. R. Proctor and W. C. Stwalley, Simple approximations for the long-range interactions of s-state alkali atoms with rare gas and hydrogen atoms, *Mol. Phys.* **37,** 1969–1974 (1979).
176. W. L. Wiese, M. W. Smith, and B. M. Miles, "Atomic Transition Probabilities. Volume II. Sodium Through Calcium," NSRDS-NBS22, U.S. Government Printing Office, Washington, DC, 1969.
177. B. Huynh, O. Dulieu, and F. Masnou-Seeuws, Associative ionization between two laser-excited sodium atoms: theory compared to experiment, *Phys. Rev. A* **57,** 958–975 (1998).
178. C. C. Tsai, J. T. Bahns, and W. C. Stwalley, Observation of $Na_2$ Rydberg states and autoionization resonances by high resolution all-optical triple resonance spectroscopy, *Chem. Phys. Lett.* **236,** 553–557 (1995).
179. A. M. Lyyra, H. Wang, T. J. Whang, L. Li, and W. C. Stwalley, CW all-optical triple resonance (AOTR) spectroscopy, *Phys. Rev. Lett.* **66,** 2724–2727 (1991).
180. A. Vardi, D. Abrashkevich, E. Frishman, and M. Shapiro, Theory of radiative recombination with strong laser pulses and the formation of ultracold molecules via stimulated photo-recombination of cold atoms, *J. Chem. Phys.* **107,** 6166–6174 (1997).
181. P. S. Julienne, K. Burnett, Y. B. Band, and W. C. Stwalley, Stimulated Raman molecule production in Bose–Einstein condensates, *Phys. Rev. A* **58,** R797-R800 (1998).
182. H. Wang and W. C. Stwalley, Ultracold photoassociative spectroscopy of heteronuclear alkali-metal diatomic molecules, *J. Chem. Phys.* **108,** 5767–5771 (1998).
183. R. de Vivie-Riedle, P. Hering, and K. L. Kompa, CARS Spectroscopy of the $NaH_2$ collision complex: the nature of the $Na(3^2p)$ $H_2$ exciplex ab initio calculations and experimental results, *Z. Phys. D* **17,** 299–308 (1990).
184. L. N. Ding, M. A. Young, P. D. Kleiber, W. C. Stwalley, and A. M. Lyyra, Photofragmentation spectroscopy of $MgD_2^+$, *J. Phys. Chem.* **97,** 2181–2185 (1993)
185. D. Veza, R. Beuc, S. Milosevic, and G. Pichler, Cusp satellite bands in the spectrum of $Cs_2$, *Eur. Phys. J. D* **2,** 45–52 (1998).
186. J. P. Burke, Ch. H. Greene, and J. L. Bohn, Multichannel cold collisions: simple dependences on energy and magnetic field, *Phys. Rev. Lett.* **81,** 3355–3358 (1998).
187. W. C. Stwalley, Stability of spin aligned hydrogen at low temperatures and high magnetic fields: new field dependent scattering resonances and predissociations, *Phys. Rev. Lett.* **37,** 1628–1631 (1976).
188. Y. H. Uang, R. F. Ferrante, and W. C. Stwalley, Model calculations of magnetic-field-induced perturbations and predissociations in $^6Li$ $^7Li$ near dissociation, *J. Chem. Phys.* **74,** 6267–6270 (1981).
189. S. Inouye, M. R. Andrews, J. Stenger, H. J. Miesner, D. M. Stamper-Kurn, and W. Ketterle, Observation of Feshbach resonances in a Bose–Einstein condensate, *Nature* **392,** 151–154 (1998).
190. J. L. Roberts, N. R. Claussen, J. P. Burke, C. E. Greene, E. A. Cornell, and C. E. Wieman, Resonant magnetic field control of elastic scattering in cold $^{85}Rb$, *Phys. Rev. Lett.* **81,** 5109–5112 (1998).
191. J. Bohn and P. S. Julienne, Prospects for influencing scattering lengths with far-off-resonant light, *Phys. Rev. A* **56,** 1486–1491 (1997).